To Jean

There was once an indian princess

named Singing Feathers

to honor the geese who bring summer on their wings...

ABSTRACT

THE REAL PART OF THE FORWARD NUCLEAR AMPLITUDE

FOR HADRON-PROTON SCATTERING

BETWEEN 70 AND 200 GEV/C

Lincoln Antonio Fajardo-Paz

Yale University

1980

We have measured the elastic scattering cross section for pp, $\bar{p}p$, π^+p, π^-p, K^+p, and K^-p at 70, 100, 125, 150, 175, and 200 GeV/c incident momenta. The range of the four momentum transfer squared, t, was a function of momentum and varied from $0.0016 \leq -t \leq 0.490$ $(GeV/c)^2$ at 200 GeV/c to $0.0018 \leq -t \leq 0.0625$ $(GeV/c)^2$ at 70 GeV/c. We have determined the ratio of the real to imaginary part of the nuclear amplitude and the nuclear slope in the same region. We have found that the nuclear slope is not a constant in this region. A suitable parametrization was found and the real parts are presented in terms of this parametrization.

THE REAL PART OF THE FORWARD NUCLEAR AMPLITUDE FOR HADRON-PROTON SCATTERING BETWEEN 70 AND 200 GEV/C

A Dissertation

Presented to the Faculty of the Graduate School

of

Yale University

in Candidacy for the Degree of

Doctor of Philosophy

by

Lincoln Antonio Fajardo-Paz

May 1980

CONTENTS

LIST OF FIGURES

LIST OF TABLES

Lovers with sullen lips or clever lines
She tries them all at least once
And then with a casual shrug moves on.
Yet I am held by her distant sway,
Searching for the touch
That like falling silk
Reveals her hidden charms.

CHAPTER 1

INTRODUCTION

Since the time of Rutherford the study of elastic scattering has been a fundamental probe of the forces between particles and of their structures. At high energies the elastic scattering of hadrons by the nuclear force has the characteristics of quantum mechanical absorption and scattering by an opaque disc: The nuclear amplitude is almost totally imaginary and sharply peaked in the forward direction. However, this simple model does not account for the shape of the elastic peak and for the small ratio of the elastic cross section to the total cross section. A detailed explanation of nuclear scattering is further complicated by the variation with energy of the shape of the elastic peak, the total elastic cross section, and the total cross section.

Because of the large coupling constant of the nuclear force, attempts at a relativistic field theory have been unsuccesful. In S-matrix theory the approach has been to identify the properties of the scatttering matrix which follow from the structure of field theory. Principal among these properties are unitarity and analyticity. The unitarity condition leads to the optical theorem which relates the total cross section to the imaginary part of the amplitude in the forward direction. In turn, the analyticity requirement leads to dispersion relations by which the global behaviour of both the total cross section and the real part of the amplitude in the forward direction are related. Thus elastic scattering not only describes the largest single process in high energy collisions but also circumscribes the behaviour of the total cross section. The determination of the real part of the nuclear amplitude gives us a check of the analyticity condition and allows us to predict the behaviour of the total cross section at higher energies.

We have measured the elastic scattering differential cross section for pp, $\bar{p}p$, π^+p, π^-p, K^+p, and K^-p. The measurements were made at Fermilab with incident momenta of 70, 100, 125, 150, 175, and 200 GeV/c. The high spatial resolution of our spectrometer allowed a very accurate determination of the scattering angle and thus of t, the four momentum transfer squared between the incident projectile and the fast forward scattered particle. The t range of of the measurements depended on the incident momentum and varied from $0.0018 \leq -t \leq 0.0625$ $(GeV/c)^2$ at 70 GeV/c to $0.0016 \leq -t \leq 0.490$ $(GeV/c)^2$ at 200 GeV/c. This t range allows us to determine the shape of the nuclear amplitude near the forward direction and by means of the interference with the Coulomb amplitude to determine the real part of the nuclear amplitude.

For pp scattering the real part of the forward nuclear amplitude has been measured extensively up to ISR (CERN Intersecting Storage Rings) energies.[1.1] The real parts for π^-p[1.2] have been measured up to 140 GeV/c, while π^+p[1.3] and K^+p[1.4] are known up to 52 GeV/c. The real parts for K^-p[1.5] and $\bar{p}p$[1.6] have not been measured above 15 GeV/c. Our experiment is the first to measure three reactions simultaneously (pp, π^+p, K^+p and $\bar{p}p$, π^-p, K^-p) and the first to measure all six reactions with the same apparatus.

Differential Cross Section

In the t range studied in this experiment the differential cross section is determined by both the Coulomb and nuclear scattering amplitudes:

$$d\sigma/dt = \pi \mid f_C + f_n \mid^2 \qquad (1.1)$$

At small -t the Coulomb amplitude is dominant and is given by the expression:

$$f_C = (2z_a e^2/c)\ G_a(t)\ G_p(t)\ \exp(iz_a\Omega)\ /\ t\ , \qquad (1.2)$$

where $z_a e$ is the charge of the incident particle a. $G_a(t)$ and $G_p(t)$ are the electromagnetic form factors of the incident particle a and the target proton. We use the dipole form for the protons and the monopole form for the pions and kaons:

$$G_p(t) = (1 + v_p\ |t|)^{-2} \tag{1.3a}$$

$$G_\pi(t) = (1 + 2v_\pi\ |t|)^{-1} \tag{1.3b}$$

$$G_K(t) = (1 + 2v_K\ |t|)^{-1} \tag{1.3c}$$

$$v_p = r_p^{\ 2} / 12\hbar^2$$

$$v_\pi = r_\pi^{\ 2} / 12\hbar^2$$

$$v_K = r_K^{\ 2} / 12\hbar^2$$

$$\hbar = h / 2\pi\ ,$$

where h is Planck's constant and the values of r are the electromagnetic form factor radii obtained from Refs. 1.7-1.9. The values of the radii used throughout the analysis are:

$$r_p = 0.805 \text{ fm}$$

$$r_\pi = 0.711 \text{ fm}$$

$$r_K = 0.565 \text{ fm}\ .$$

In Eq. 1.2 the Coulomb phase shift, Ω, is given by West and Yennie[1.10] as:

$$\Omega = \alpha \ln[\ 1.124 / (\ (b(0) + 4v_p + 4v_a)\ |t|\ )\ ]\ ,$$

where α is the fine structure constant and b(0) is the nuclear slope at t = 0. We define b(t) below.

Traditionally real part measurements have been analyzed with the nuclear amplitude parametrized as an exponential with a constant slope,

B. However, recent results from experiments at Fermilab,[1.11,1.12] SLAC,[1.13] and the CERN ISR[1.14] show a more complicated t dependence of the nuclear slope. To explore this behaviour we employ two parametrizations for the nuclear amplitude. For convenience they are called the exponential and form factor parametrizations. We define the exponential nuclear amplitude as follows:

$$f_n^{\,e} = (\sigma_{tot}/4\pi\hbar)\ (i + \rho)\ \exp[\ (Bt + Ct^2)/2\ ]\ , \tag{1.4}$$

where σ_{tot} is the total cross section and where B and C are the constant nuclear slope and curvature. The real and imaginary parts are assumed to have the same functional dependence on t and spin effects are neglected.[1.15] Thus we define ρ as the ratio of the real to imaginary part of the nuclear amplitude at t = 0.

As we show in Ref. 1.11, the nuclear amplitude can be parametrized by a form suggested in the theoretical models of Chou and Yang[1.16] and versions of the Additive Quark Model (AQM). These models attribute the major part of the small t elastic cross section variation to the hadronic form factors of the target and the projectile. These form factors are assumed to be the same as the electromagnetic ones. In the AQM form factors describe the spatial distribution of clothed quarks; in the very small -t region, the scattering is dominated by single quark-quark scattering. Specifically we use the form for the nuclear amplitude suggested by Bialas et. al.[1.17] and Levin and Shekhter.[1.18] We define the form factor nuclear amplitude as follows:

$$f_n^{\,ff} = (\sigma_{tot}/4\pi\hbar)\ (i + \rho)\ G_a(t)\ G_p(t)\ \exp(ut/2)\ , \tag{1.5}$$

where σ_{tot}, $G_a(t)$, $G_p(t)$ are defined above and u is the reduced nuclear slope. One can identify the u with the quark radius[1.19], r_q, where $u = r_q^2/2\hbar^2$. In Appendix D we give a summary of the arguments used by Bialas et al. in their theory. Again we assume that the real and imaginary parts have the same functional dependence on t, neglect spin effects, and define ρ to be the ratio of real to imaginary parts.

In summary, we can write the differential cross section as the sum of three terms:

$$d\sigma/dt = \sigma_C + \sigma_I + \sigma_n$$

where σ_C, σ_I, and σ_n are the Coulomb, interference and nuclear contributions. The exponential cross section is given by sum of the three terms below:

$$\sigma_C = (4\pi e^4/c^2)\, G_a^2\, G_p^2 \,/\, t^2 \tag{1.6a}$$

$$\sigma_I^e = \alpha\, \sigma_{tot}\, G_a\, G_p\, (z_a\rho \cos\Omega + \sin\Omega) \exp[(Bt+Ct^2)/2] \,/\, t \tag{1.6b}$$

$$\sigma_n^e = (\sigma_{tot}^2/16\pi\hbar^2)\,(1+\rho^2) \exp(Bt+Ct^2) \tag{1.6c}$$

Similarly the form factor cross section is given by the sum of the three terms below:

$$\sigma_C = (4\pi e^4/c^2)\, G_a^2\, G_p^2 \,/\, t^2 \tag{1.7a}$$

$$\sigma_I^{ff} = \alpha\, \sigma_{tot}\, G_a^2\, G_p^2\, (z_a\rho \cos\Omega + \sin\Omega) \exp(ut/2) \,/\, t \tag{1.7b}$$

$$\sigma_n^{ff} = (\sigma_{tot}^2/16\pi\hbar^2)\,(1+\rho^2)\, G_a^2\, G_p^2 \exp(ut) \tag{1.7c}$$

In both cases the magnitude and sign of ρ can be determined from the interference term. While the Coulomb term is sharply decreasing ($1/t^2$) and the nuclear term is nearly flat, the interference term is distinguished by a $1/t$ dependence and has its maximum effect in the range $0.001 \leq -t \leq 0.003$ $(\mathrm{GeV}/c)^2$. However, the value of ρ depends strongly on the nuclear slope in this neighborhood. The accurate determination of ρ requires considerable care in the determination of the nuclear slope near $t = 0$. We have paid particular attention to the problem of determining the correct nuclear cross section.

We define the nuclear slope, $b(t)$, and the nuclear curvature, $c(t)$, as follows:

$$b(t) = d[\ \ln \sigma_n\ ]/dt$$

$$c(t) = (1/2)\ db/dt\ .$$

Thus for the exponential cross section b and c are:

$$b^e(t) = B - 2C\ |t| \tag{1.8a}$$

$$c^e(t) = C\ . \tag{1.8b}$$

For pp scattering the form factor slope and curvature are:

$$b_p^{ff}(t) = u + 8v_p\ \ (1 + v_p|t|)^{-1} \tag{1.9a}$$

$$c_p^{ff}(t) = 4v_p^2\ \ (1 + v_p|t|)^{-2}\ . \tag{1.9b}$$

While for πp or Kp scattering the form factor slope and curvature are:

$$b_a^{ff}(t) = u + 4v_a\ (1 + 2v_a|t|)^{-1} + 4v_p\ (1 + v_p|t|)^{-1} \tag{1.9c}$$

$$c_a^{ff}(t) = 4v_a^2\ (1 + 2v_a|t|)^{-2} + 2v_p^2\ (1 + v_p|t|)^{-2}\ . \tag{1.9d}$$

Dispersion Relations

In 1954 Gell-Mann, Goldberger, and Thirring[1.20] used causality arguments in the context of quantum electrodynamics to show that the transition amplitudes can be analytically continued to complex values of the energy and to obtain dispersion relations for the amplitude. However, for S-matrix theory it is difficult to rigorously establish the connection between causality and analyticity.[1.21] S-matrix dispersion relations are thus based on the reasonable assumption of analyticity. The dispersion relations for πp elastic scattering (by virtue of the pions spin zero and non-exotic channels) have been proved from axioms of field theory[1.22]. For pp and Kp elastic scattering, dispersion relations have only been shown to be valid to all orders in pertubation theory.

Although the evaluation of dispersion relations goes beyond the scope of this thesis, we give brief discussion of the mathematical and physical bases of dispersion relations. By Cauchy's integral representation theorem we write:

$$f(z) = (1/2\pi i) \int_C dz' \, f(z') \,/\, (z' - z) \, ,$$

where C is a closed smooth curve, f(z') is a function analytic within C, and z is contained within C. Thus the real part of f(z) is given by:

$$\mathrm{Re}[\, f(z) \,] = (1/2\pi) \int_C dz' \, \mathrm{Im}[\, f(z') \,] \,/\, (z' - z) \qquad (1.10)$$

To apply the above equation to the scattering of particles, we associate the real part of z with s, the center of mass energy squared, and f(s) with $T_{ap}(s,t)$, the relativistically invariant amplitude for ap elastic scattering. We assume that $T_{ap}(s,t)$ is analytically continued under the simultaneous application of charge conjugation and time reversal. This condition, known as crossing symmetry, relates the reaction $a + p \rightarrow a + p$ with initial and final momenta $(p_a^{\,i}, p_p^{\,i}, p_a^{\,f}, p_p^{\,f})$ to the reaction $\bar{a} + p \rightarrow \bar{a} + p$ with $(-p_a^{\,f}, p_p^{\,i}, -p_a^{\,i}, p_p^{\,f})$. Thus the center of mass energy squared for $\bar{a}p$ scattering is given by:

$$
\begin{aligned}
s_{\bar{a}p} &= (-p_a^{\,f} + p_p^{\,i})^2 \\
&= u_{ap} \\
&= M^2 - s_{ap} - t \;,
\end{aligned}
$$

where s, t, and u are the standard Mandelstam variables and $M = 2m_a^{\,2} + 2m_p^{\,2}$. Since the variable t remains the same for both reactions, the amplitude $T_{ap}(s, t)$ is given by:

$$
\begin{aligned}
T_{ap}(s,t) &= T_{a^+p}(s,t) && \text{for } s \geq (m_a+m_p)^2 \\
&= T_{a^-p}(M^2-s-t,\, t) && \text{for } s \leq (m_a-m_p)^2 - t \;,
\end{aligned}
$$

where T_{a^+p} and T_{a^-p} are amplitudes for a^+p and a^-p scattering. In Fig. 1.1 we show the contour needed to evaluate the integral 1.10. Howerver, this contour includes contribution from poles due to intermediate states, M_I, and exchange reactions and from unphysical cuts along the real axis, $M_C^{\,2}$.

Figure 1.1

CONTOUR FOR ANALYTIC DISPERSION RELATIONS

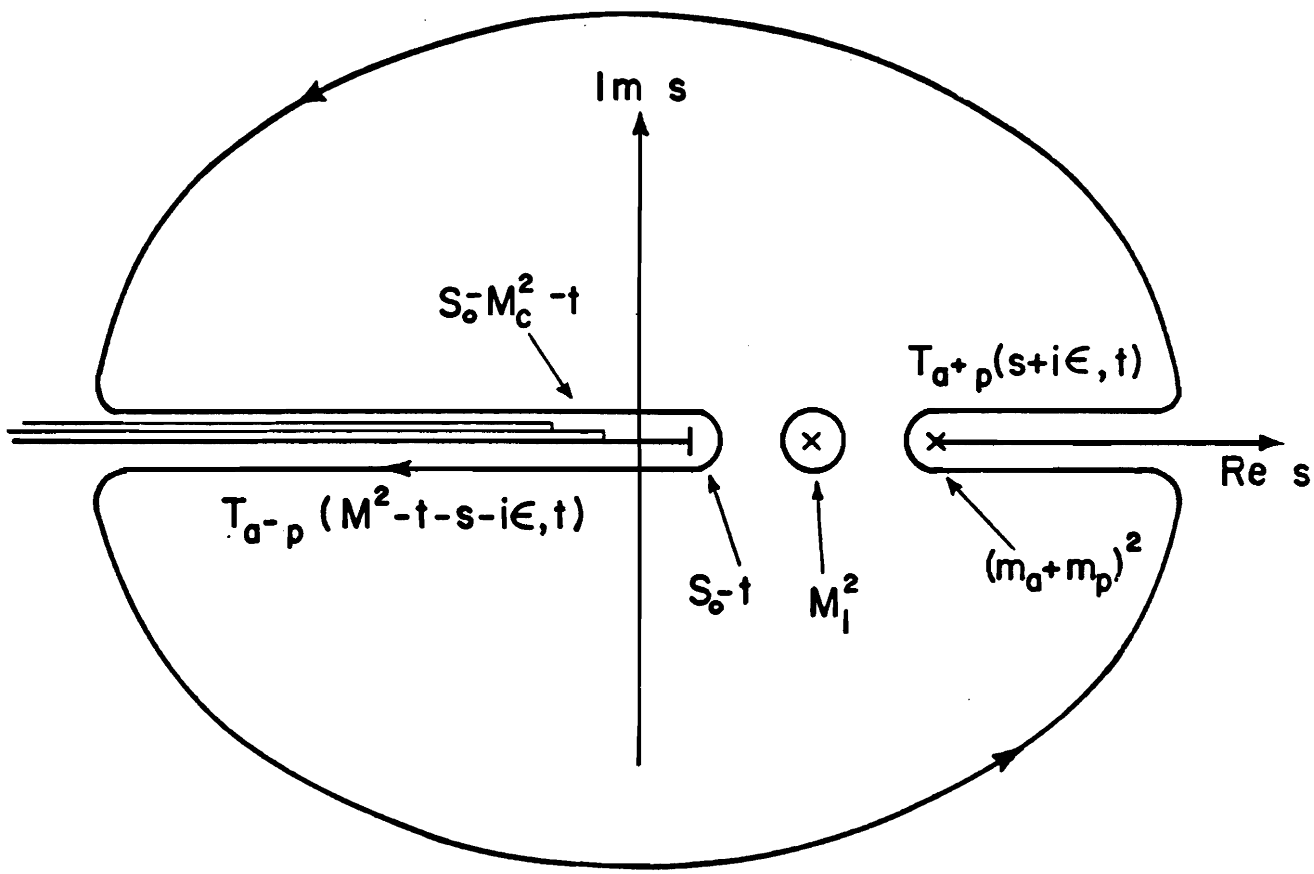

$$M^2 = (m_a + m_p)^2$$

$$s_o = (m_a - m_p)^2$$

Since we are interested in dispersion relations in the forward direction, we set t = 0. It is more convenient to reformulate the integrals in terms of the energy, E. The optical theorem then has the form

$$\mathrm{Im}[\, T_{ap}(E)\,] = 2m_p\, (E^2 - m_a{}^2)^{1/2}\, \sigma_{ap}(E)\ ,$$

where E is the incident energy of particle a. The dispersion relation can then be written as:

$$\begin{aligned}\mathrm{Re}[\, T_{ap}(E) - T_{ap}(0)\,] = {} & E \textstyle\sum_I R_I \,/\, (E_I - E) \\ & + (E/\pi) \int_{\overline{M}_C}^{m_a} dE'\ \mathrm{Im}[T_-(E')] \,/\, (E'^2 - E^2) \\ & + (4m_pE/\pi)\ \mathbb{P} \int_{m_a}^{\infty} dE'\ (E'^2 - m_a{}^2)^{1/2}\, E'^{-1} \\ & \qquad \times [\ \sigma_{ap}(E')\, (E'-E)^{-1} - \sigma_{\overline{a}p}(E')\, (E'+E)^{-1}\ ]\ ,\end{aligned} \tag{1.11}$$

where the first term represents the sum over poles due to intermediate states and exchanges. In the second term Im[T_] represents the unphysical cuts discontinuity and $\overline{M}_C$ is the unphysical cut threshhold. The last term is the principal value of the of the integral over the total cross sections. Since the difference between the particle and antiparticle total cross sections does not go to zero rapidly enough at high energies, the real part of T_{ap} at E = 0 has been subtracted to make the integral convergent.

In Fig. 1.2 we show the principal pole and unphysical

Figure 1.2

PRINCIPAL POLE TERMS
and UNPHYSICAL CONTRIBUTIONS

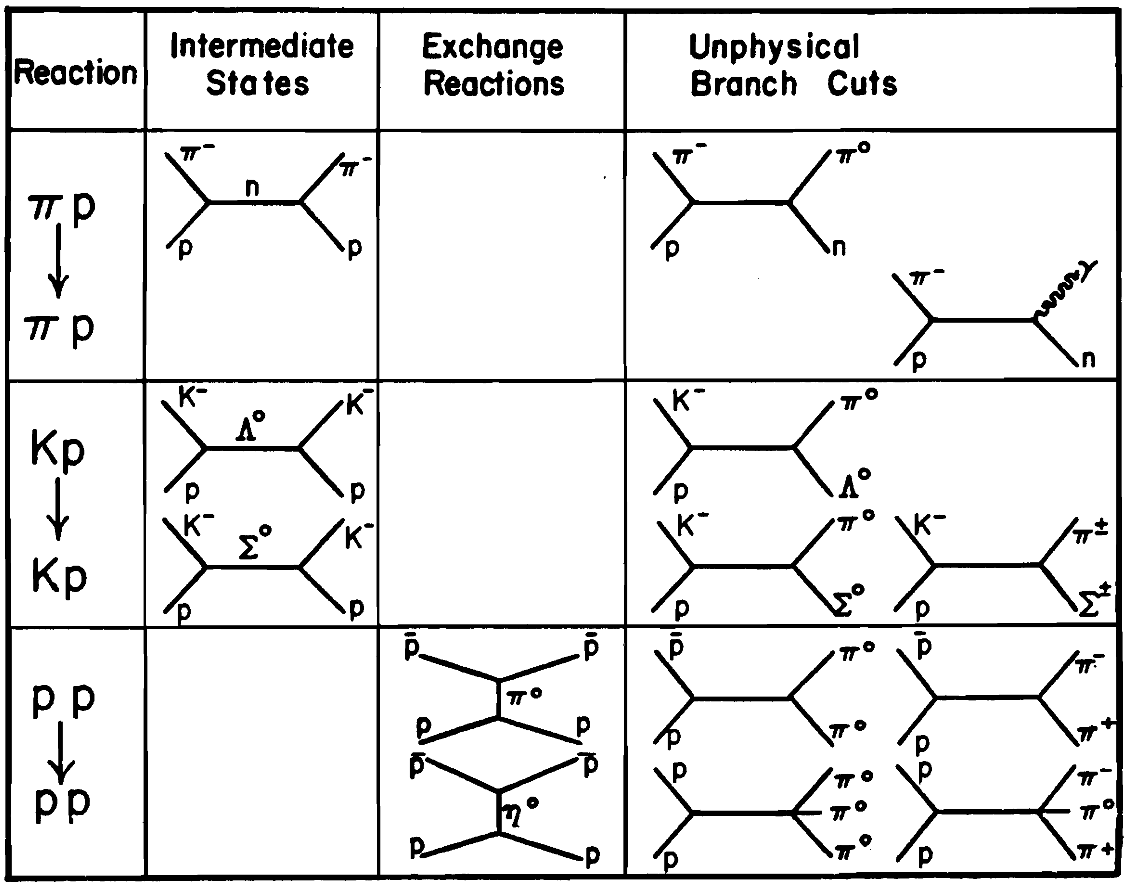

contributions. For πp scattering these contributions are small and well understood, while for Kp and pp they are substantial and have large uncertainties. On a practical level the evaluation of the third term in 1.11 is made difficult by regions at low energies where the total cross sections have not been measured. At high energies the total cross section varies slowly, while the integral is sharply peaked in the neighborhood of $E' = E$. By means of a clever Taylor series expansion, derivative dispersion relations[1.23] show that the real part becomes a local function of the total cross section and is insensitive to its value at very high energies.

We compare our results with the calculations of Hendrick et al.[1.24], Hohler et al.[1.25], Dumbrajs[1.26], and Lipkin[1.27]. The first three calculations use analytic dispersion relations and a detailed fit to total cross section measurements. Hendrick et al. and Hohler et al. extrapolate the total cross sections to very high energies using a $\ln^2(E)$ dependence, while Dumbrajs uses a $[\ln(E)]^{.967}$ dependence. Lipkin uses derivative dispersion relations[1.28] and fits the total cross sections at Fermilab energies with a two component Pomeron model. This model gives the total cross section as rising with an $E^{.13}$ dependence.

CHAPTER 2

APPARATUS

Overview

The apparatus used in this experiment was a single arm forward spectrometer that measured the momentum and trajectory of the incident particle and of a fast forward secondary. High pressure proportional wire chambers (PWC's) surrounding a liquid hydrogen (LH_2) target measured the scattering angle with a precision of 30 μrad, σ . The difference between the incoming and outgoing momentum was determined to an accuracy of 0.03% ($\Delta p/p$; σ) and was used to identify inelastic scatters and scatters off electrons. Four Cerenkov counters simultaneously identified pions, kaons, and protons, while two calorimeters tagged electrons and muons in the beam. A diagram of the apparatus is shown in Fig. 2.1 and the distances along the beam line of the major elements are presented in Table 2.1. In Ref. 2.1 Alan Schiz gives a detailed description of the apparatus. In this chapter we summarize its salient features.

Beam

The experiment was performed in the M6 West beam line of the Meson Lab at Fermilab. The beam properties are summarized in Refs. 2.2.

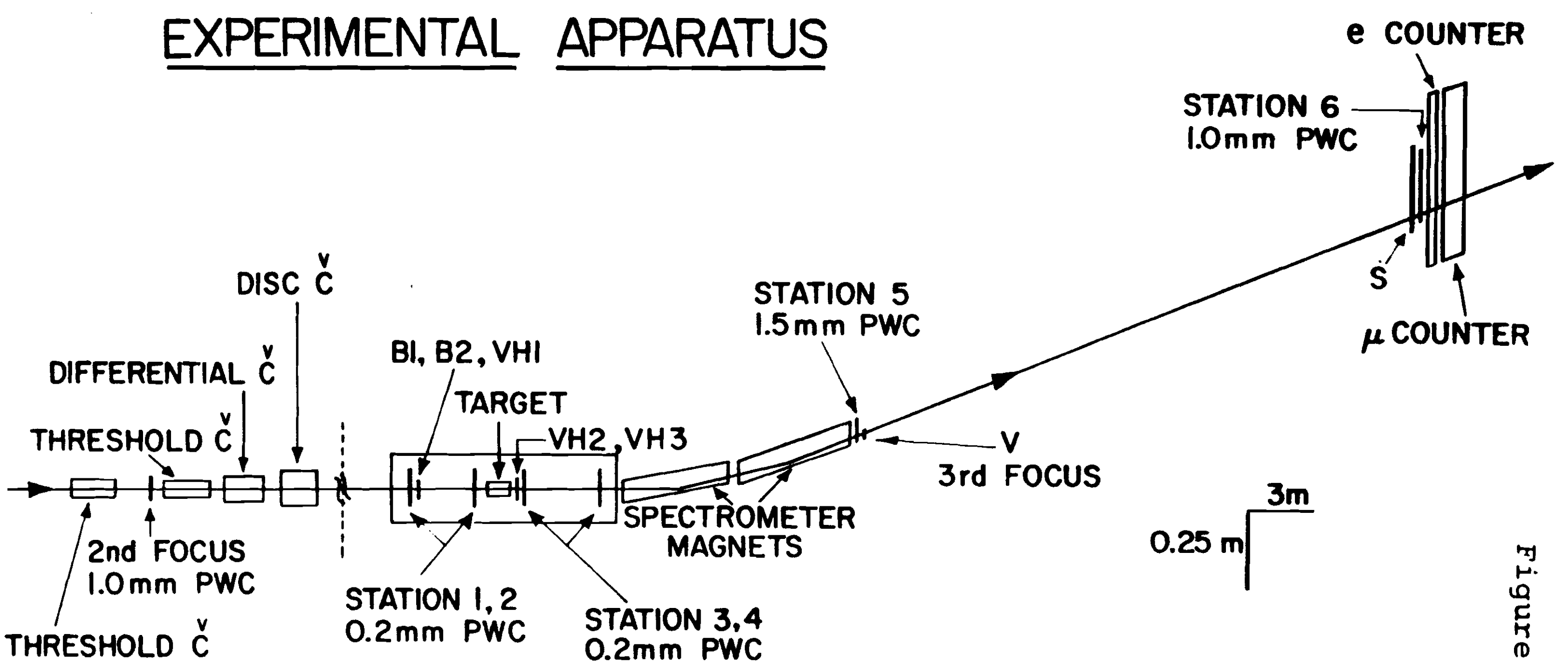
EXPERIMENTAL APPARATUS
e COUNTER
STATION 6
1.0mm PWC
S
μ COUNTER
DISC Č
DIFFERENTIAL Č
THRESHOLD Č
B1, B2, VH1
TARGET
VH2, VH3
STATION 5
1.5mm PWC
V
3rd FOCUS
3m
0.25 m
SPECTROMETER
MAGNETS
2nd FOCUS
1.0mm PWC
THRESHOLD Č
STATION 1, 2
0.2mm PWC
STATION 3, 4
0.2mm PWC

Figure 2.1

TABLE 2.1

Layout of Apparatus

Simplified trajectory of an on-axis on-momentum unscattered beam particle is as follows (not to scale):

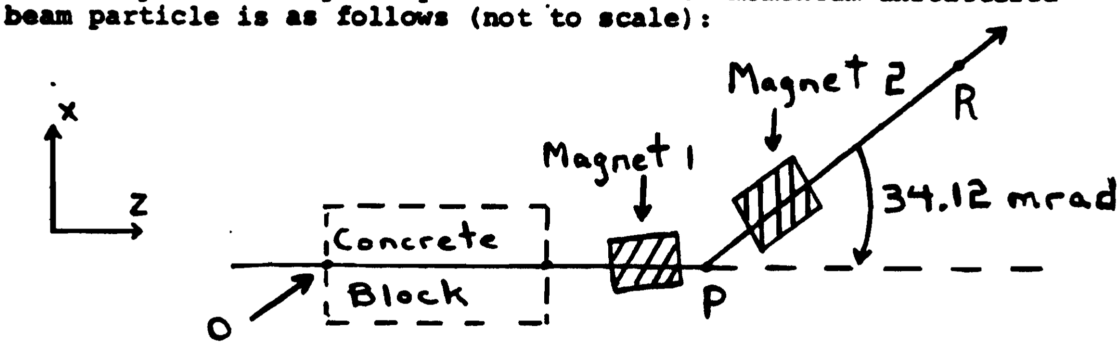

The following elements are measured with respect to upstream end of concrete block (pt.O)

Element	Z (cm)
High Resolution PWC1	23.18
High Resolution PWC2	373.38
High Resolution PWC3	625.12
High Resolution PWC4	1075.04
Magnet 1 Entrance[a]	1122.67
Magnet 2 Entrance [a]	1729.68
Bend Point, P	1751.90
Magnet 2 Entrance[a]	1774.12
Magnet 2 Exit[a]	2380.91

The following elements are measured along $\overline{PR}$ with respect to the bend point P:

Element	Z (cm)
PWC5[b]	674.92
Veto Plane	705.47
PWC6	3640.14

[a]Refers to Z of center of aperture as projected down to unbent beam line

[b]These chambers (an x and y) were tilted 8.477° with respect to line PR

Typically protons with 300 or 400 GeV/c incident momentum were focused on a beryllium production target. The production angle of the M6 beam was 2.65 mrad from the direction of the incident protons. The beam momentum could be varied from 20 to 200 GeV/c. The beam had three stages, each with point to parallel to point optics. The momentum spread (maximum ±1%) was selected via a horizontal collimator at the first focus.

At the second focus a PWC with 1mm wire spacing measured the momentum of the incoming particle with a $\Delta p/p = 0.03\%$ standard deviation. The scintillation counters SA, SB, E, W, U, and D defined the upstream aperture. Further downstream, two other scintillation counters, H1 and H2 also rejected particles with improper trajectories.

Four Cerenkov counters simultaneously identified pions, kaons, and protons. The upstream counters, M6K1 and M6K2[2.3], were used as threshhold counters to identify pions. M6K3[2.4] and M6K4[2.5] were differential counters to identify kaons and protons. Figures 2.2 and 2.3 show typical pressure curves for these counters; Figure 2.4 shows the beam composition at the target as a function of beam momentum. At 200 GeV/c the contamination of kaons by pions was largest and was approximately 0.5%.

At the third focus the beam was recombined in both space and momentum. Here the beam was focused on a very small scintillation counter V1, described below.

Figure 2.2

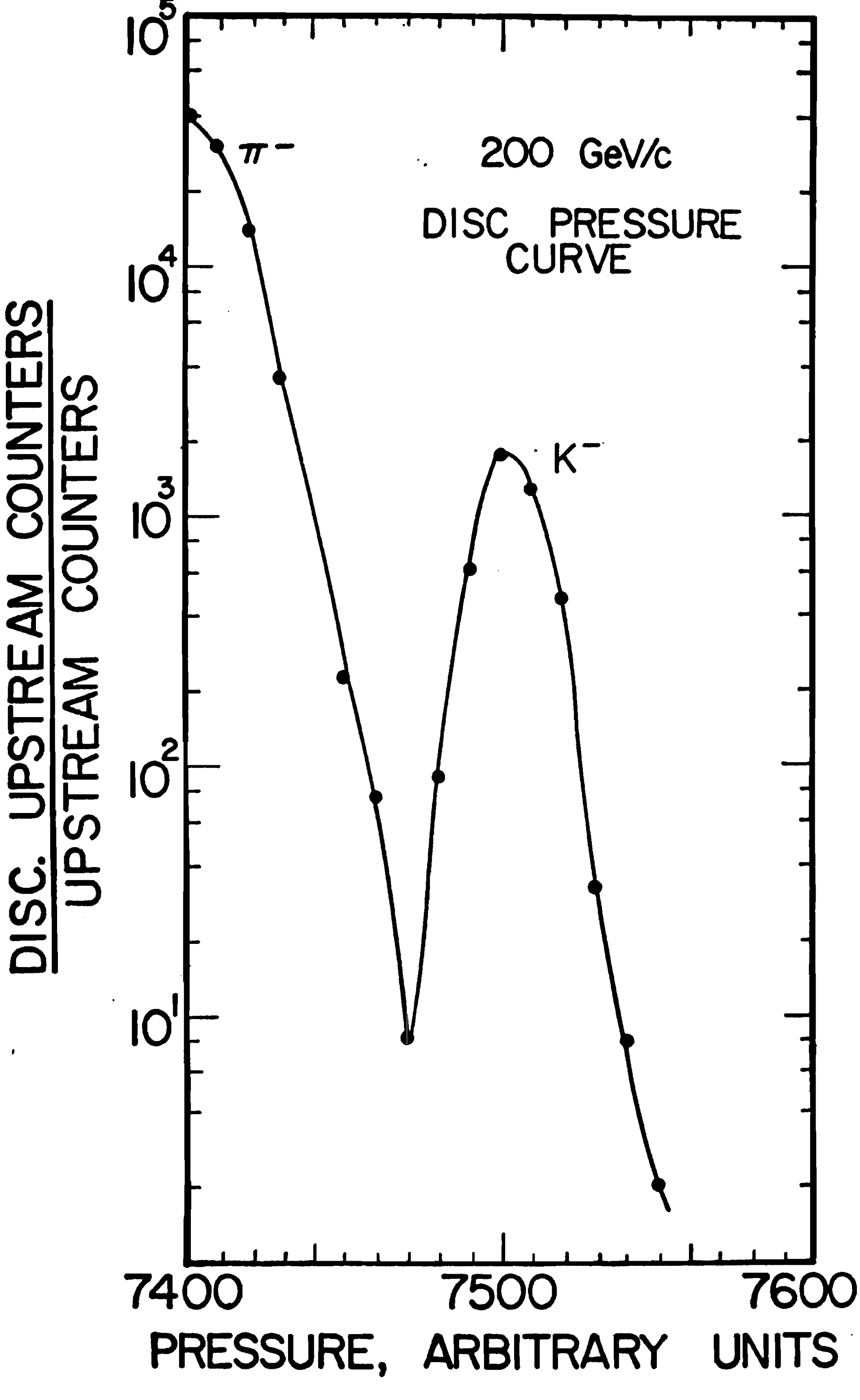

10^5
10^4
10^3
10^2
10^1
π^-
200 GeV/c
DISC PRESSURE CURVE
K^-
DISC. UPSTREAM COUNTERS / UPSTREAM COUNTERS
7400
7500
7600
PRESSURE, ARBITRARY UNITS

Figure 2.3

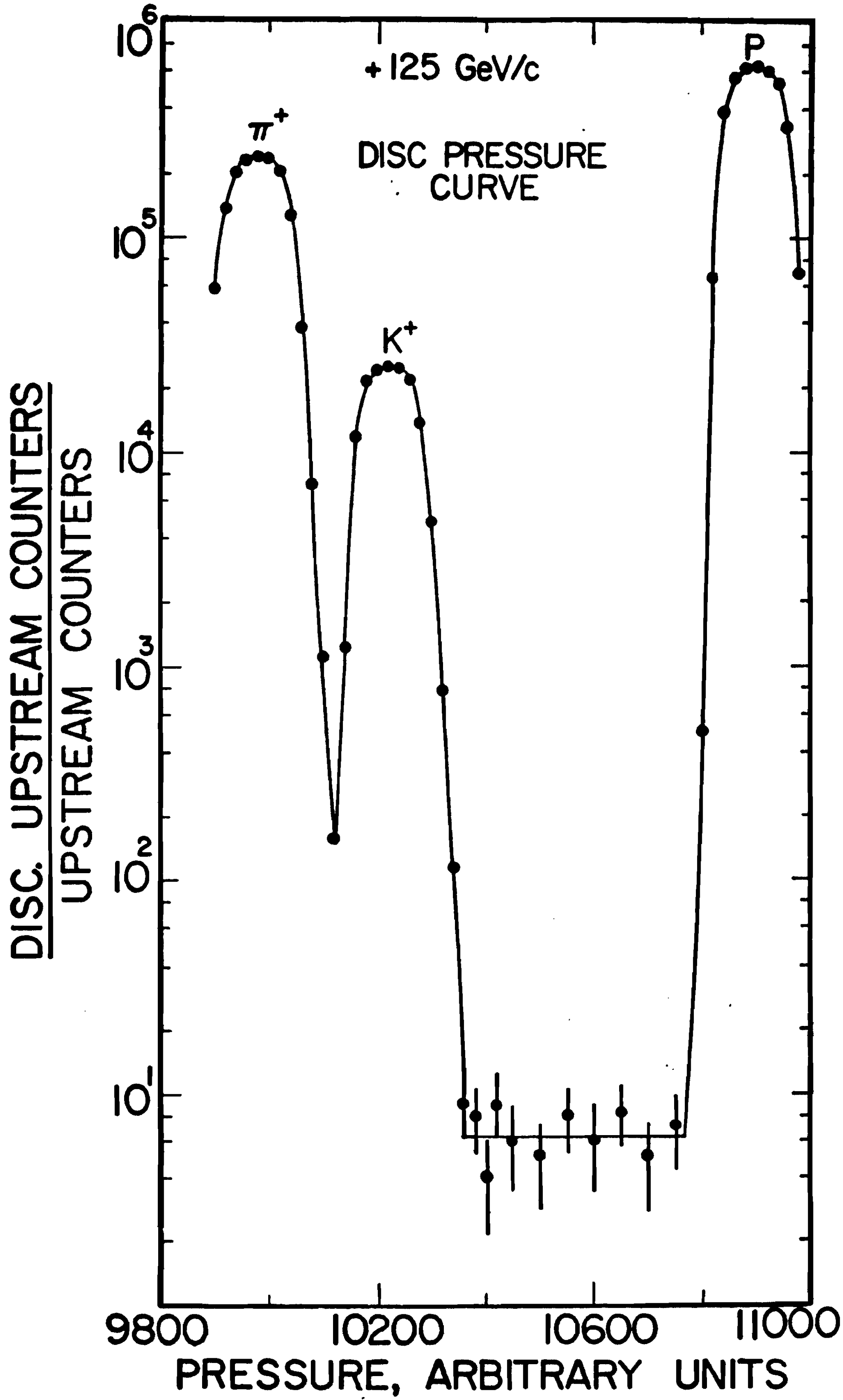
+125 GeV/c
DISC PRESSURE CURVE
π+
K+
P
DISC. UPSTREAM COUNTERS / UPSTREAM COUNTERS
10^6
10^5
10^4
10^3
10^2
10^1
9800
10200
10600
11000
PRESSURE, ARBITRARY UNITS

Figure 2.4

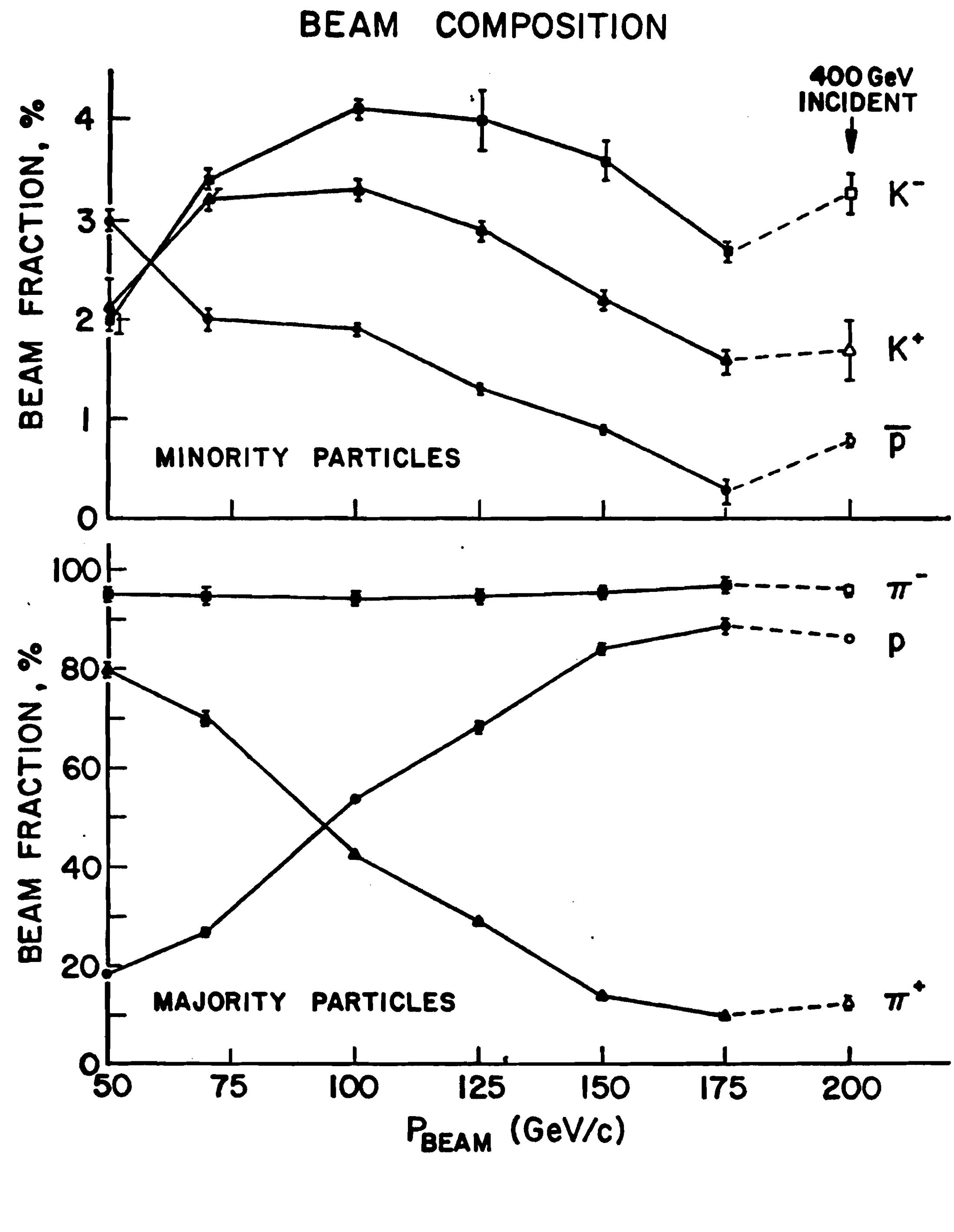
BEAM COMPOSITION
400 GeV
INCIDENT
BEAM FRACTION, %
4
3
2
1
0
K⁻
K⁺
p̄
MINORITY PARTICLES
100
80
60
40
20
0
π⁻
p
π⁺
MAJORITY PARTICLES
50
75
100
125
150
175
200
P_BEAM (GeV/c)

Detectors and Targets

Scintillation Counters

B1, B2, VH1, VH2, VH3, V1, and S (Fig. 2.1) were all scintillation counters. B1 and B2 defined the beam, while VH1 was a hole veto that removed beam halo. VH2 and VH3 were hole vetoes used to remove large angle secondary particles.

The beam was focused on V1 at the third focus: To first order a scattered particle missed V1. The different sizes of V1 are shown in Table 2.2 as a function of incident momentum. V1 was supported in an aluminum foil coated box and viewed via an air light guide (Fig. 2.5). The relative placement of V1 and the last magnet aperture projected to the veto plane is shown in Fig. 2.6.

Finally, the scintillator S subtended the full downstream aperture of the apparatus and defined a particle that had traversed its full length.

Liquid Hydrogen Target

The target assembly (Fig. 2.7) consisted of a mylar cylinder contained within a vacuum pipe. The liquid hydrogen was held in the cylinder which was 52.7 cm long and 4.4 cm in diameter. To minimize extraneous material near the LH_2 the vacuum pipe extended from just downstream of PWC station 2 to just upstream of station 3. The hydrogen pressure was kept at 15.5 ± 0.05 psia; the density of the liquid hydrogen was then 0.0705 ± 0.0008 gm/cm^3. In the analysis the atomic density, N, used was:

TABLE 2.2

Dimensions of V1

Momentum (GeV/c)	Vertical (mm)	Horizontal (mm)	Thickness (mm)
70	4.90	20.25	10.32
100 125 150	4.11	20.22	10.32
175 200	2.52	20.15	10.18

Figure 2.5

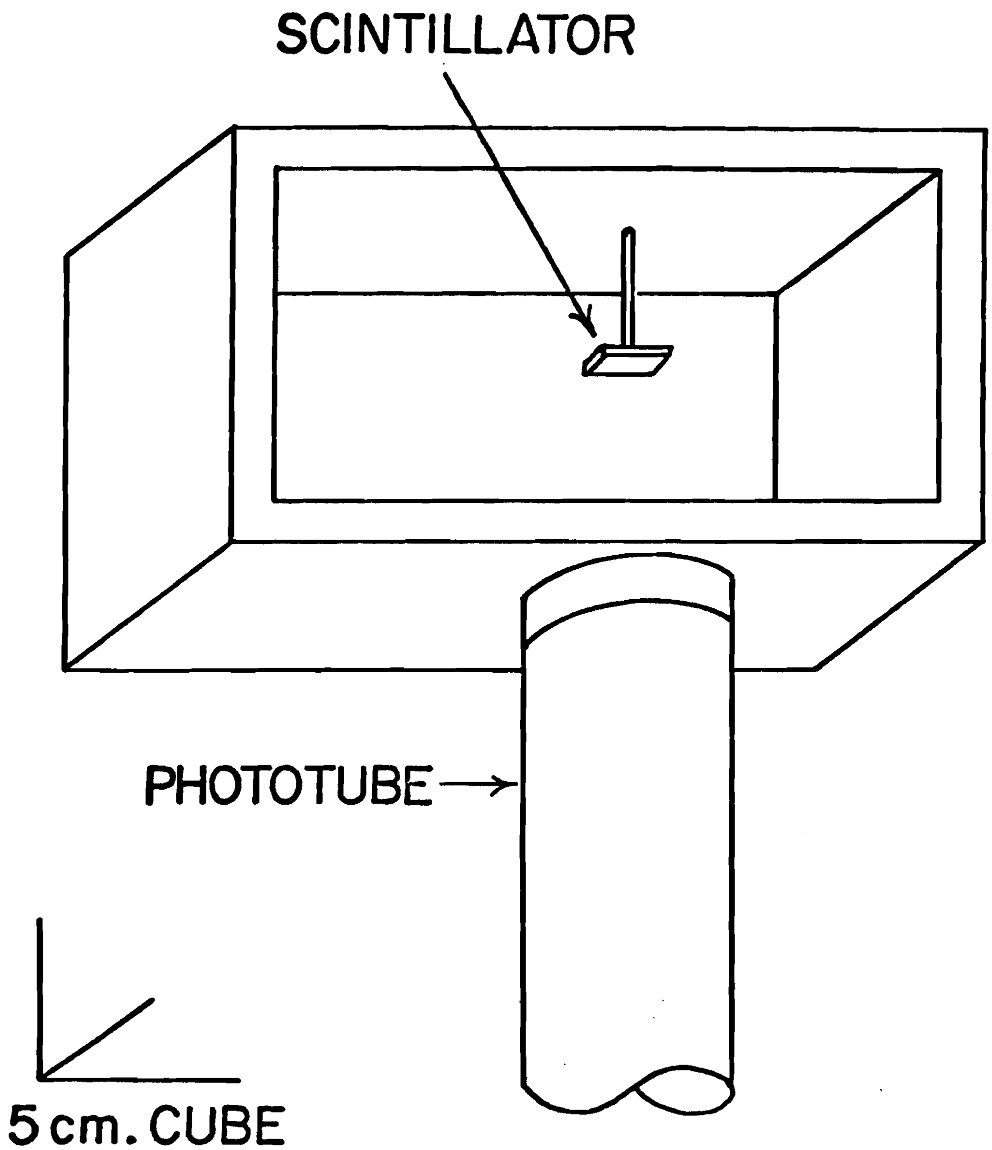

Figure 2.6

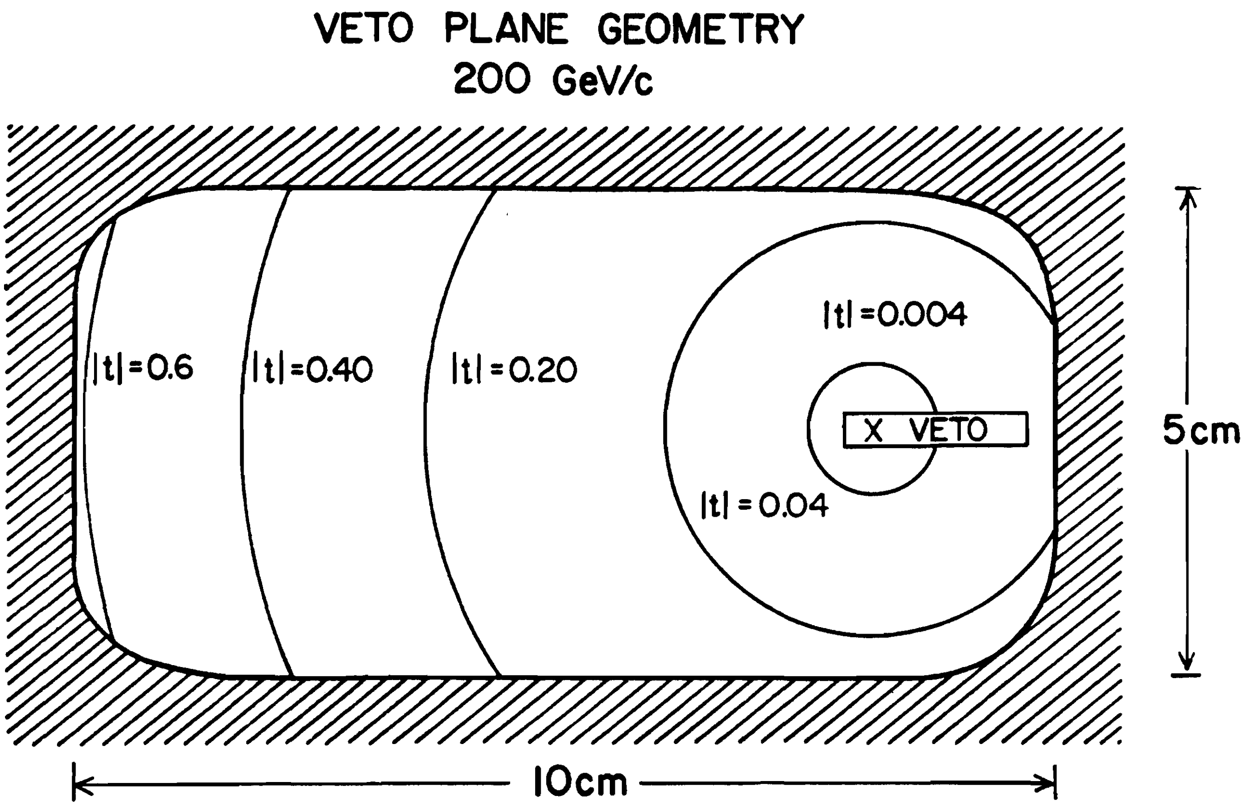
VETO PLANE GEOMETRY
200 GeV/c
|t|=0.6
|t|=0.40
|t|=0.20
|t|=0.004
|t|=0.04
X VETO
5cm
10cm

$N = 4.28 \times 10^{22}$ atoms/cm^3.

Two sets of carbon resistors in the liquid hydrogen monitored the liquid level. The target was emptied by using a small heat leak into the target to drive the hydrogen into a reservoir. The residual gas density was then estimated to vary from 4.4×10^{-4} to 0.9×10^{-4} gm/cm^3.

Recoil Detector

The recoil detector[2.6] as shown in Fig. 2.8 consisted of four U-shaped scintillation counters centered about the target. Its function was to help distinguish elastic from inelastic reactions. The outer two counters, RV1 and RV2, are 1 cm thick and 40.64 cm in length along the beam. A 1.0 cm thick lead plate was sandwiched between them and this combination was used to detect gamma rays from neutral pions produced in inelastic collisions. A recoil proton needed a kinetic energy of at least 150 MeV (corresponding to an elastic scatter with $-t = 0.281$ (GeV/c)^2) to reach RV2. The remaining parts of the detector were not used in the analysis of this experiment.

Electron Scattering Rejection

The recoil electron from a hadron-electron scatter is ejected in the forward direction for t range of interest. To detect these forward recoil electrons, two hole veto scintillation counter, VH2 and VH3, were located immediately upstream of PWC station 3. In addition the upstream face of VH2 was covered by a 1.0 cm lead sheet to detect gamma rays from π^0 decays. Both lead sheet and scintillator had 3.8 cm diameter holes. VH3 was downstream of VH2 and had an inner hole

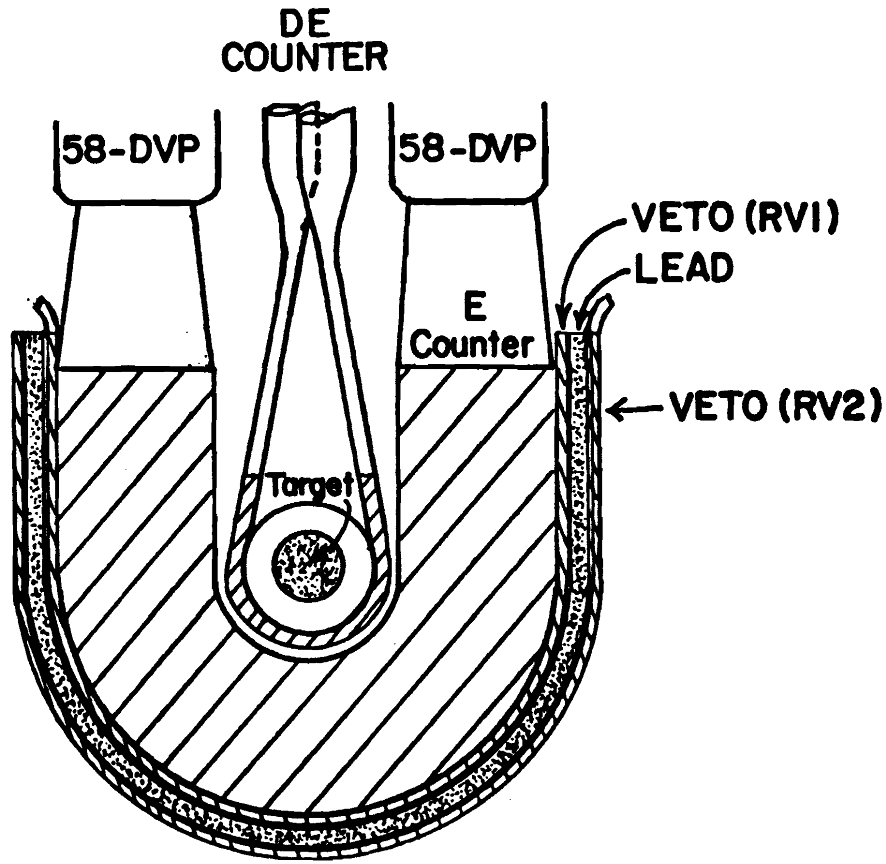

CROSS SECTION VIEW OF RECOIL DETECTOR

Figure 2.8

diameter of 2.5 cm.

Proportional Wire Chambers

All track position measurements were done by PWC's. In addition to the momentum tagging chamber at the second focus, there were six sets or stations of PWC's. Table 2.3 summarizes the chamber characteristics.

Stations 1 through 4 consisted of PWC planes with a wire spacing of 400 μm and an active area 1.5 cm in radius. These planes were assembled into pairs of planes (doublets) offset by a half wire spacing. The signals from the two planes of a doublet were interleaved by a special connector before being encoded. In Reference 2.7 the construction and testing of these high resolution, high pressure PWC's is detailed. Each plane had and efficiency of 99 ± 1% and the spatial resolution of a doublet was 70 μm standard deviation.

The PWC doublets in Stations 1 through 4 measured tracks in the horizontal (x) and vertical (y) directions. Station 3 also had PWC doublets rotated 45 and 135 degrees from the horizontal to measure the track position in the u and v directions. These four stations determined the scattering angle with an accuracy of 30.0 μrad.

Station 5 consisted of 1.5 mm wire spacing x and y PWC single planes and was located just downstream of the spectrometer magnets. This station was used primarily to monitor the beam position and size at the third focus. Station 6 at the end of the apparatus consisted of a pair of 2mm wire spacing PWC single planes. These planes were

TABLE 2.3

PROPORTIONAL WIRE CHAMBER CHARACTERISTICS

Chamber	High Voltage Plane	Signal Wire	Number of Wires	Wire Spacing (mm)	Gap[a] (mm)	Window Size
Momentum Tagging	25μm Al Foil	25μm W	64	1	8	8.2cm diameter
High Resolution[b] PWC's (Station 1-4)	25μm Al Foil	5μ Tungsten @ 4.6gm Tension	76	0.4	1	3cm diameter active area
Station 5 (x, y)	25μm Al Foil	25μm W	32	1.5	8	10.2cm diameter
Station 6[c]	75μm Cu Wire	25μm W	160	2.0	1.65	17.8 x 35.6cm rectangle

[a]Means distance between ground plane and signal plane.

[b]Data given for single plane. Chambers composed of doublet comprised of two singlets offset by 200μ and separated by 3.8cm.

[c]Data given for single plane. Chamber had two planes offset by 1mm.

staggered 1 mm to give an effective wire spacing of 1mm. Stations 3, 4, and 6 were used to determine the outgoing momentum.

The details of the PWC encoding and readout to the computer are described in Refrences 2.1 and 2.8.

Muon and Electron Calorimeters

Electrons were identified by a lead scintillator sandwich counter; muons by an iron-scintillator sandwich counter (Fig. 2.9). Each counter had two phototubes whose summed outputs gave a response indepedent of the particle position in the counter.

Energetic electrons in the beam would be identified as pions by the Cerenkov counters. This contamination was largest at 50 GeV/c; at this momentum the electron calorimeter distribution (Fig. 2.10) shows an energy deposition peak for the 'pions' but not for the protons. We identify this peak as electrons. At 50 GeV/c the electrons were 2.5% of the pions but at higher momenta they rapidly disappeared. Since electrons deposit all their energy in the electron calorimeter, they have none to deposit in the muon calorimeter. Thus a cut requiring that more than the minimum ionizing energy be deposited in the muon counter also removes the electron contamination.

Muons were produced not only in the Meson production target but also by pion and kaon decays in the beam line. A fraction of these decays occured in the liquid hydrogen target, simulating a scatter. This muon contamination was removed by requiring that more than the minimum ionization energy be deposited in the calorimeter. Figure 2.11

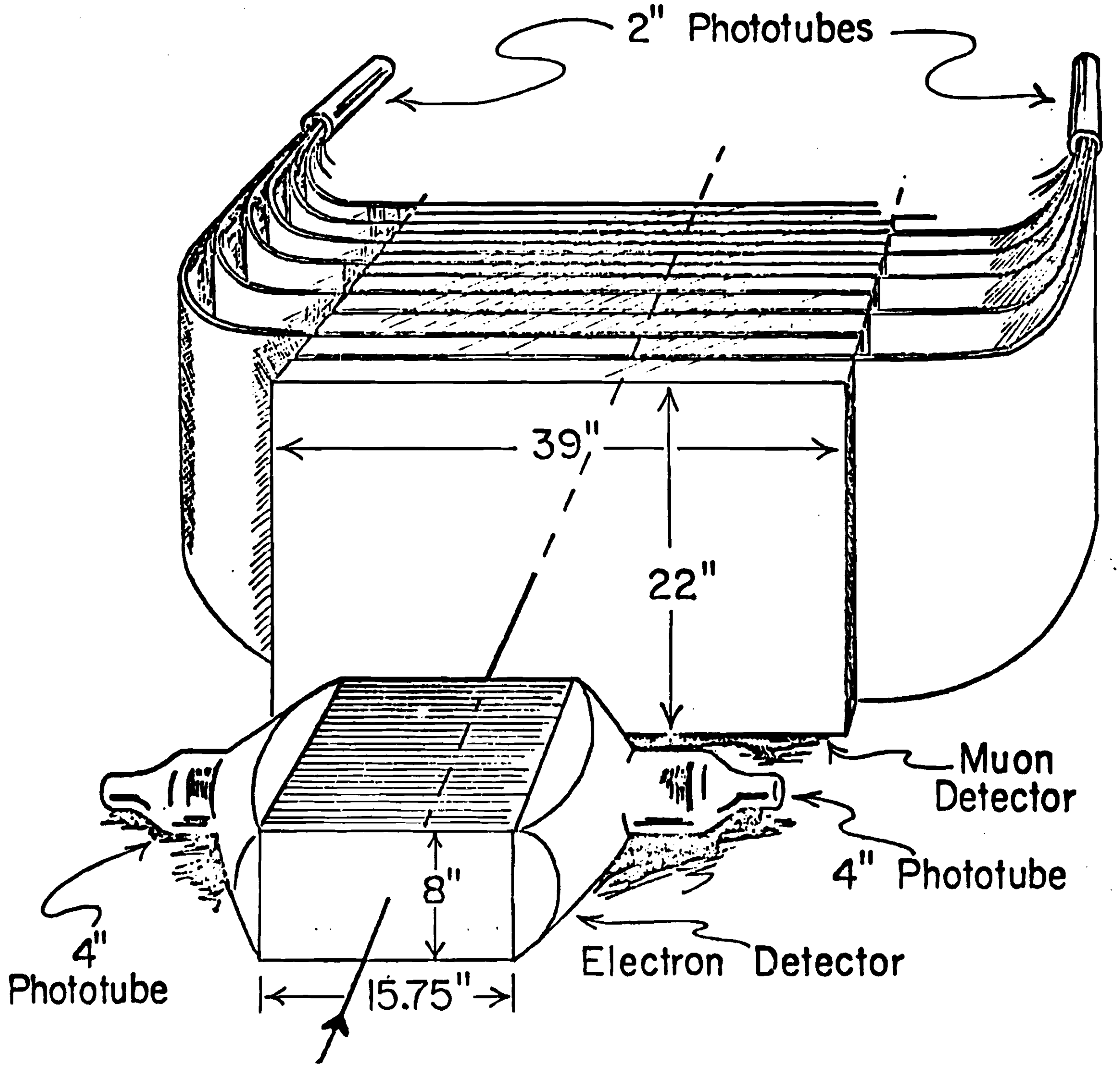
2" Phototubes
39"
22"
Muon Detector
4" Phototube
8"
4" Phototube
15.75"
Electron Detector

Figure 2.9

Figure 2.10

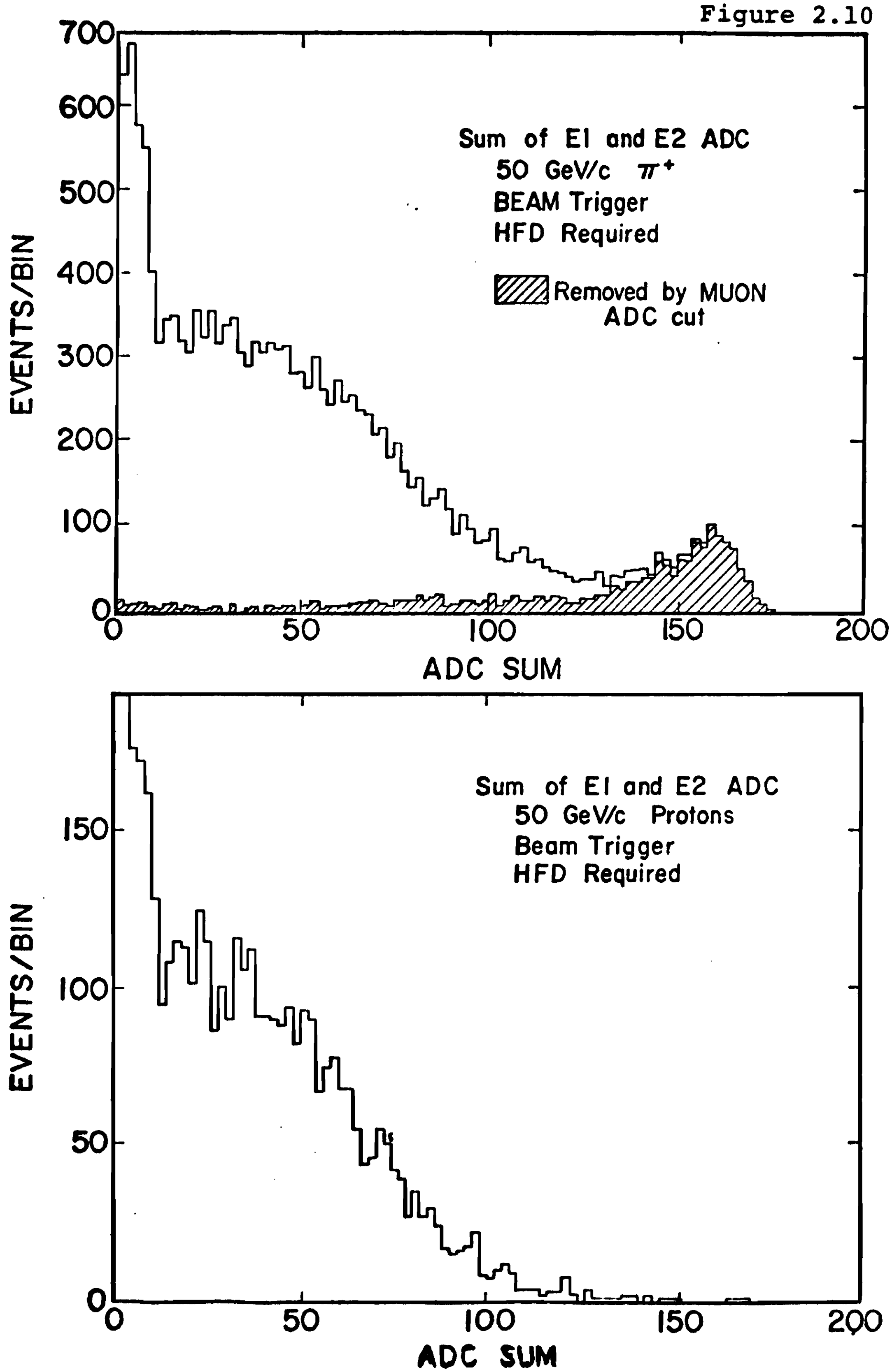
700
600
500
400
300
200
100
0
EVENTS/BIN
Sum of E1 and E2 ADC
50 GeV/c π^+
BEAM Trigger
HFD Required
Removed by MUON
ADC cut
0
50
100
150
200
ADC SUM
150
100
50
0
EVENTS/BIN
Sum of E1 and E2 ADC
50 GeV/c Protons
Beam Trigger
HFD Required
0
50
100
150
200
ADC SUM

Figure 2.11

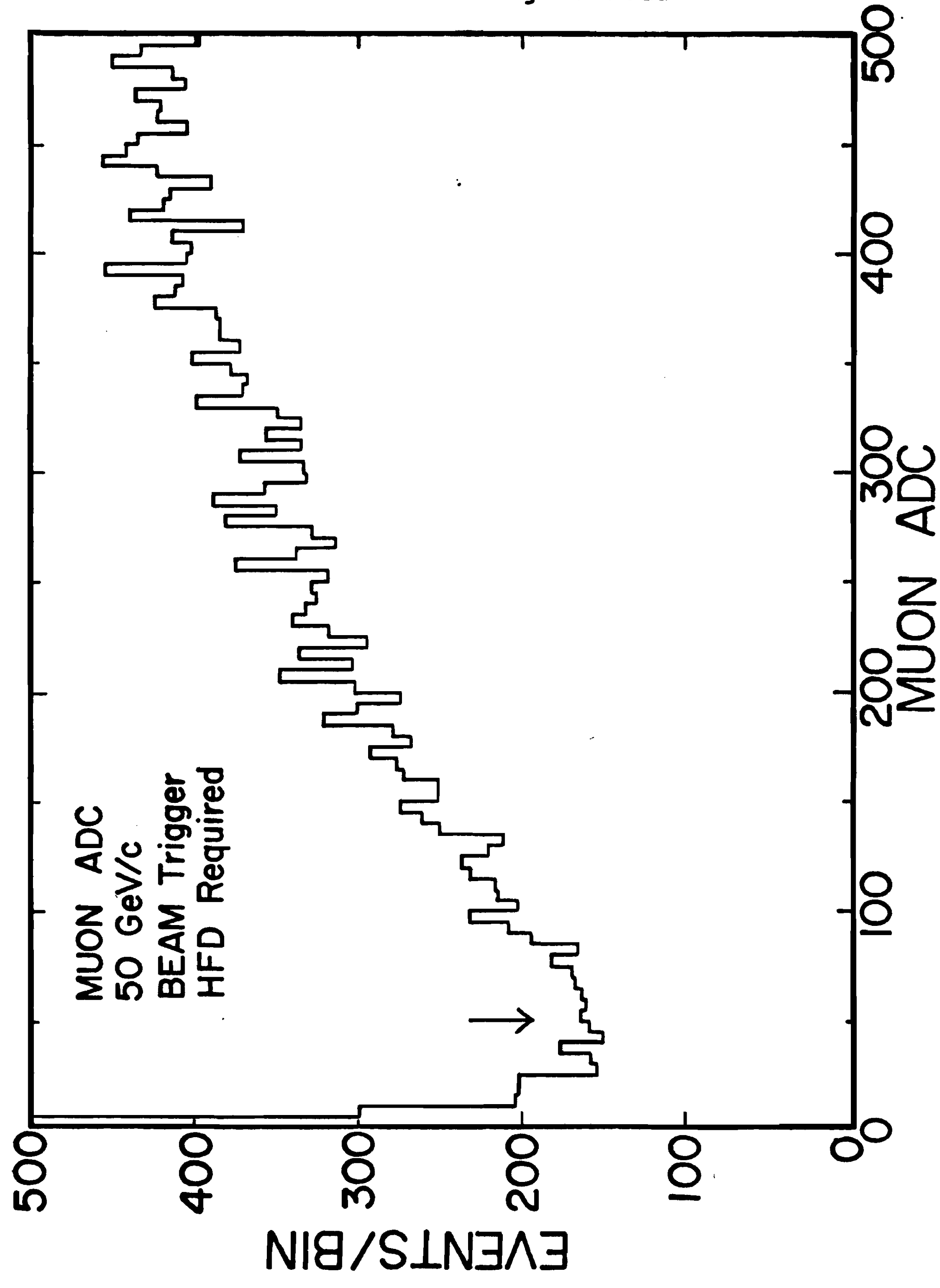
MUON ADC
50 GeV/c
BEAM Trigger
HFD Required
EVENTS/BIN
MUON ADC
0
100
200
300
400
500

shows the distribution in the muon calorimeter and the muon cut.

Spectrometer Magnets

The two spectrometer magnets were identical in design to the Fermilab main ring B2 dipole magnets. They had a 5 cm vertical by 10 cm horizontal aperture and a magnetic length, $\int B \cdot dl \,/\, B_{center}$, of 6.07 meters. A 670.5 cm by 1.0 cm single turn flip coil and a precision charge digitizer were used to map the field as a function of horizontal and vertical position with an accuracy of 0.01%. The upstream magnet had a maximum horizontal and vertical variation over the physical volume of 0.02% and 0.04%, respectively. The downstream magnet had no measurable variation.

During the experiment the field in both the upstream beam line magnets and in the spectrometer magnets were monitored by NMR probes located in two 0.91 m monitor magnets. The currents in the monitoring magnets were in series with the appropriate magnet string. The current in the spectrometer magnets was scaled such that at all momenta an unscattered beam particle was bent through an angle of 34.12 mrad. The magnetic fields were maintained to $\Delta B/B = 0.03\%$, σ .

CHAPTER 3

DATA ACQUISITION

Overview

The data collection logic involved a two level trigger. The first level used the scintillation counters to provide a fast trigger (400 nsec). The second level then required a good incident track and a minimum scattering angle. An analog device called the Hardware Scatter Focus Detector (HSFD)[3.1] performed the second level calculation in 5 μsec.

The three basic trigger types defined by the data acquisition logic were SCATTER, BEAM, and PSACVT. The SCATTER trigger (60% of the raw data) defined a single incident particle that scattered in the target region with a -t greater than 0.001 $(GeV/c)^2$ and produced a fast forward secondary that traversed the rest of the apparatus. The BEAM trigger (35% of the raw data events) was a sample of incident beam particles in the good beam phase space. The third trigger type, PSACVT, was used to study the systematics of the HSFD.

Scintillation Triggers

The first part of the various scintillation triggers involved the scintillation and Cerenkov counters upstream of the concrete block (Fig. 3.1). All three trigger types required a signal from JV and from CGT, where:

$$JV = SA \cdot SB \cdot \overline{H} \cdot \overline{H1} \cdot \overline{H2}$$

$$H = D + U + W + E$$

$$CTG = \text{Pion} + \text{Kaon} + \text{Proton}$$

The counters SA, SB, D, U, W, E, H1, and H2 were described in the last chapter. A signal from JV implied that the beam particle had a correct trajectory. A signal from CGT signified a positive particle identification. To balance the beam compostion (Fig. 2.4) in favor of the rarer particles, only one out of 2^n abundant particles was accepted. (This scaling varied from 2^1 to 2^5.)

Figure 3.2 exhibits the remaining part of the scintillation trigger system. A BEAM trigger is defined as

$$BEAM = B1 \cdot B2 \cdot \overline{VH1} \cdot \text{Beam Rationer} \cdot JV \cdot CTG$$

The beam rationer used signals from B1 to reject incident particles within 400 nsec of each other. A sample of BEAM triggers (one out of 2^m, where m was between 5 and 10) were recorded by the online computer, regardless of the particle's trajectory downstream of B1 and B2. This sample of recorded BEAM triggers were used to determine the normalization and the alignment and to study systematics of the apparatus.

BEAM INSTRUMENTATION AND PARTICLE IDENTIFICATION

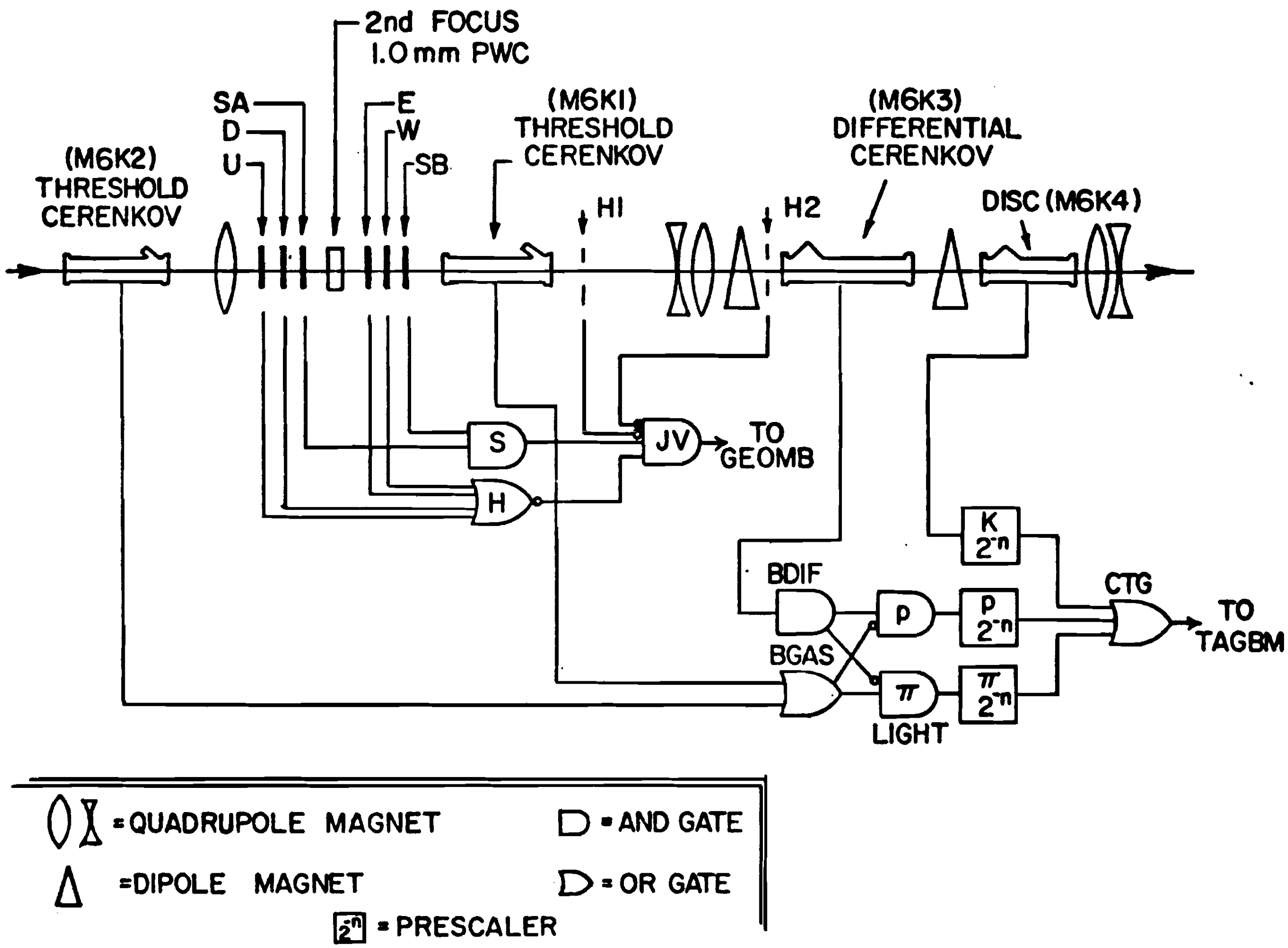

Figure 3.1

DATA COLLECTION LOGIC

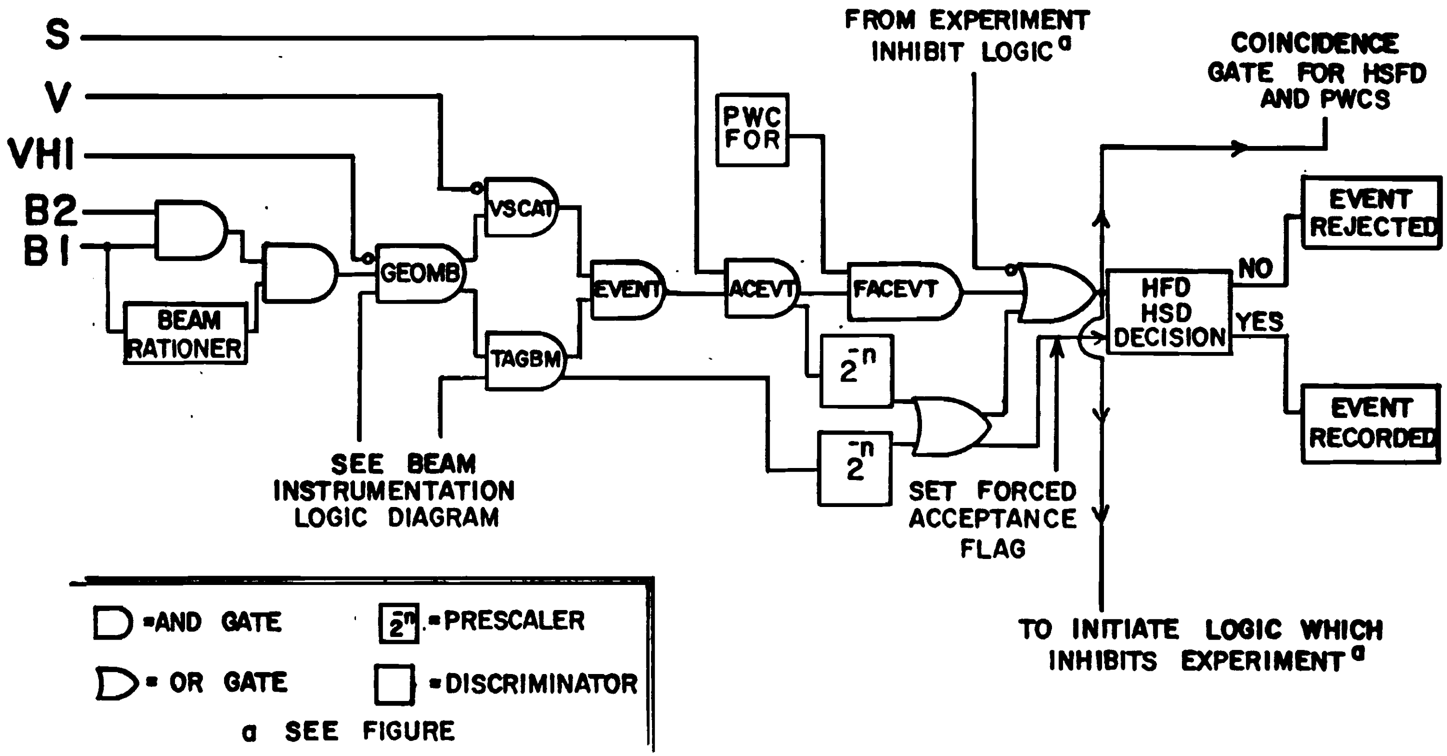

Figure 3.2

The scintillation trigger for a first level scatter, FACEVT, was

$$\text{FACEVT} = \text{BEAM} \cdot \overline{\text{V1}} \cdot \text{S} \cdot \text{PWCFOR} ,$$

where $\overline{\text{V1}}$ means that the particle missed the veto at the third focus, while a signal from S implied that the fast forward particle had traversed the entire length of the spectrometer. PWCFOR required the x and y chambers of stations 1, 2, and 4 had at least one coordinate.

Hardware Scatter/Focus Detector

Because of multiple scattering in the beam line only 95% of the beam could be focused onto V1. Since the elastic scattering rate was less than 0.5%, the 5% beam halo would have saturated our data handling capacity. The Hardware Scatter/Focus Detector used the track coordinates from PWC stations 1, 2, and 4 to perform two analog calculations, shown schematically in Fig. 3.3. Each calculation was made in both the horizontal (x) and vertical (y) directions.

The Hardware Focus Detector (HFD) calculation projected the incident track to the veto plane and required the track to be within a preset window, matched to the position of V1. If the horizontal (vertical) track projection was within the horizontal (vertical) window, then HFDX (HFDY) was set true. The HFD thus selected particles with tracks focused on the veto, V1, and reduced the possiblity of the HSD being fooled by a missing or spurious coordinate in stations 1 and 2.

The Hardware Scatter Detector (HSD) calculation projected the incident track to PWC station 4. If the projected coordinate and the

HFD and HSD Geometry

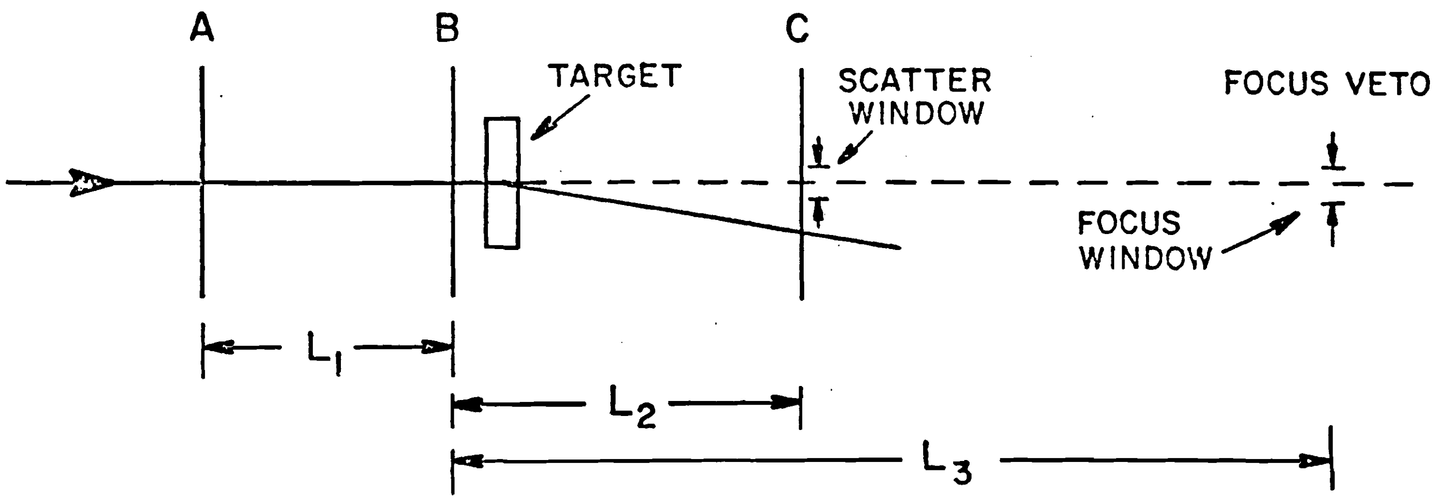

SCATTER: $\frac{L_2}{L_1} A + C - \left(\frac{L_1 + L_2}{L_1}\right) B$ > Scatter Window

FOCUS: $\frac{L_3}{L_1} A - \left(1 + \frac{L_3}{L_1}\right) B$ < Focus Window

Figure 3.3

actual coordinate differed by more than a fixed amount in the x (y) direction, then HSDX (HSDY) was set true. The preset amount corresponded to a -t of approximately 0.001 $(GeV/c)^2$.

To study possible biases of the HSFD, a sample of FACEVT triggers were recorded (PSACVT). This sample showed that no scatters with -t greater than the preset amount were rejected. In Figure 3.4 a sample of PSACVT events are shown; the shaded area are those events rejected by the HSD.

The trigger for a SCATTER events was then:

$$\text{SCATTER} = \text{FACEVT} \cdot (\text{HFDX} \cdot \text{HFDY}) \cdot (\text{HSDX} + \text{HSDY}).$$

Online Computer

A PDP15/40 computer[3.2] recorded the data and monitored the apparatus performance. The online program was designed primarily for speed in data acquisition and could read up to 800 events per one second spill. Two factors were instrumental in achieving this high rate.

First an economical event format was implemented. An event generated about thirty 18 bit words: 2 words of latch information, 6 words with 2 ADC's per word, and 22 words of encoded PWC hit locations. Second, a double buffer system filled one area of core with events, while another area was written onto a disk. In between spills these

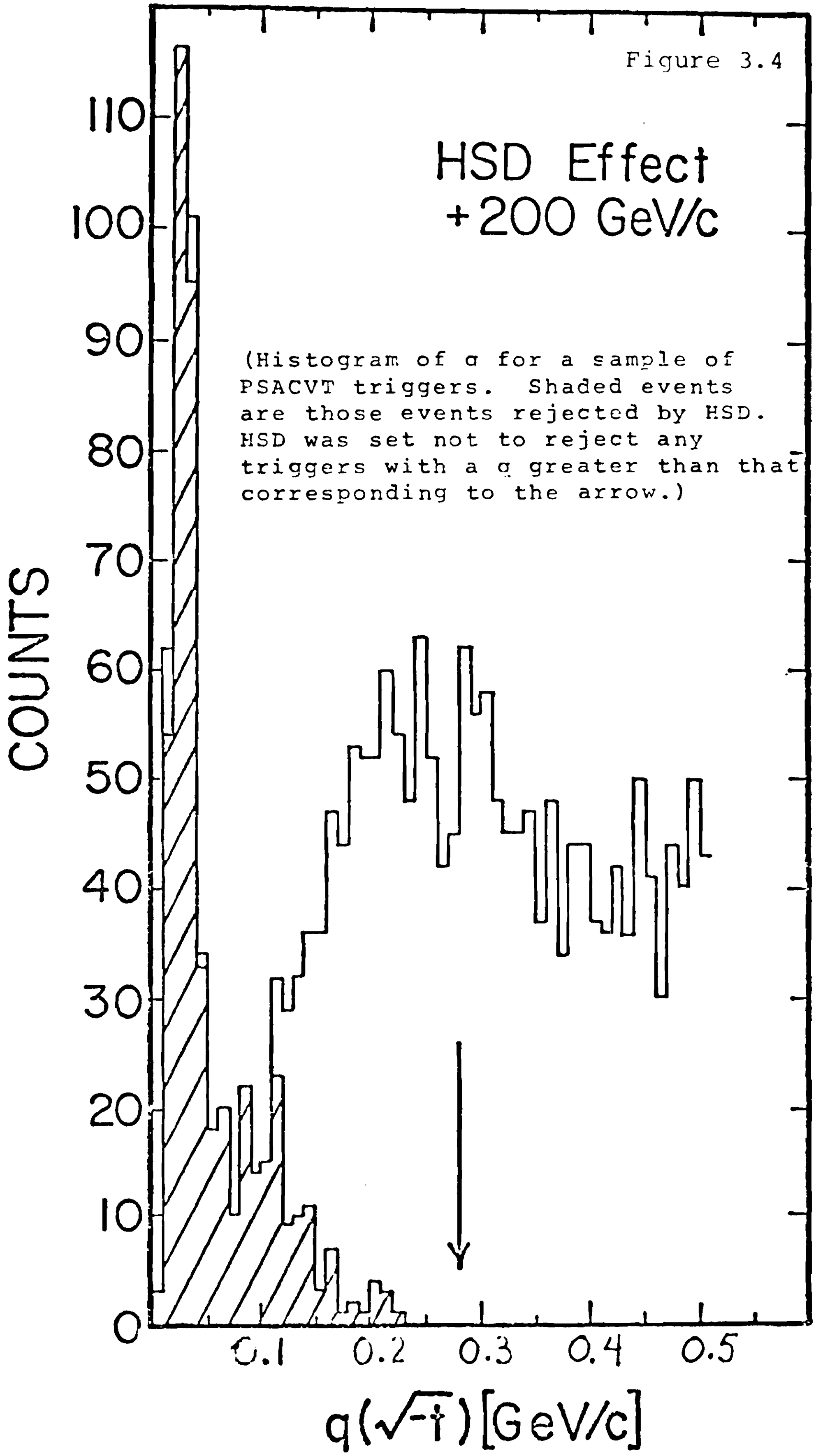

Figure 3.4

(Histogram of q for a sample of PSACVT triggers. Shaded events are those events rejected by HSD. HSD was set not to reject any triggers with a q greater than that corresponding to the arrow.)

records were transfered from disk to magnetic tape via the same buffers. The online monitoring was performed while the events were in these buffers.

The apparatus information was transferred to the computer via CAMAC modules. The PWC encoded information was stored in special word buffers with outputs to HSFD and which were read out by the computer. Standard CAMAC modules were used for scalers, ADC's and latch information. In addition, the computer read in periodically from a scanning digital voltmeter (DVM) values of various phototube voltages and of the LH_2 resistors.

In Table 3.1 we list the different latches read into the computer. Similarly in Table 3.2 the ADC's are listed. The PWC encoded word format is presented in Table 3.3.

To monitor the apparatus, the PDP15 generated histograms and scattergrams of the beam position, PWC efficiencies, latch and ADC distributions.

Trigger Rates

Under typical running conditions 500,000 particles per one second spill were incident upon the apparatus. In order to record as many of the rarer particles (K^+, K^-, $\overline{p}$) as possible, only a fraction of the abundant (π^+, π^-, p) incident particles were considered. Typically, the predominant particles were scaled until a live time of 60% was attained. The effective incident beam was then 40,000 particles per one second spill of which one out of 250 particles was recorded on tape

TABLE 3.1

Computer Latch Information

Latch	Latch
B1	HFDX (HFD in x plane)
STROBE (from beam rationer)	MGK2 (most upstream Cerenkov counter)
B2	HSDX (HSD in x plane)
JV	HSDY (HSD in y plane)
V1	BEAM
VH2	PSACVT
VH3	FACEVT
DISC[a]	HFDY (HFD in y plane)
RV1	VH1
RV2	FO1[b] (for x of PWC station 1)
S	FO2[b] (for y of PWC station 1)
LIGHT[a]	FO3[b] (for x of PWC station 2)
HEAVY[a]	FO4[b] (for y of PWC station 2)
BDIF[a]	FO9[b] (for x of PWC station 4)
BGAS[a]	FO10[b] (for y of PWC station 4)
V2	FOP[c]

[a] See Figure

[b] FOn on if PWC plane had a wire activated

[c] FOP on if any plane in PWC stations 1 and 2 had [illegible] 1 hit

TABLE 3.2

ADC Information (512 channels/ADC)

ADC

Muon Counter (sum of both phototubes)

TR R1 R2 R3 R4	Recoil Detector Scintillators (see Fig.)

Electron Counter A

Electron Counter B

HSDX
HSDY
HFDX
HFDY

TABLE 3.3 .

PWC Encoded Word Format

(18 bits per word)

Bits 1 - 8	corresponded to a group of eight wires. A bit was set to 1 when a signal was recieved from its appropriate wire. Otherwise, it was set to 0.
Bits 9 - 14	specified which group of eight wires.
Bits 15 - 17	were used for diagnostic purposes.
Bit 18	when set to 1, identified the first word from a PWC; when set to 0, it identified an additional word from that PWC.

A PWC word was generated for a group of 8 wires that contained at least one hit. If a PWC did not have any hits a word was generated with Bits 1 - 8 set to zero and with Bits 9 - 14 and Bit 18 set to 1.

as a BEAM event. The number of events that satisfied the first level of the scatter trigger was between 2000 and 4000 of which one out of 250 particles was recorded as a PSACVT event. The number of scatter triggers that passed the HSFD requirements was between 200 and 300 and all these events were recorded as SCATTER events.

CHAPTER 4

ANALYSIS

Overview

The task of the analysis was to reduce the data into a manageable form, to determine the efficiency of the apparatus, and to compare the data with theoretical models. This task was complicated by the large data sample and by the effects of resolution and multiple scattering. The massive 100 million raw data events written on 800 tapes forced the analysis to proceed in several steps as shown in Fig. 4.1. This procedure allowed the information per event to be reduced gradually and made practical iterative studies of the apparatus with increasing number of events. The analysis was done at the Fermilab Computer Center using either a CDC 6600 or a CDC Cyber 175 computer system.

The significant effects of multiple scattering and resolution near $-t = 0.0016\ (GeV/c)^2$ prompted the comparison between data and theory to be made by modifying the theory to include the effects of the apparatus. At their largest the sum of these corrections is between 4 and 6% near $-t = 0.0016\ (GeV/c)^2$. These corrections depend strongly on the t dependence of the differential cross section. The three contributions to the differential cross section, σ_C, σ_I, and σ_n, have corrections each with a different functional dependence on t. However, σ_I and σ_n have to be determined from the data. Assuming the

ANALYSIS

FLOW

CHART

Figure 4.1

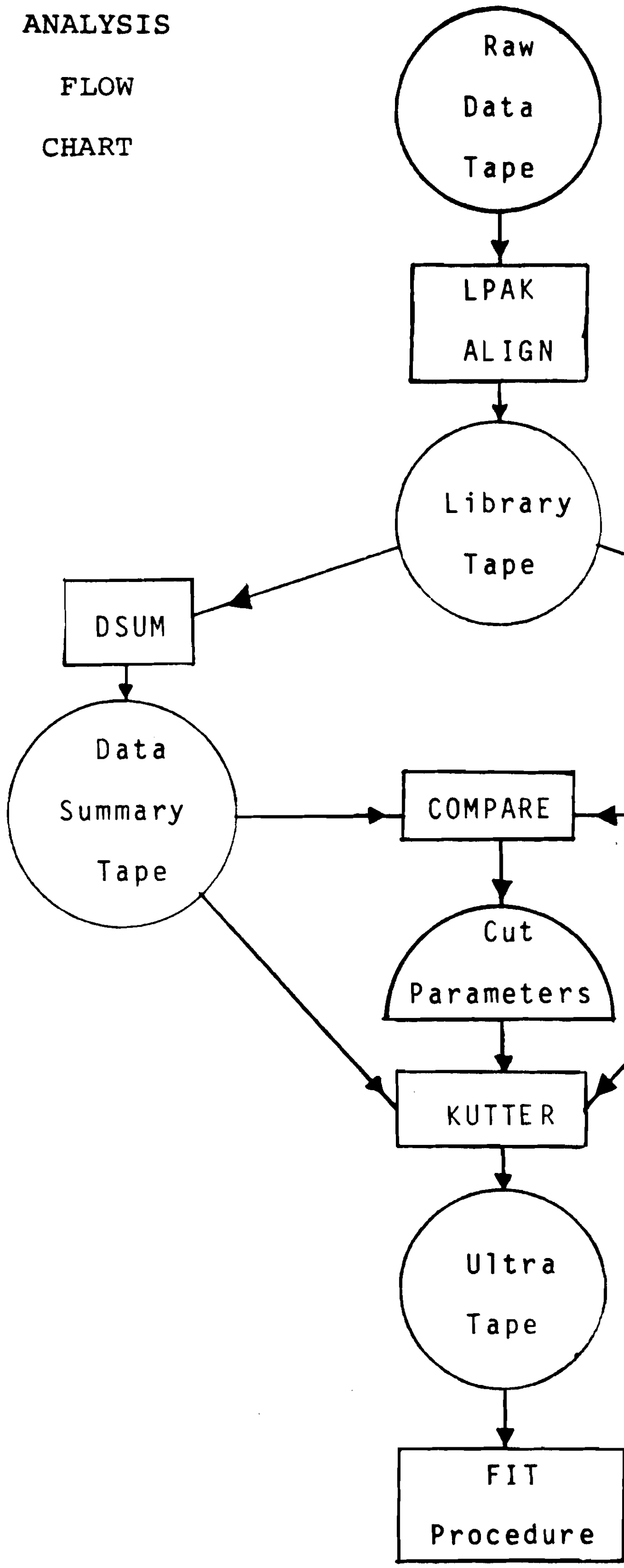

theoretical cross sections, Eqs. 1.6 and 1.7, the LH_2 multiple scattering corrections were found analytically. The resolution and acceptance corrections were then included numerically via a Monte Carlo simulation. The corrected theoretical cross sections were then fit to the data.

To facilitate the analysis, the variable q was used:

$$q = (-t)^{1/2} \simeq p_{beam}\,\theta$$

and

$$d\sigma/dq = -2 (-t)^{1/2} \; d\sigma/dt ,$$

where p_{beam} is the incident momentum. The horizontal and vertical projections of q were called q_x and q_y. There are two major reasons for this choice of variables. First the resolution of the apparatus was constant as a function of the scattering angle, θ . The large dynamic range of -t (0.0016 to 0.360 $(GeV/c)^2$ at 200 GeV/c) caused the resolution as a function of t to vary substantially (a factor of 14 at 200 GeV/c). However, since q is proportional to θ, the resolution is constant in q and the data could be subdivided in uniform q bins. Secondly, the cross section $d\sigma/dq$ versus q is a more slowly varying function than $d\sigma/dt$ versus t. Thus the binning of $d\sigma/dq$ populates the bins more uniformly. This reduces the sensitivity of the fitting to the integration over the bin and to the migration of events between bins due to resolution and multiple scattering. While the analysis was made using q and $d\sigma/dq$, for convenience we present our final results in terms of t and $d\sigma/dt$.

Library Tapes

The library tapes were produced by the programs LPAK and ALIGN (Fig. 4.1). LPAK deciphered the raw data tapes, rejected events with insufficient track information, and packed the event data in a convenient format. Using a subsample of these events, ALIGN determined the relative spatial positions of the PWC's. The PWC coordinates, latches, ADC's, DVM information, and alignment parameters were written on 150 library tapes.

LPAK

The events of interest in this experiment consisted of sampled beam tracks and small angle elastic scatters. The events have only one track throughout the apparatus. Thus the first task of LPAK was to look for one unambiguous coordinate in each PWC. In Table 4.1 the PWC's are defined. The algorithm used by LPAK to determine a coordinate is a function of the number of clusters and their pattern. A cluster is a group of adjacent struck wires. This algorithm is specified in Table 4.2. PWC's 11 through 15 are single planes with no redundancy; their algorithm requires one and only one cluster of 3 wires or less.

The algorithm for the high resolution, high pressure PWC's (1 through 10) incorporates the redundancy of having two physical planes and allows 90% of the raw events to be reconstructed. In any given doublet 97% of the events had a single unambiguous cluster, such that the position of the track was known to within a wire spacing. The distribution of unambiguous clusters (as defined in Table 4.2a)in a

TABLE 4.1

PWC Definitions Used in the Analysis

PWC Number	Description[a]
1	x, Station 1
2	y, Station 1
3	x, Station 2
4	y, Station 2
5	x, Station 3
6	y, Station 3
7	u, Station 3
8	v, Station 3
9	x, Station 4
10	y, Station 4
11	x, Station 5
12	y, Station 5
13	x, Station 6
14	x, Station 6
15	Momentum Tagging

[a]See Chapter 2 for a detailed description of the PWC's.

TABLE 4.2a

Principal PWC Cluster Types

Cluster Type Number	Wire Map[a]
1	1 0 1 0 1 0 1
2	1 0 1 0 1
3	$1\ \underset{\star}{0}\ 1$
4	$\underset{\star}{1}$
5	$1_{\star}1$
6	$1\ \underset{\star}{1}\ 1$
7	$1_{\star}1\ 0\ 1$ or $1\ 0\ 1_{\star}1$

[a]This map gives the pattern of PWC wires hit. For the high resolution doublet planes (PWC's 1 -10) the wire spacing is 200 μm. The coordinate position is assigned in units of half wire spacings and are indicated for the valid clusters with an asterisk.

TABLE 4.2b

Valid PWC Cluster Types

PWC Plane	Cluster Type
1 - 10: Single hit	3, 4, 5, 6, 7
1 - 10: Multiple hits	5, 6, 7
11 - 15: All hits	3, 4, 5, 6

doublet was as follows:

1. 70% - The cluster had one wire hit in each plane of a pair. This configuration is called a type 5 cluster.

2. 20% - The cluster had one hit in one plane and the two adjacent wires hit in the other plane. This is a type 6 cluster.

3. 5% - The cluster had one hit in one plane and no hits in the other plane. This is a type 4 cluster.

4. 2% - The cluster had two adjacent wires hit in one plane and no hits in the other plane. This is a type 3 cluster.

The remaining 3% had either no hits or multiple clusters. Since the PWC's were uncorrelated, this implies that 50% of all the events would have been lost outright. Of these 3%, however, 2/3 had multiple clusters that could be salvaged. Track matching studies using the four PWC's of station 3 revealed that clusters with hits in only one plane could be ignored when there was a cluster elsewhere in the doublet with hits in both planes. We believe these one-plane clusters were delta rays emitted perpendicular to the incident track such that they appear in only one plane. The angular resolution of events with salvaged clusters was the same as that of normal events. In Table 4.2b the valid cluster types are specified for all the PWC's.

The PWC resolution, $\sigma_{R,C}$ depended on the cluster type and on the angle of the track. We found that $\sigma_{R,C}$ could be written as

$$\sigma_{R,C} = (W_{R,C}^{2} / 12) + (L_{R}^{2} / 2)\ \theta_{R}^{2} \quad , \tag{4.1}$$

where θ_R is the angle of the track to the perpendicular of the PWC plane, L_R is the effective separation between doublet planes, and $W_{R,C}$ is the effective wire spacing. For PWC's 1 through 10 we measured the following values:

L_R = 3.35 ± 0.14 cm

$W_{R,C}$ = 0.180 ± 0.001 mm for cluster type 5

= 0.106 ± 0.015 mm for cluster type 6

The quantity L_R is in reasonable agreement with the actual separation between planes of 3.0 cm. Similarly $W_{R,C}$ for cluster type 5 reflects the actual wire spacing of the staggered pair of 0.2 mm. $W_{R,C}$ for cluster type 6 is indicative of the small region where a track will activate two adjacent wires on a plane. Since the resolution of PWC's 11 through 15 is not critical, we approximated their resolution as their actual wire spacing divided by 3.46. These resolution functions were used in the Monte Carlo simulation.

Once the coordinate assignment was completed, LPAK required that the event had enough information to reconstruct the track throughout the apparatus. The criteria was as follows:

1. One unambiguous coordinate in each of PWC's 1, 2, 3, 4, 9, 10,and 15

2. At least two unambiguous coordinates from PWC's 5, 6, 7, and 8

3. At least one unambiguous coordinate from either PWC 13 or 14.

If the event satisfied the above criteria, LPAK would then write the following onto the library tape:

1. Latches

2. ADC's

3. For each PWC

   a. the coordinate expressed in units of half wire spacing

   b. a bit indicating a valid coordinate (needed only for planes 5, 6, 7, 8, 13, and 14)

   c. the cluster type

   d. the cluster multiplicity

LPAK also wrote bookkeepping information, DVM readouts, and computer scaler totals for each spill.

ALIGN

The elements of the apparatus were surveyed into position with a precision of a few millimeters. However, the precise determination of t requires a spatial precision of a few microns. The great majority of BEAM events were essentially unaffected by their passage througth the apparatus. Thus they were used by ALIGN to determine the relative spatial position of the PWC's. ALIGN used only BEAM triggers that had:

1. one coordinate in each PWC (1 through 15)

2. no significant scatter in the apparatus

The major drawback of the beamline was its inability to transport the beam to station 6 with no magnetic field in the spectrometer magnets. Thus the determination of the position of PWC's 13 and 14 relative to PWC's 1 through 10 depended on the incident momentum and the magnetic field of the spectrometer magnets. By using the pressure separations between pions, kaons, and protons in the very precise M6K4[2.5] Cerenkov counter (see Figs. 2.1-2.3), the central value of the beam momentum was checked. In Table 4.3 the central momentum and per cent error used in the analysis are presented.

ALIGN first assigned the central beam momentum to the center of the beam distribution in the momentum tagging PWC at the dispersed second focus. Next, straight lines were fit in each projection, x (horizontal) and y (vertical), to the hits in the x and y PWC's of stations 1 through 4. These lines were then projected to the u and v PWC's of station 3. The projection to PWC's 11 through 14 was made by tracking through the uniform magnetic fields of the spectrometer magnets.

A residual is defined as the difference between the fitted track and the coordinate at that PWC. To remove BEAM tracks that underwent a large angle scatter, each residual had to be within 1.732 standard deviations of the residual distribution for that particular PWC. If all the residuals of a track were within those limits, the residuals for each PWC were averaged to give the shift of the PWC center. The center of the x and y PWC's of station 1 were defined as the origin of the coordinate system and were kept fixed. The current regulators of the beamline magnets were only stable to one per cent. Since a change in the spectrometer magnetic field could not be distinguished from a

TABLE 4.3

Momenta Used in the Analysis

Nominal Momentum (GeV/c)	Beam Momentum (GeV/c)	Momentum Uncertainty ($\Delta p/p$)
70	70.00	0.0036
100	100.00	0.0030
125	124.77	0.0016
150	151.44	0.0033
175	174.33	0.0037
200	200.80	0.0038

shift in the position of station 6, the residuals of station 6 were used to adjust the magnetic field and the chamber position remained fixed to its initial value. The initial position of station 6 was determined by using the first run at a momentum setting, fixing the spectrometer magnetic field to its nominal value and allowing the position of station 6 to vary.

Because of the statistical power of the experiment, the above procedure had to be applied in a particular way to avoid systematic effects. Each run (usually one raw data tape containing 250,000 events) had its own alignment parameters. To obtain finely tuned parameters throughout the run, groups of 500 good BEAM events at the beginning of the run were used to give starting values. Then, starting over at the beginning of the run, parameters were determined every 1000 to 3000 good BEAM events. The values for the 8 to 10 segments of the run were averaged to give the alignment parameters for the entire run. This procedure was quite succesful in giving parameters constant within a run and in between runs. Table 4.4 lists for different momenta (the beam charge sign was positive) the average values q_x and q_y (the x and y projected scattering angle) and the square of the recoil mass:

$$m_r^2 = t + m_p^2 + 2m_p \text{ (momentum in - momentum out)}$$

for a large sample of beam events. We see that the scattering angle distributions are centered at 0 to better than 1 μradian and the recoil mass agrees with the proton mass squared to better than 0.005 $(\mathrm{GeV}/c)^2$.

The widths of the distribuitons of q_x, q_y and m_r^2 for BEAM events provide a measure of the resolution in scattering angle and recoil mass

TABLE 4.4

Results of Alignment Procedure[a]

Momentum (GeV/c)	$\langle q_x \rangle$ (Mev/c)	$\langle q_y \rangle$ (Mev/c)	$\langle m_r^2 \rangle$ $(GeV/c)^2$	Number[b] of BEAM Events
70	0.055	0.020	0.883	238,600
100	-0.057	-0.016	0.884	250,000
125	0.011	-0.004	0.882	144,400
150	-0.092	-0.006	0.884	276,700
175	-0.035	0.012	0.881	143,700
200	-0.024	-0.042	0.884	52,400

[a]Distributions are truncated at 4 standard deviations.

[b]Approximately 1/4 to 1/3 of the total sample at that momenta and beam charge were used.

achieved by the apparatus. The standard deviations of the same samples of BEAM triggers listed in Table 4.4 are plotted versus incident momentum in Figs. 4.2a,b. Estimates of the main contributions to the resolution, the PWC resolution and multiple scattering, are indicated. The PWC contribution is represented by a band, since, as discussed above, the PWC resolution is a function of cluster type and the angle of the incident track. Since BEAM triggers pass through the veto counter but SCATTER triggers do not, the m_r^2 distribution for SCATTER events is slightly narrower than shown in Fig. 4.2b.

Another contribution to the momentum resolution which has not been included in the curves is intra spill ripple of magnet power supplies. This ripple can affect both the spectrometer field and the dispersion at the second focus. We corrected for such effects in the Monte Carlo by smearing the incoming momentum by a small amount (0.05% at 200 GeV/c; .07% at 70 GeV/c) in order to give agreement between the Monte Carlo and the data in the recoil mass squared distribution.

Summary Tapes

By recording only a few kinematic and geometric quantities for events that passed a latch cut, the library tapes were reduced to 75 data summary tapes. In parallel 75 Monte Carlo summary tapes were generated from the library tapes to simulate the apparatus acceptance and resolution effects. These summary tapes were used to determine the cuts to be applied to both data and Monte Carlo events.

Figure 4.2

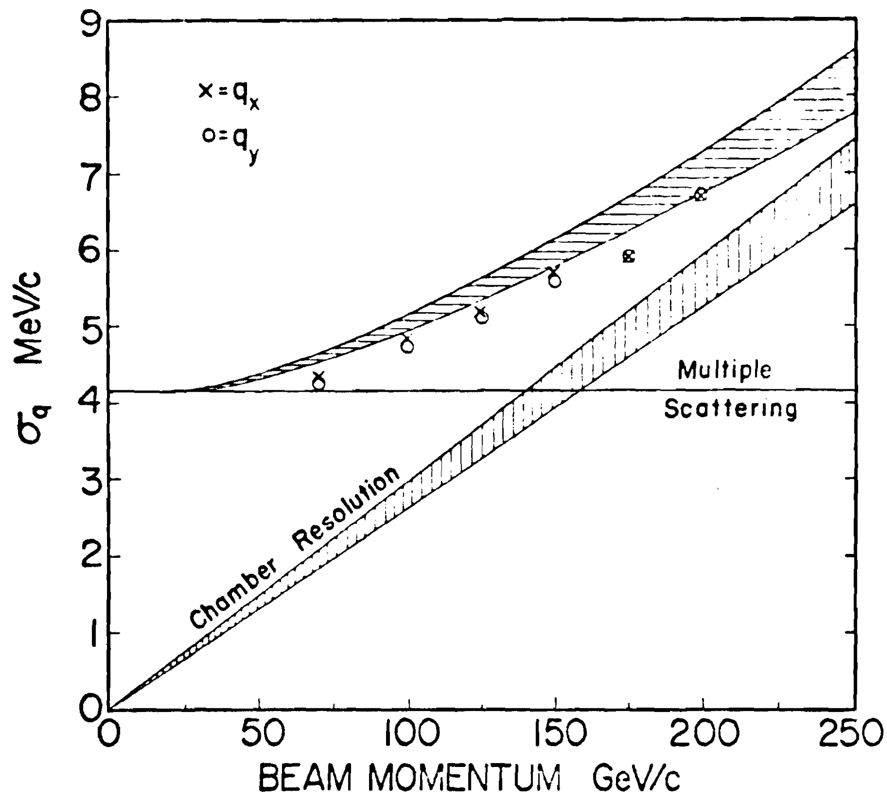
x = q_x
o = q_y
σ_q MeV/c
Multiple Scattering
Chamber Resolution
BEAM MOMENTUM GeV/c
0
1
2
3
4
5
6
7
8
9
0
50
100
150
200
250

(a)

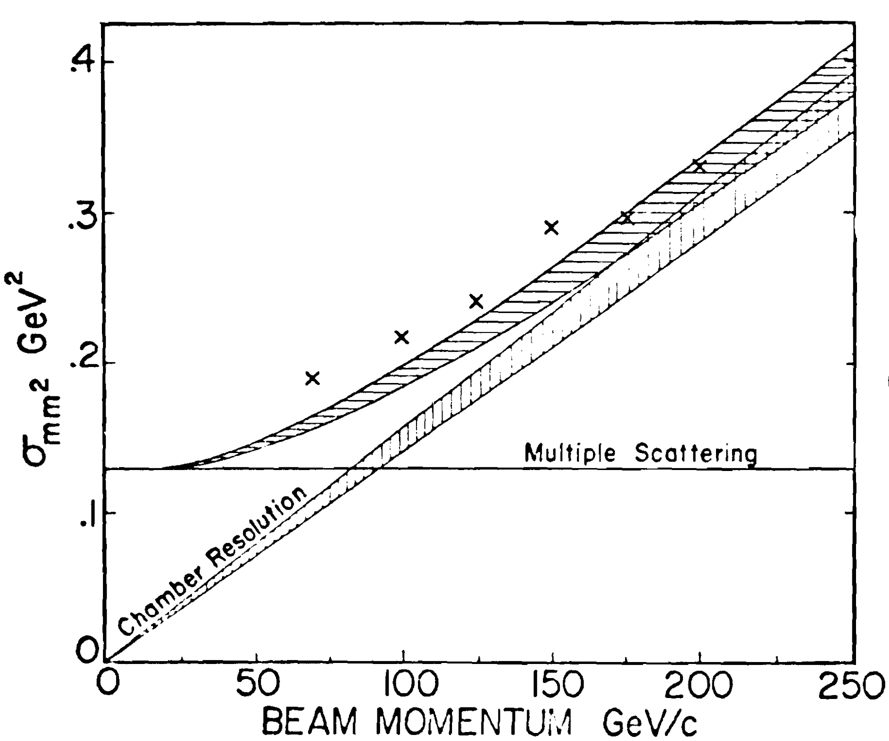
σ_{mm^2} GeV^2
Multiple Scattering
Chamber Resolution
BEAM MOMENTUM GeV/c
0
.1
.2
.3
.4
0
50
100
150
200
250

(b)

DSUM

The program DSUM used the library tapes and alignment prameters to produce the data summary tapes. The only requirement on an event was for the following latches to be set;

B1, STROBE, B2, JV, F01, F02, F03, F04, F09, F010, $\overline{\mathrm{FOR}}$, $\overline{\mathrm{VHI}}$

(where F0n refers to the fast or from PWC plane n). This latch cut requires the BEAM events to have passed the same requirements (in beam phase space and PWC efficiencies) as SCATTER events which have this latch cut in their trigger. For events that passed the latch cut the geometric and kinematic quantities in Table 4.5 were written on the data summary tape.

CSUM

The objectives of the Monte Carlo program, CSUM, were twofold: 1) to simulate the geometric efficiency of the apparatus apertures and 2) to simulate the finite resolution of the PWC's and multiple scattering outside of the target.

BEAM events that had B1, JV, STROBE, B2, S1, HFDX, HFDY, $\overline{\mathrm{VHI}}$ and $\overline{\mathrm{FOR}}$ latches set came from the same beam phase space as SCATTER events. Each of these BEAM events was used 10 times to provide initial track coordinates. These coordinates were made random to within a half wire spacing each time.

The interaction in the liquid hydrogen target was simulated by generating a flat random $q_{generated}$ distribution, such that the θ

TABLE 4.5

Event Quantities Written onto Data Summary Tapes

	Description
1.	q of scatter
2.	θ_x, θ_y projections of scattering angle
3.	ϕ , azimuthal angle of scatter
4.	m_r^2, missing mass squared
5.	z_v, distance along beam where scatter occured
6.	x, y at PWC Station 4
7.	x, y at Veto Plane (See Table 2.1)
8.	x, y at PWC Station 6
9.	PWC status word
10.	Muon ADC
11.	Latch information: Particle type, BEAM, SCATTER, PSCAVT, VH2, VH3, RV1, RV2, HSDX, HSDY, and V1.

distribution was flat between 0. and 5. mrad and the ϕ distribution was flat between $-\pi$ and π. These variables are related as follows:

$$\theta_x = \theta \cos\phi$$

$$\theta_y = \theta \sin\phi$$

$$q_{generated} = p_{beam} \left[\theta_x^{\,2} + \theta_y^{\,2} \right]^{1/2} \quad .$$

Since all SCATTER events traverse the full length of the target, no absorbtion correction as a function of z_v the longitudinal position of the scattering vertex, is needed. Thus the z_v position was generated with a flat random distribution extending past the physical limits of the target. This slightly longer length allowed corrections to the z_v distribution to be made as the physical limits of the target were better determined.

This track was propagated through the apparatus such that at stations 2, 3 and 4 the track suffered small deflections due to multiple scattering. These small angular deflections were generated with a random gaussian distribution of a width appropriate to the amount of material in that station. The track was required to be within apertures slightly larger than the physical apertures. No veto cut was applied at this time. Events that did not meet these loose requirements were removed from further consideration.

CSUM next simulated the PWC resolution by generating measured track coordinates at each PWC. The measured track coordinates were distributed about the generated track coordinates by a random gaussian distribution with a standard deviation, $\sigma_{R,C}$ (Eq. 4.1). The cluster type used in the simulation was that of each BEAM track used at each PWC. The same subroutine that calculated the geometric and kinematic quantities for the data events was used to reconstruct the Monte Carlo events from the 'measured' tracks. The generated and 'measured' quantities listed in Table 4.6 were then written on the Monte Carlo summary tape.

Cut Parameters

The geometric and kinematic cuts to be applied to both data and Monte Carlo events were determined by iteration. Using the data summary tapes cut parameters were obtained. The program COMPARE (Fig. 4.1) applied these first rough cuts (also later on the more refined cuts were also used) to both data and Monte Carlo events. Histograms for the majority particles were made for both data and Monte Carlo events. The Monte Carlo events were weighted by the appropriate cross section. The distribution of all geometric and kinematic quantities on the summary tapes were then compared to verify that data and Monte Carlo events had matching distributions in all quantities. This procedure allowed fine tuning of the cuts.

We now give a detailed description of the cuts used in the analysis. Cuts 1 and 2 were applied only to the data; cuts 3 through 9 to the data and the measured quantities of the Monte Carlo; cuts 10 through 12 to only the generated quantities of the Monte Carlo. The cuts 1 through 12 form the basic set of cuts and are used to determine the final distribution of the data and Monte Carlo. Cuts 13 through 17 were used to test the sensitivity of the results to the basic cuts.

TABLE 4.6

Event Quantities Written onto Monte Carlo Summary Tapes

A. Generated Quantities

1. initial q of scatter
2. z_v, initial position of scatter
3. initial x, y at veto plane

B. Reconstructed Quantities (PWC resolution included)

1. reconstructed q of scatter
2. θ_x, θ_y of scatter
3. z_v
4. x, y at PWC Station 4
5. x, y at veto plane
6. x, y at PWC Station 6

The cuts are as follow:

Data only

1. LATCH CUT. The final latch cuts on the data events required HSDX, HSDY, $\overline{VH2}$, $\overline{VH3}$, $\overline{RV1}$, $\overline{RV2}$ and $\overline{V1}$. $\overline{VH1}$ and $\overline{VH2}$ remove events that scattered off electrons. The $\overline{RV1}$ and $\overline{RV2}$ was applied to remove inelastic scatters. This cut is applied only if $-t < .15$ $(GeV/c)^2$, since an elastic scatter with $t > .2$ $(GeV/c)^2$ would impart sufficient energy to the recoil proton to traverse the full depth of the recoil detector.

2. MUON CUT. The electron and muon contamination was removed by requiring the summed output of the muon calorimeter to be greater than MUON. A typical calorimeter distribution is shown in Fig. 2.11. The peak at the low end corresponds to minimum ionizing muons and electrons that have deposited all their energy in the upstream electron calorimeter.

Data and Monte Carlo

3. RAD4 CUT. The limiting aperture of the PWC's on the concrete block was the sensitive area of station 4, which had a radius of 1.5 cm. All tracks were required to be within RAD4 cm's of the center of station 4.

4. EGG CUT. The spectrometer magnet channel cross section was a rectangle with rounded corners as shown in Fig. 2.6. The limiting

aperture of the spectrometer magnets was its most downstream exit. The projection of this aperture onto the veto plane (x_v, y_v) is given by $EGG(x_v, y_v) = 1$, where

$$EGG(x_v, y_v) = [((x_v-27.4cm)/5cm)^6 + ((y+0.24cm)/2.5cm)^6]^{1/6}$$

The projected track of all events onto the veto plane were required to have $EGG(x_v, y_v)$ less than EGGM.

5. STATION 6 CUT. The final aperture of the apparatus was station 6. All tracks were required to be within the rectangle defined by X6LO, X6HI, Y6LO and Y6HI.

6. VETO CUT. Tracks in the veto plane were required to be outside the veto region, defined by the rectangle (XVLO, XVHI, YVLO and YVHI). Typically this rectangle was 0.2 cm larger than the physical veto in both x and y dimensions. See Fig. 2.6.

7. Z_v CUT. The longitudinal position of the interaction vertex, z_v, was required to be in the target region defined by ZLO and ZHI. In Fig. 4.3 a typical z_v for scatters with $-t > 0.001\ (GeV/c)^2$ is shown. The solid lines indicated the physical target position and the dashed lines the Z_v CUT.

8. MM^2 CUT. The recoil mass squared, m_r, defined above was required to be between MMLO and MMHI. This cut removes scatters with high energy losses (some inelastics and scatters off electrons). In Fig. 4.4 a typical m_r^2 distribution is shown.

9. DEAD WIRE CUT. Since Stations 1 and 2 defined the incident beam

Figure 4.3

Z DISTRIBUTION : 200 GeV/c

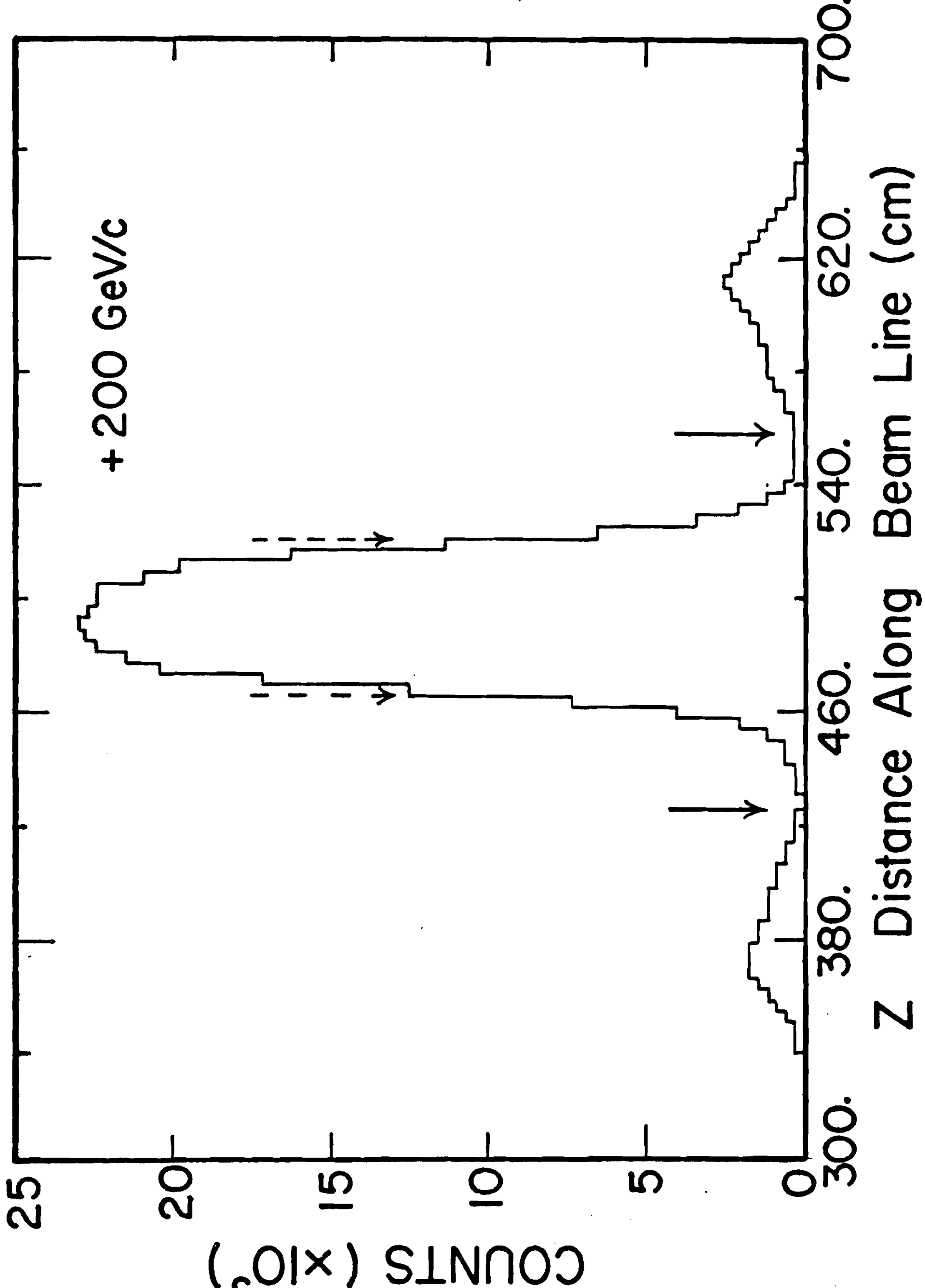

Figure 4.4

RECOIL MASS SQUARED DISTRIBUTION : 200 GeV/c

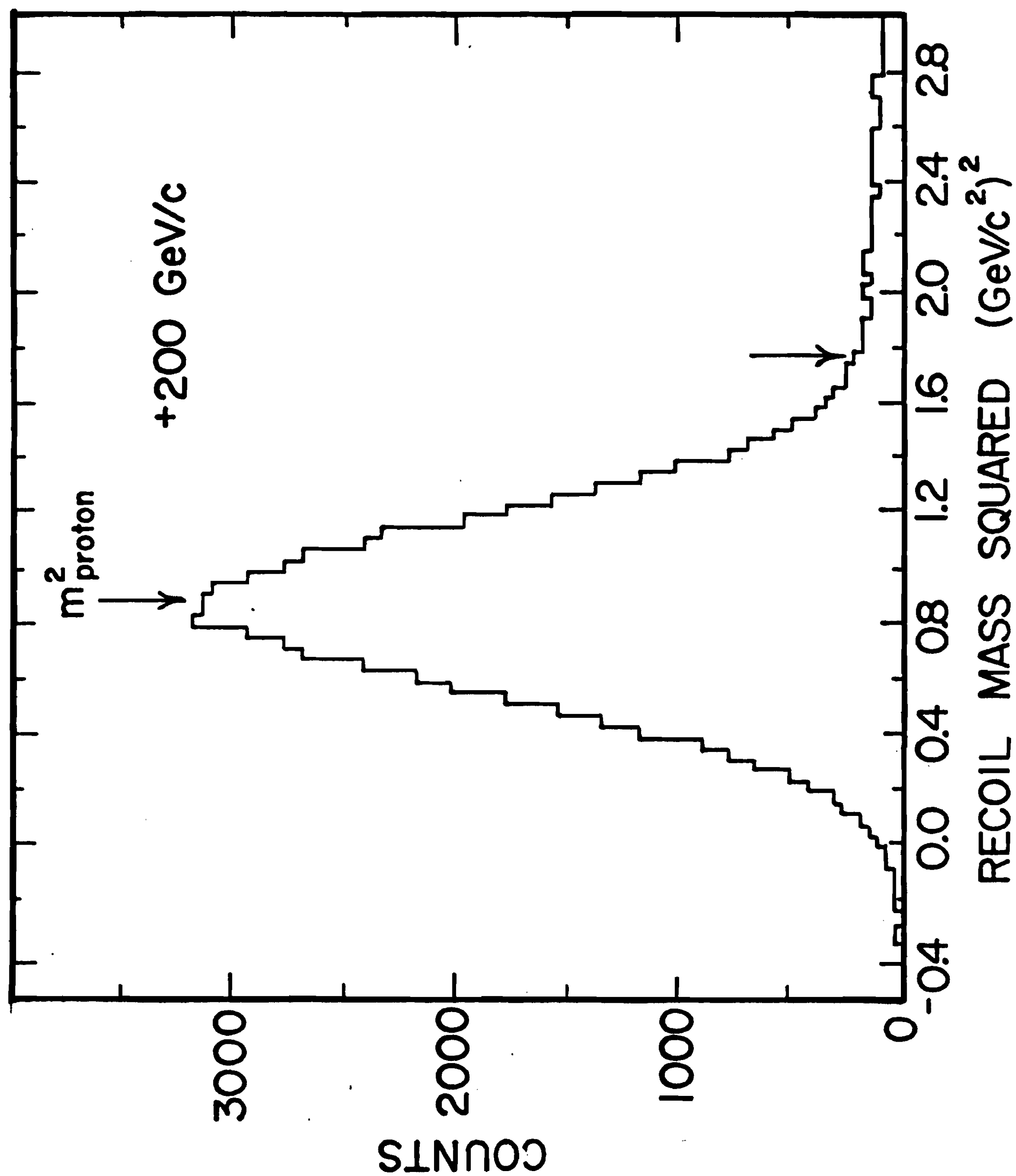

phase space an inefficient or inactive PWC electronics channel was of no consequence. In station 3 the redundancy of x, y, u and v measurements made such inefficiencies negligible. However, in station 4 there is no redundancy and these inefficient areas must be removed. If a track's horizontal position was between X4ALO and X4AHI or between X4BLO and X4BHI, then the event was rejected. Similarly, if a tracks vertical position was between Y4ALO and Y4AHI or between Y4BLO and Y4BHI, the event was also rejected. These inefficient regions were found by sampling through x_4 and y_4 histogram distributions of the data.

Monte Carlo only

10. EGG_g CUT. The projection of the generated track onto the veto plane was required to have $EGG(x_{v,g}, y_{v,g})$ less than EGGG.

11. $VETO_g$ CUT. The projection of the generated track onto the veto plane was required to be outside the veto area defined by the rectangle XVLOG, XVHIG, YVLOG, and YVHIG. This area corresponded exactly to the physical veto area.

12. $Z_{v,g}$ CUT. The generated z position of the track vertex was required to be within the target volume and was defined by ZLOG and ZHIG.

TIGHT CUTS

The above cuts form the basic set of cuts. The following cuts were applied to both data and Monte Carlo events to study the sensitivity of the results to the more important cuts.

13. $RAD4_t$ CUT. The track was contrained to be within the tighter radius, RAD4T, from the center of station 4.

14. EGG_t CUT. The track was required to have $EGG(x_v, y_v)$ less than EGGT.

15. $VETO_t$ CUT. The track was required to be outside of a region defined by the rectangle XVLOT, XVHIT, YVLOT, and YVHIT. This region was 0.4 cm larger in x and y than the physical veto.

16. $Z_{v,t}$ CUT. The z_v of the interaction vertex was required to be within the even smaller region between ZLOT and ZHIT.

17. MM_t CUT. The recoil mass sqared was required to be within the smaller region MMLOT and MMHIT.

In Table 4.7 the values for the cuts are given as a function of incident momentum.

Ultra Tapes

The Ultra tapes made by KUTTER (Fig. 4.1) contained the data and Monte Carlo distributions with the basic cuts and with the tighter set of cuts. The program KUTTER applied the basic cuts to the data and Monte Carlo events on the Summary tapes, determined the HSD efficiency and found the normalization coefficients for both data and Monte Carlo events. In Table 4.8 the information written on the Ultra tapes is listed.

The basic cuts for the data were 1 through 9 and for the Monte Carlo 3 through 12. If an event passed these basic cuts, KUTTER would

TABLE 4.7a

Cuts Used in Analysis[a]

	Cuts	Momentum +200	-200[b]	-200[b]	+175	-175
2.	MUON	250.000	250.000	250.000	100.000	100.000
3.	RAD4	1.450	1.450	1.450	1.450	1.450
4.	EGG	0.900	0.900	0.900	0.900	0.900
5.	X6LO	120.000	120.000	120.000	120.000	120.000
	X6HI	147.000	147.000	147.000	147.000	147.000
	Y6LO	-6.500	-7.000	-7.000	-7.000	-7.000
	Y6HI	6.000	5.600	5.600	6.000	6.000
6.	XVLO	0.000	0.000	0.000	0.000	0.000
	XVHI	24.550	24.530	24.470	24.470	24.600
	YVLO	-0.276	-0.280	-0.160	-0.180	-0.180
	YVHI	0.176	0.160	0.280	0.270	0.270
7.	ZLO	440.000	440.000	440.000	440.000	440.000
	ZHI	550.000	550.000	550.000	550.000	550.000
8.	MMLO	0.200	0.200	0.200	0.200	0.200
	MMHI	1.560	1.560	1.560	1.560	1.560
9.	X4ALO	0.310	0.300	0.300	1.220	1.220
	X4AHI	0.380	0.390	0.390	1.360	1.360
	X4BLO	1.220	1.220	1.220	---	---
	X4BHI	1.360	1.360	1.360	---	---
	Y4ALO	---	---	---	-0.320	---
	Y4AHI	---	---	---	-0.180	---
	Y4BLO	---	-0.260	-0.260	---	---
	Y4BHI	---	-0.180	-0.180	---	---
10.	EGGG	0.980	0.980	0.980	0.980	0.980
11.	XVLOG	0.000	0.000	0.000	0.000	0.000
	XVHIG	24.450	24.430	24.370	24.370	24.500
	YVLOG	-0.176	-0.180	-0.060	-0.080	-0.080
	YVHIG	0.076	0.060	0.180	0.170	0.170
12.	ZLOG	468.020	468.020	468.020	468.020	468.020
	ZHIG	520.770	520.770	520.770	520.770	520.770
13.	RAD4T	1.300	1.300	1.300	1.300	1.300
14.	EGGT	0.750	0.750	0.750	0.750	0.750
15.	XVLOT	0.000	0.000	0.000	0.000	0.000
	XVHIT	24.650	24.630	24.570	24.570	24.700
	YVLOT	-0.376	-0.380	-0.260	-0.280	-0.280
	YVHIT	0.276	0.260	0.380	0.370	0.370
16.	ZLOT	455.000	455.000	455.000	455.000	455.000
	ZHIT	535.000	535.000	535.000	535.000	535.000
17.	MMLOT	0.400	0.400	0.400	0.400	0.400
	MMHIT	1.360	1.360	1.360	1.360	1.360

[a]Cuts 2,4,10,14 are unitless; Cuts 8 and 17 are in $(GeV/c)^2$; The remaining cuts are in cm.

[b]During the -200 GeV/c data taking the veto phototube had to be replaced, changing the veto position.

TABLE 4.7b

Cuts Used in Analysis

Cuts		Momentum +150	-150	+125	-125
2.	MUON	480.000	480.000	480.000	480.000
3.	RAD4	1.450	1.450	1.450	1.450
4.	EGG	0.900	0.900	0.900	0.900
5.	X6LO	120.000	120.000	120.000	120.000
	X6HI	147.000	147.000	147.000	147.000
	Y6LO	-7.000	-7.000	-7.000	-7.000
	Y6HI	5.200	6.000	6.000	6.000
6.	XVLO	0.000	0.000	0.000	0.000
	XVHI	24.670	24.670	24.700	24.700
	YVLO	-0.620	-0.620	-0.640	-0.620
	YVHI	-0.010	-0.010	-0.030	-0.010
7.	ZLO	440.000	440.000	440.000	440.000
	ZHI	550.000	550.000	550.000	550.000
8.	MMLO	0.200	0.200	0.200	0.200
	MMHI	1.560	1.560	1.560	1.560
9.	X4ALO	---	-0.200	1.220	-0.200
	X4AHI	---	-0.120	1.340	-0.120
	X4BLO	1.220	1.220	---	1.220
	X4BHI	1.360	1.360	---	1.340
	Y4ALO	-0.460	0.000	-0.200	-0.200
	Y4AHI	-0.420	0.060	-0.120	-0.120
	Y4BLO	0.280	---	0.040	---
	Y4BHI	0.340	---	0.080	---
10.	EGGG	0.980	0.980	0.980	0.980
11.	XVLOG	0.000	0.000	0.000	0.000
	XVHIG	24.570	24.570	24.600	24.600
	YVLOG	-0.520	-0.520	-0.540	-0.520
	YVHIG	-0.110	-0.110	-0.130	-0.110
12.	ZLOG	468.020	468.020	468.020	468.020
	ZHIG	520.770	520.770	520.770	520.770
13.	RAD4T	1.300	1.300	1.300	1.300
14.	EGGT	0.750	0.750	0.750	0.750
15.	XVLOT	0.000	0.000	0.000	0.000
	XVHIT	24.770	24.770	24.800	24.800
	YVLOT	-0.720	-0.720	-0.740	-0.720
	YVHIT	0.090	0.090	0.070	0.090
16.	ZLOT	455.000	455.000	455.000	455.000
	ZHIT	535.000	535.000	535.000	535.000
17.	MMLOT	0.400	0.400	0.400	0.400
	MMHIT	1.360	1.360	1.360	1.360

TABLE 4.7 c

Cuts Used in Analysis

Cuts		Momentum			
		+100	-100	+70	-70
2.	MUON	450.000	450.000	90.000	90.000
3.	RAD4	1.450	1.450	1.450	1.450
4.	EGG	0.900	0.900	0.900	0.900
5.	X6LO	120.000	120.000	120.000	120.000
	X6HI	147.000	147.000	147.000	147.000
	Y6LO	-6.500	-7.000	-6.500	-7.000
	Y6HI	6.000	6.000	6.000	6.000
6.	XVLO	0.000	0.000	0.000	0.000
	XVHI	24.700	24.750	24.800	24.800
	YVLO	-0.630	-0.630	-0.280	-0.280
	YVHI	-0.020	-0.020	0.410	0.410
7.	ZLO	440.000	440.000	440.000	440.000
	ZHI	550.000	550.000	550.000	550.000
8.	MMLO	0.200	0.200	0.200	0.200
	MMHI	1.560	1.560	1.560	1.560
9.	X4ALO	---	-0.240	---	---
	X4AHI	---	-0.200	---	---
	X4BLO	1.220	1.180	---	1.480
	X4BHI	1.360	1.360	---	1.520
	Y4ALO	-0.180	-0.480	---	-0.320
	Y4AHI	-0.060	-0.420	---	-0.260
	Y4BLO	---	-0.260	---	-0.440
	Y4BHI	---	-0.160	---	-0.360
10.	EGGG	0.980	0.980	0.980	0.980
11.	XVLOG	0.000	0.000	0.000	0.000
	XVHIG	24.600	24.650	24.700	24.700
	YVLOG	-0.530	-0.530	-0.180	-0.180
	YVHIG	-0.120	-0.120	0.310	0.310
12.	ZLOG	468.020	468.020	468.020	468.020
	ZHIG	520.770	520.770	520.770	520.770
13.	RAD4T	1.300	1.300	1.300	1.300
14.	EGGT	0.750	0.750	0.750	0.750
15.	XVLOT	0.000	0.000	0.000	0.000
	XVHIT	24.800	24.850	24.900	24.900
	YVLOT	-0.730	-0.730	-0.380	-0.380
	YVHIT	0.080	0.080	0.510	0.510
16.	ZLOT	455.000	455.000	455.000	455.000
	ZHIT	535.000	535.000	535.000	535.000
17.	MMLOT	0.400	0.400	0.400	0.400
	MMHIT	1.360	1.360	1.360	1.360

TABLE 4.8

Event Quantities Written on Ultra Tapes

A. Data Events

1. q of scatter
2. Latch word: Particle type, SCATTER, BEAM
3. Cut status word indicating which of the following cuts were passed: Basic cuts, cut 13, cut 14, cut 15, cut 16, or cut 17.

B. Monte Carlo Events

1. initial q of scatter
2. reconstructed q of scatter
3. Cut status word: defined above.

then generate a code word indicating which of the additional cuts 13 through 17 were also satisfied.

Using the SCATTER events that passed the basic cuts, KUTTER would then determine the HSD efficiencies, $E_x(q_x)$, $E_y(q_y)$, and $E_{HSD}(q)$. E_x and E_y were the projected effiencies, while E_{HSD} is given by the OR of E_x and E_y. In Figure 4.5 we show $E_x(q_x)$ at 70 and 200 GeV/c.

The resolution function $R(q', q'')$ is given by the Monte Carlo events that passed the appropriate cuts. $R(q', q'')$ is the number of events generated with $q = q'$ that passed all cuts, and was reconstructed with $q = q''$ divided by the total number generated with $q = q'$. We define the acceptance, $A(q')$, as the probablity of a track generated with $q = q'$ passed all cuts. $A(q')$ is given as follows:

$$A(q') = \int_{-\infty}^{\infty} dq'' \, R(q',q'').$$

In Fig. 4.6 we show $A(q')$ at 200 GeV/c. The sharp fall off of the acceptance at $\theta = 1$ mrad ($q = 0.2$ GeV/c at 200 GeV/c) is due to the overlap of the three limiting apertures of the apparatus, given by Cuts 3, 4, and 5.

Target Empty Subtraction

After the cuts were applied to the data, the target full and target empty q distributions were first normalized and then subtracted. The normalized distributions, N^F and N^{MT}, were obtained as follows:

$$N^F(q_i) = N_s{}^F(q_i) \cdot R_s{}^F \,/\, N_b{}^F$$

$$N^{MT}(q_i) = N_s{}^{MT}(q_i) \cdot R_s{}^{MT} \,/\, N_b{}^{MT} \;,$$

Figure 4.5a

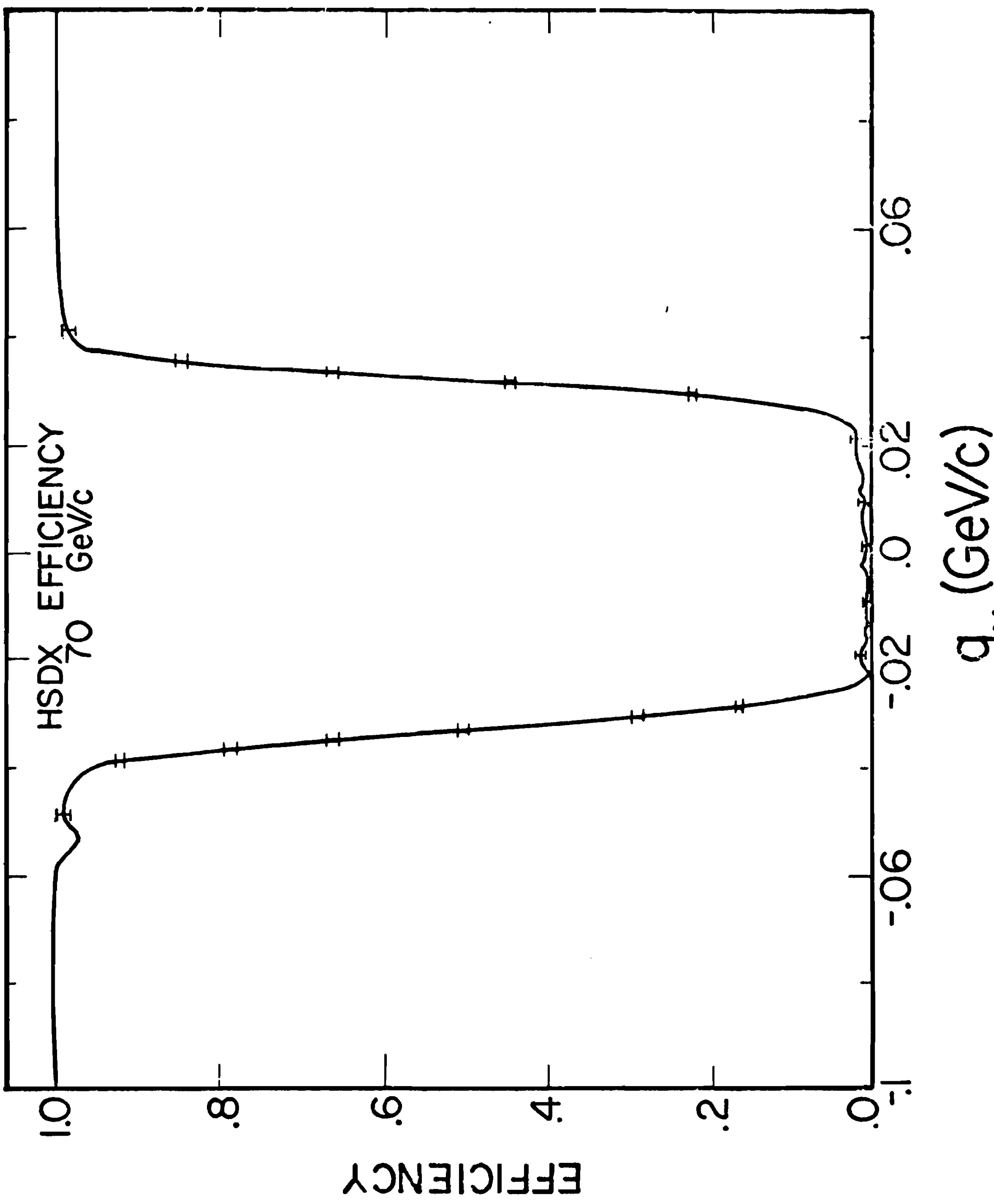
HSDX70 EFFICIENCY GeV/c
EFFICIENCY
1.0
.8
.6
.4
.2
0
-.1
-.06
-.02
.0
.02
.06
q_x (GeV/c)

Figure 4.5b

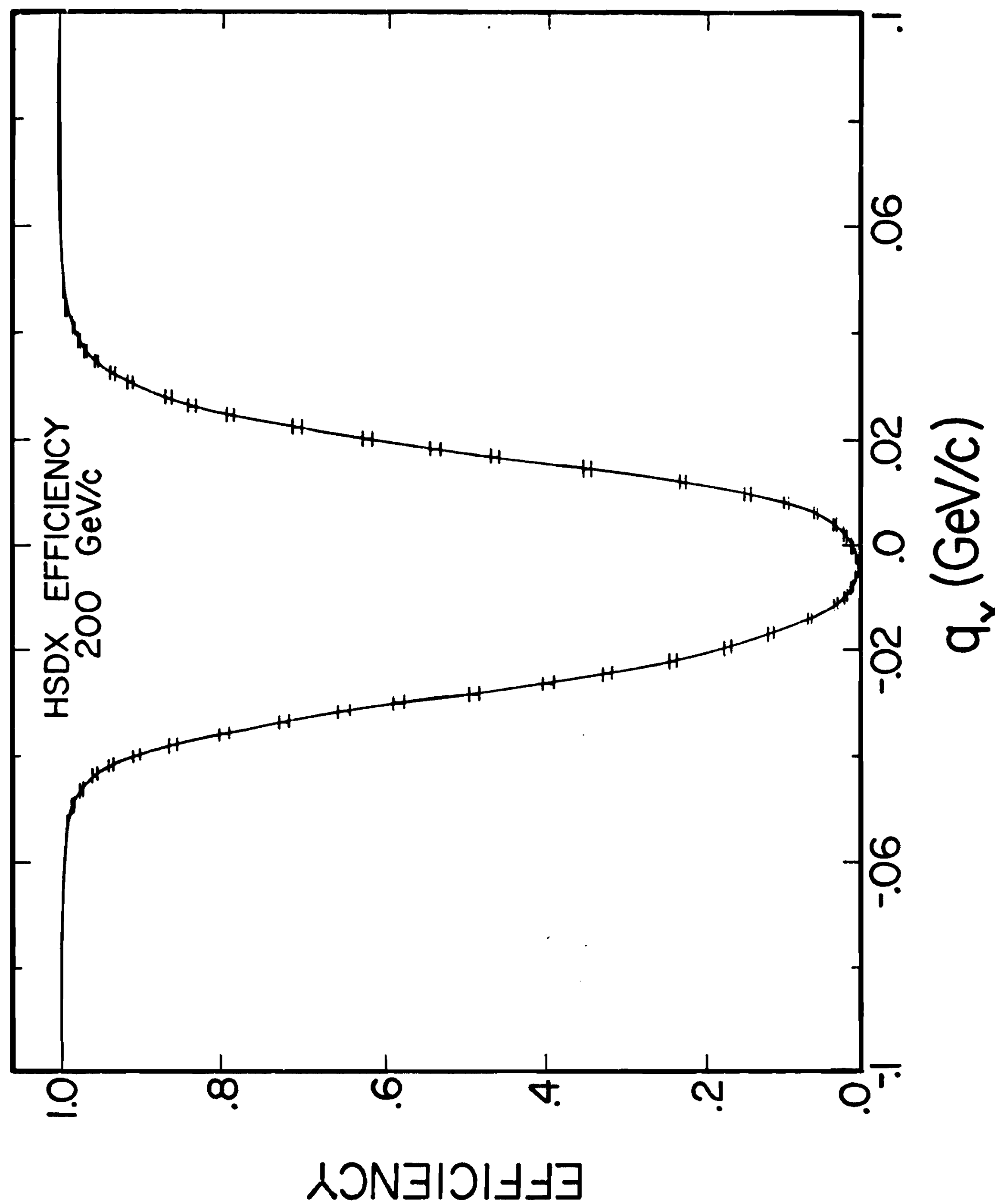
HSDX EFFICIENCY
200 GeV/c
EFFICIENCY
1.0
.8
.6
.4
.2
0.
-.1
-.06
-.02
.0
.02
.06
.1
qx (GeV/c)

Figure 4.6

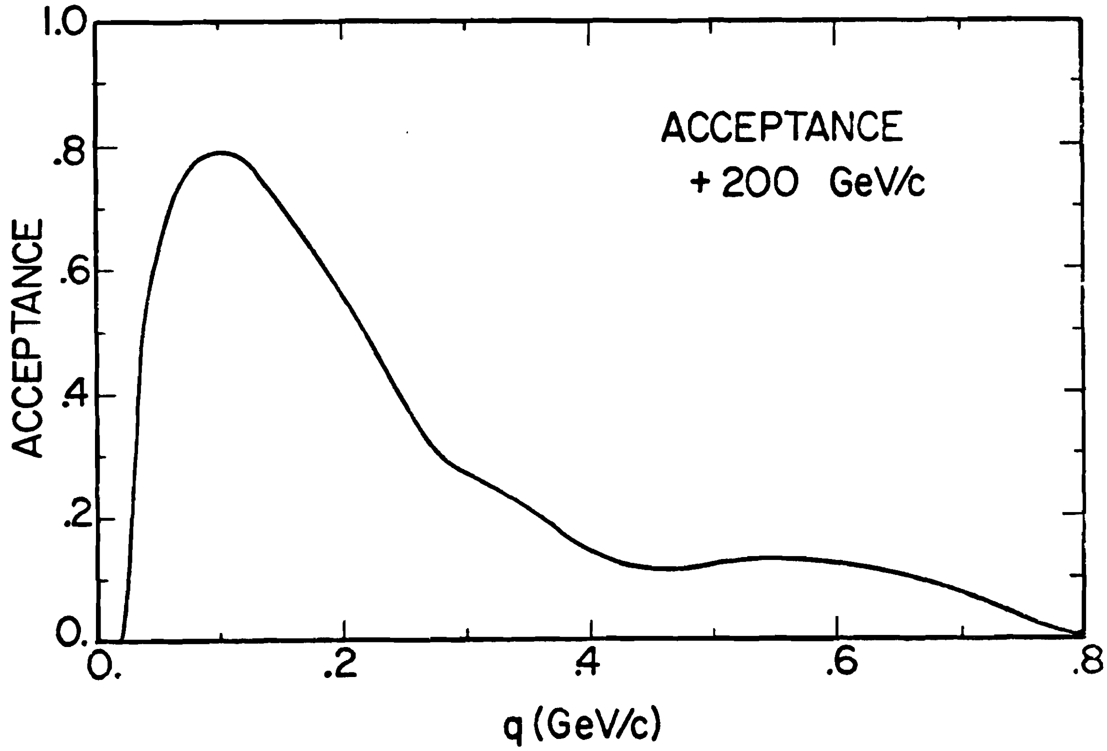

where $N_s^F(q_i)$ and $N_s^{MT}(q_i)$ are the number of full and empty target, SCATTER events that passed all the cuts and had q in the range $q_i-\Delta q/2 \leq q \leq q_i+\Delta q/2$; N_b^F and N_b^{MT} are the number of full and empty target reconstructed BEAM events. The bin size of the distribution, Δq, varied from 0.002 GeV/c at 70 GeV/c to 0.005 GeV/c at 200 GeV/c. The sampling rate R_s is given by:

$$R_s = N_{s \cdot b} / N_s,$$

where N_s is the total number of reconstructed SCATTER events and $N_{s \cdot b}$ is the total nubmer of reconstructed SCATTER events that are also BEAM events. The ratio, N_b / R_s, is the total incident flux corrected for dead time corrections and absorbtion losses in the apparatus.

The data scattering distribution, $S_D(q_i)$, is given by:

$$S_D(q_i) = (N^F(q_i) - N^{MT}(q_i)) / (D \cdot L \cdot \Delta q),$$

where D is the number of protons per volume of LH_2 and L is the target length. The target empty correction N^{MT} is largest at 200 GeV/c where it is 30% of N^F at $-t = 0.0016$ $(GeV/c)^2$, but rapidly decreases to zero at $-t = 0.01$ $(GeV/c)^2$. The statistical error of N^F and N^{MT} are dominated by the statistical errors of R_s^F and R_s^{MT} which are typically 1% and 3% respectively. In summary, $S_D(q_i)$ is the differential cross section for scattering in the liquid hydrogen as measured by our apparatus.

Corrections to Theoretical Cross Section

The theoretical cross sections given by Eqs. 1.6 and 1.7 were modified to include the following corrections: multiple scattering, resolution, acceptance, HSD efficiency, and radiative losses.

Since our multiple Coulomb scattering distribution width is in very good agreement with Moliere's prediction,[4.1] we extend the Moliere formalism to include the interference and nuclear contributions. This transforms the theoretical cross sections of Eqs. 1.6 and 1.7 into Moliere distributions, $S_{MS}{}^{e}$ and $S_{MS}{}^{ff}$, due to multiple scattering in the liquid hydrogen. In the t range of interest these distributions are approximated by:

$$S_{MS}{}^{e} = \sigma_C (1-\varepsilon_C)^{-1} + \sigma_I{}^{e} (1+\varepsilon_I) + \sigma_n{}^{e} (1+\varepsilon_n{}^{e})$$
$$S_{MS}{}^{ff} = \sigma_C (1-\varepsilon_C)^{-1} + \sigma_I{}^{ff} (1+\varepsilon_I) + \sigma_n{}^{ff} (1+\varepsilon_n{}^{ff}),$$

where ε_C is Bethe's result in Ref. 4.1 due to pure Coulomb scattering, ε_I is the multiple scattering correction due to the interference term, and ε_n is the double nuclear scattering correction. These corrections are given as follows:

$$\varepsilon_C = (4w^2 / |t|) [1 + .043 \ln(.16 |t| / w^2)]$$

$$\varepsilon_I = (w^2 / |t|) + (1.333 w^4 / t^2)$$

$$\varepsilon_n{}^{e} = (D L \sigma_{tot}{}^2 (1+\rho^2)) / (64\pi\hbar^2 b^e(0) \exp[(Bt+Ct^2)/2])$$

$$\varepsilon_n{}^{ff} = (D L \sigma_{tot}{}^2 (1+\rho^2)) / (64\pi\hbar^2 b^{ff}(0) G_a(t) G_p(t))^{-1},$$

where w is the 1/e of the projected Coulomb multiple scattering gaussian distribution. D and L, as defined above, are the number of protons per volume of LH_2 and the target length. Since L is 52.7 cm, then w is 3.68 MeV/c. At $-t = 0.0016\ (\mathrm{GeV/c})^2$, ε_C and ε_I are 4% and 1% corrections and rapidly decrease with increasing -t. The double scattering correction, ε_n is less than 1% in our t range. The details of the multiple scattering corrections are found in Appendix A.

The acceptance and resolution corrected theoretical cross section, $S_{MS,A,R}(q_i)$ is given by:

$$S_{MS,A,R}(q_i) = \int_{q_i-\Delta q/2}^{q_i+\Delta q/2} dq' \int_0^\infty 2q''dq''\ S_{MS}(q'')\ R(q'',q')$$

where $R(q'',q')$ is the probability that a scatter generated with $q = q''$ passed all the aperture and kinematic cuts and was reconstructed as a scatter with $q = q'$. The function $R(q'',q')$ is numerically generated by the Monte Carlo. It would by extremely time consuming to evaluate the above integral every time a parameter was changed in the fitting procedure. To avoid this, the cross section, $S_{MS}(q)$ was expanded into a series such that the parameters of the fit are decoupled from q. For the exponential case we write symbolically:

$$S_{MS}{}^{e} = \sum_j\ g_j{}^{e}(\rho,\ B,\ C,\ \sigma_{tot})\ h_j{}^{e}(q).$$

We found that a series expansion of 100 terms was sufficiently accurate(1 part in 10^8). The integration over the Monte Carlo events is performed only once and $S_{MS,A,R}(q_i)$ is written as:

$$S_{MS,A,R}(q_i) = \sum_j\ g_j{}^{e}(\rho,\ B,\ C,\ \sigma_{tot})\ \ \langle h_j{}^{e}(q_i)\rangle\ ,$$

where

$$\langle h_j{}^{e}(q_i)\rangle = \int_{q_i-\Delta q/2}^{q_i+\Delta q/2} dq' \int_0^\infty 2q''dq''\ h_j{}^{e}(q'')\ R(q'',q').$$

A similar procedure was followed for the form factor cross section. In Appendix B we present the expansion method in detail.

The theoretical cross section with all our corrections is given by:

$$S_{Th}(q_i) = S_{MS,A,R}\,(1+\varepsilon_{rad}(q_i)) \,/\, E_{HSD}(q_i)\ ,$$

where ε_{rad} is the radiative correction and E_{HSD} is the total HSD efficiency. We use the calculations of Sogard[4.2] to determine the loss of events, ε_{rad}, from the elastic peak due to the radiation of photons. In this experiment the correction is significant only for pions: ε_{rad} increases from zero at $t = 0$ to about 5% at $-t = 0.36$ $(GeV/c)^2$ for the missing mass squared cut used in the analysis and for the width of the elastic peak. The HSD efficiency, E_{HSD}, is 0.99 at $-t = 0.0016$ $(GeV/c)^2$ and rapidly becomes 1.0 with increasing $-t$.

The scintillator counters, RV1, RV2, VH2, and VH3 were used to remove a 2 to 3%, non-elastic background. After these cuts were applied, no significant contamination of the elastic peak is observed in our t range. No additional correction for inelastic contamination was made.

Fitting Procedure

The fitting procedure consisted of minimizing the following χ^2:

$$\chi^2 = \sum_i (S_D(q_i) - A_n\, S_{Th}(q_i))^2 \,/\, \sigma_i^2\ ,$$

where σ_i is the statistical error of $S_D(q_i)$ and A_n is an arbitrary normalization parameter. The χ^2 was minimized by the program

MINUIT[4.3] and the statistical errors on the parameters were calculated by the subroutine HESSE.

The corrected data cross section, $d\sigma^D/dt$, is given by:

$$d\sigma^D/dt = d\sigma/dt \left[S_D(q_i) / (A_n \; S_{Th}^*(q_i)) \right] \tag{4.2}$$

where $d\sigma/dt$ is the cross section given by Eq. 1.7 and $S_{Th}^*(q_i)$ is $S_{Th}(q_i)$ evaluated with our final parameters. The corrected cross section tables are found in Appendix C.

CHAPTER 5

RESULTS AND CONCLUSIONS

The Nuclear Slope

Since the value of ρ is strongly correlated to the nuclear slope at small -t, we first discuss the structure of the nuclear cross section. As mentioned above recent experimental results[1.11-1.14] have observed substantial deviations from a constant exponential slope for $-t > 0.025$ $(GeV/c)^2$. As we show below, the nuclear curvature, C from Eq. 1.9, is approximately 5 $(GeV/c)^{-4}$ for all six reactions. In the absence of direct experimental evidence below $-t = 0.025$ $(GeV/c)^2$, we assume that this curvature extends down to $t = 0$. This assumption is inherent in the nuclear amplitudes given by Eqs. 1.4 and 1.5. Thus even in the small t range, $0.0 \leq -t \leq 0.10$ $(GeV/c)^2$, the variation of the nuclear slope, b(t), is about 1 $(GeV/c)^{-2}$ which has a significant effect on ρ.

The nuclear curvature at large -t is demonstrated in Fig. 5.1, where $d\sigma/dt$ for pp scattering at 200 GeV/c is shown. The theoretical curve was obtained by fitting the data in the range $0.0016 \leq -t \leq 0.09$ $(GeV/c)^2$ with the exponential cross section Eq. 1.6 and $C = 0$. We note that the experimental cross section does not decrease as a simple

Figure 5.1

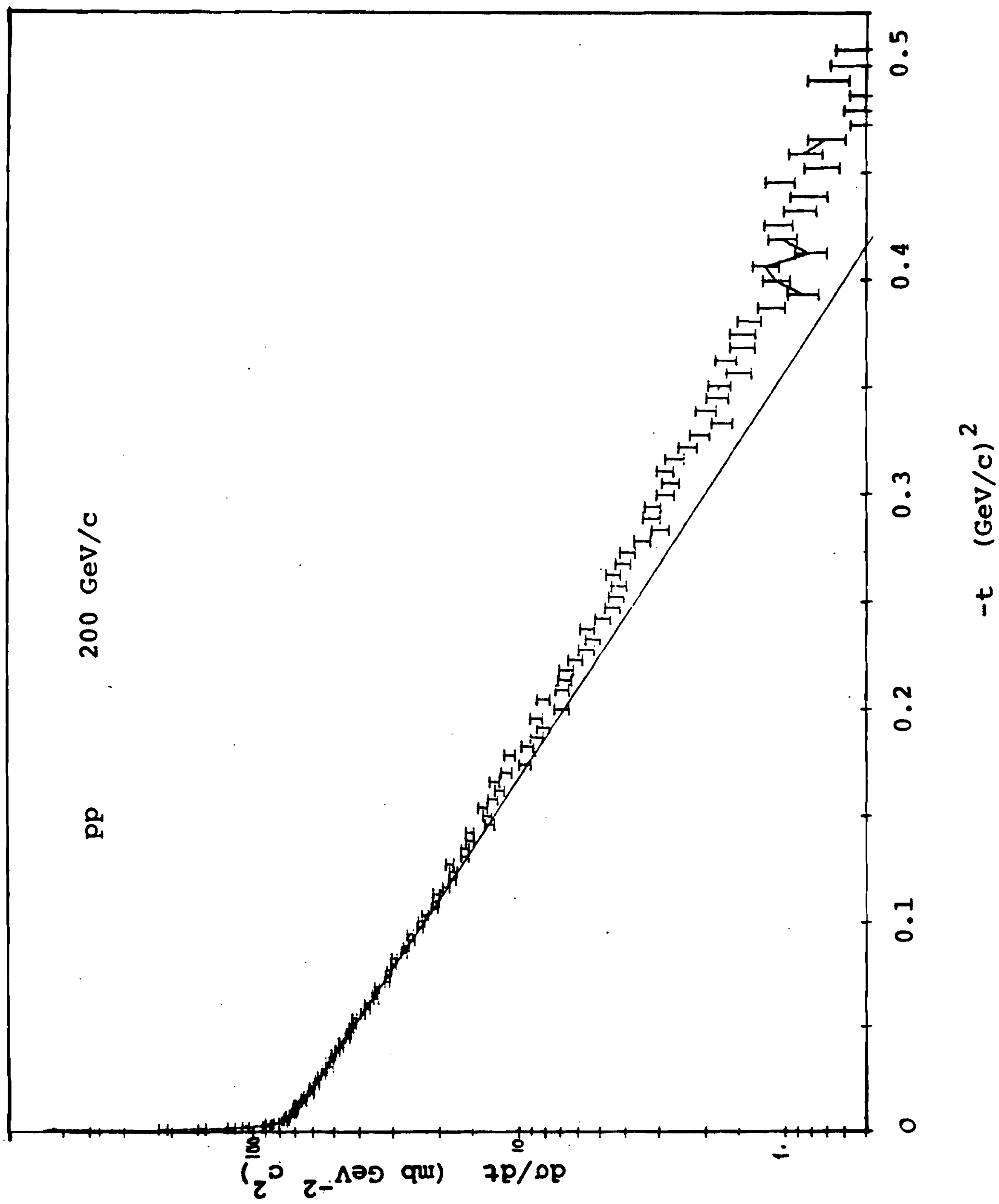

exponential. Similar behaviour is observed for all six reactions between 125 and 200 GeV/c (below 125 GeV/c our t range is too small to observe curvature). By fitting the data with Eq. 1.6 and allowing B and C to vary, we get a much better representation of the data. In Table 5.1 we present B and C for all six reactions at 200 GeV/c. The data was fit in the range $0.01 \leq -t \leq 0.36$ $(GeV/c)^2$ with the exponential cross section Eq. 1.6 and ρ fixed to our final value (presented in the next section). We see that the values of C are substantial and nearly particle independent. At lower momenta our reduced t range and reduced statistics at high -t do not allow a very accurate simultaneous determination of both B and C.

We found in a related experiment[1.11] on elastic scattering of pp, π^+p, and π^-p with a high statistical sample in the range $0.025 \leq -t \leq 0.62$ $(GeV/c)^2$, that the AQM formulation fit the data rather well. Similarly we find with this experiment that the form factor cross section, Eq. 1.7, with only one parameter, u, allowed to vary fits all six hadronic interactions. We find that the χ^2 's for the form factor fits are comparable to those of the exponential cross section with both B and C free to vary.

Using the values of u from our final fits at 200 GeV/c (presented in the next section), we calculate the form factor nuclear slope, $b^{ff}(t)$, given by Eq. 1.9. Similarly we find the exponential slope, $b^e(t)$, given by Eq. 1.8 and B and C from Table 5.1. In Figure 5.2 we compare $b^{ff}(t)$ and $b^e(t)$ to previous measurements of the nuclear slope for pp, π^+p, and π^-p at 200 GeV/c. In the t range of the fits, $b^{ff}(t)$ is represented by the solid line and $b^e(t)$ is shown by the dashed line.

TABLE 5.1

Exponential Fit[a] at 200 GeV/c

Parameter	Reaction					
	pp	π^+p	K^+p	$\bar{p}p$	π^-p	K^-p
B $(GeV/c)^{-2}$	12.64 ± 0.12	10.72 ± 0.15	9.60 ± 0.22	13.27 ± 0.24	10.85 ± 0.14	9.51 ± 0.19
C $(GeV/c)^{-4}$	5.06 ± 0.44	6.08 ± 0.54	4.37 ± 0.79	4.54 ± 0.97	5.87 ± 0.51	3.38 ± 0.69
A_n	1.10 ± 0.01	1.11 ± 0.01	1.10 ± 0.01	1.10 ± 0.01	1.11 ± 0.01	1.05 ± 0.01
χ^2/DF[b]	1.09	1.57	1.19	1.07	0.86	1.18

[a]The range of the fit was $0.01 \leq -t \leq 0.36$ $(GeV/c)^2$

[b]The number of degrees of freedom, DF, was 97 for all six fits.

Figure 5.2

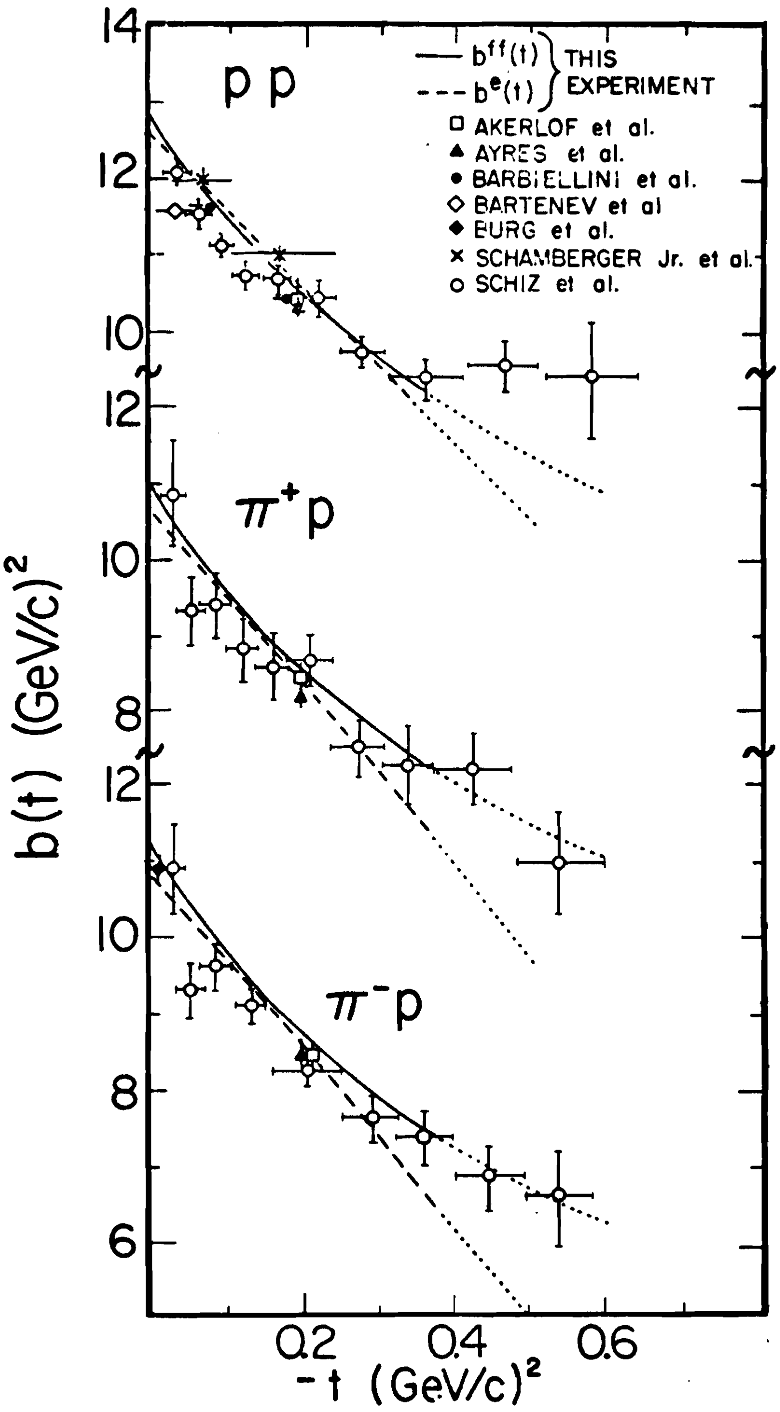

b(t) (GeV/c)²
-t (GeV/c)²
pp
π⁺p
π⁻p
— $b^{ff}(t)$ } THIS
--- $b^{e}(t)$ } EXPERIMENT
□ AKERLOF et al.
▲ AYRES et al.
● BARBIELLINI et al.
◇ BARTENEV et al
◆ BURG et al.
× SCHAMBERGER Jr. et al.
○ SCHIZ et al.
14
12
10
8
6
0.2
0.4
0.6

Both curves are continued with dotted lines. We note that for all three reactions the slope is increases more rapidly than a constant curvature measured at higher -t would predict. We see that the form factor slope gives a good prescription for this increase. Both form factor and exponential slopes are slightly higher than our previous result[1.11], but we attribute this to the statistical bias of the this sample towards low -t. We also note that the nuclear slope is increasing with increasing momentum.

In Figure 5.3 we compare $b^{ff}(t)$ at $-t = 0.1$ and 0.2 $(GeV/c)^2$ with the exponential determinations ($B - 2C|t|$) of Ayres et al.[1.12] and Ackerlof et al.[1.12] for all six reactions from 50 to 200 GeV/c. We note the excellent agreement of the local slopes at $-t = 0.2$ $(GeV/c)^2$. At $-t = 0.1$ $(GeV/c)^2$ our local slopes are substantially higher than the predicted values of Ayres et al. and Ackerlof et al., indicating that the curvature is increasing for all six reactions.

An elegant feature of the form factor cross section is to explain the large curvature that we measure at low -t and the small curvature that Ayres et al. and Akerlof et al. measured at high -t. In pp scattering the form factor curvature, $c^{ff}(t)$ (Eq. 1.9), equals 4.9 $(GeV/c)^{-4}$ at $t = 0.2$ $(GeV/c)^2$, which is good agreement with $C = 5$ $(GeV/c)^{-4}$. While at $t = 0.4$ $(GeV/c)^2$, the curvature has decreased to $c^{ff}(t) = 2.3$ $(GeV/c)^{-4}$ which is in good agreement with previous measurements[1.12] of C in this t range. Calculating $c^{ff}(t)$ for other reactions, we see that the curvature is almost particle independent. This is also in good agreement with previous measurements.

Figure 5.3

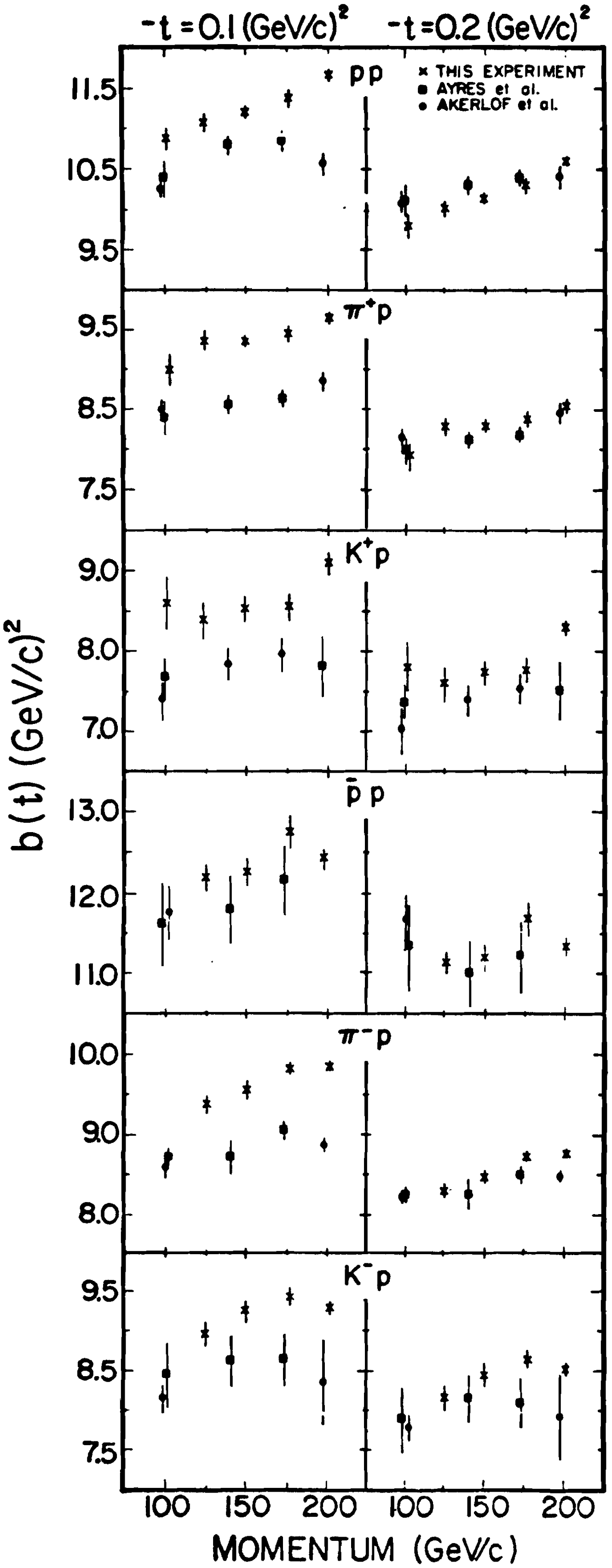
-t = 0.1 (GeV/c)^2
-t = 0.2 (GeV/c)^2
× THIS EXPERIMENT
■ AYRES et al.
● AKERLOF et al.
pp
π^+p
K^+p
$\bar{p}$p
π^-p
K^-p
b(t) (GeV/c)^2
MOMENTUM (GeV/c)
11.5
10.5
9.5
8.5
7.5
9.0
8.0
7.0
13.0
12.0
11.0
10.0
100
150
200

Again because of the short leverage arm and low statistics at large -t of this data we are unable to fit for the nuclear form factor radii. However in our previous result[1.11], we were able to fit for the proton and pion nuclear radii. The fits tended to give values of proton radius 7% smaller than the electromagnetic values, while the pion radius was consistent with the electromagnetic measurements. For kaons we have no such independent check and only one experimental measure of the kaon radius.[1.9] To first order our values of ρ are insensitive to small changes in the radii, since the values of u will vary to compensate.

In Fig. 5.2 we also note that $b^{ff}(t)$ and $b^{e}(t)$ are rather close in our t range. Our data does not have the statistical power to distinguish the two formulations by a χ^2 test. However, we are sensitive to variations of the fits as we vary the t range. To illustrate the stability of the form factor fits, the data at 200 GeV/c was fit with the exponential cross section (C was fixed to 0.0) and with the form factor cross section in the intervals $0.0016 \leq -t \leq -t_{max}$. The values of $-t_{max}$ ranged from 0.05 to 0.36 $(GeV/c)^2$. In Fig. 5.4a the fitted values of B and u are plotted as a function of $-t_{max}$ for all six reactions at 200 GeV/c. For convenience B and u are superimposed and a dashed line goes through the value of u from our final fits. The scales for u and B are the left and right hand sides, respectively. We note as the range of the fit increased B decreased, while u remained constant within statistical errors. The χ^2 per degree of freedom also rapidly increased for the exponential case but remained near one for the form factor case. Since ρ is strongly

Figure 5.4a

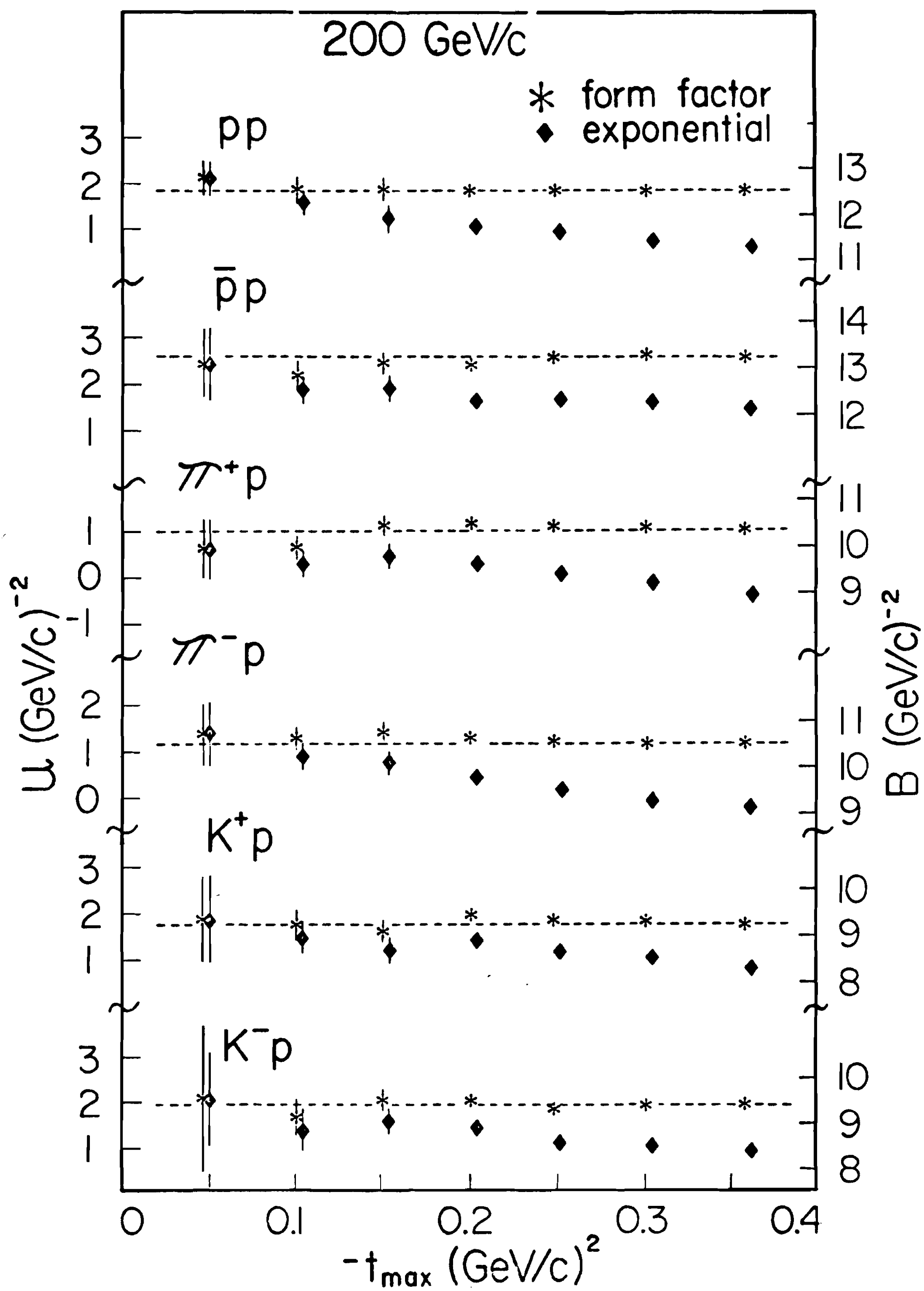
200 GeV/c
form factor
exponential
pp
p̄p
π⁺p
π⁻p
K⁺p
K⁻p
μ (GeV/c)⁻²
B (GeV/c)⁻²
-t_max (GeV/c)²
0
0.1
0.2
0.3
0.4

correlated to the nuclear slope, the variation of ρ follows the variation of B and u. Since z_a changes sign in Eqs. 1.6 and 1.7 for particle and anti-particle, the variation of ρ will be reversed for the two cases. This behaviour is shown in Fig. 5.4b, where a dashed line goes through the value of ρ from our final fits. For small $-t_{max}$ the values of ρ for both formulations converge, although with large uncertainties. At lower momenta the same behaviour is noted, but over reduced t ranges. Fitting the data with the exponential cross section and C fixed to the values of Table 5.1, results in fits similar to those of the form factor, but with slightly larger undulations of ρ and B as a function of $-t_{max}$. In summary, the form factor cross section, Eq. 1.7, gives a good representation of the data and makes the determination of ρ less sensitive to the fitting range. A fit over a larger t interval increases the statistical certainty in ρ by increasing the certainty in the slope parameter.

The Real Part

In Tables 5.2a-f we present the results of fitting the data with the form factor cross section over the indicated t ranges. The parameters ρ, u and A_n were allowed to vary except at 70 Gev/c, where u was held constant. The value of u at 70 GeV/c was determined by fitting the values of u between 100 and 200 GeV/c to the function $a + b \ln(p_{beam})$. The total cross section, σ_{tot}, was held fixed to the values of Carroll et al.[5.1]

In Figs. 5.5a-f the corrected data and the fitted form factor cross sections are compared over the full t range for all six particles

Figure 5.4b

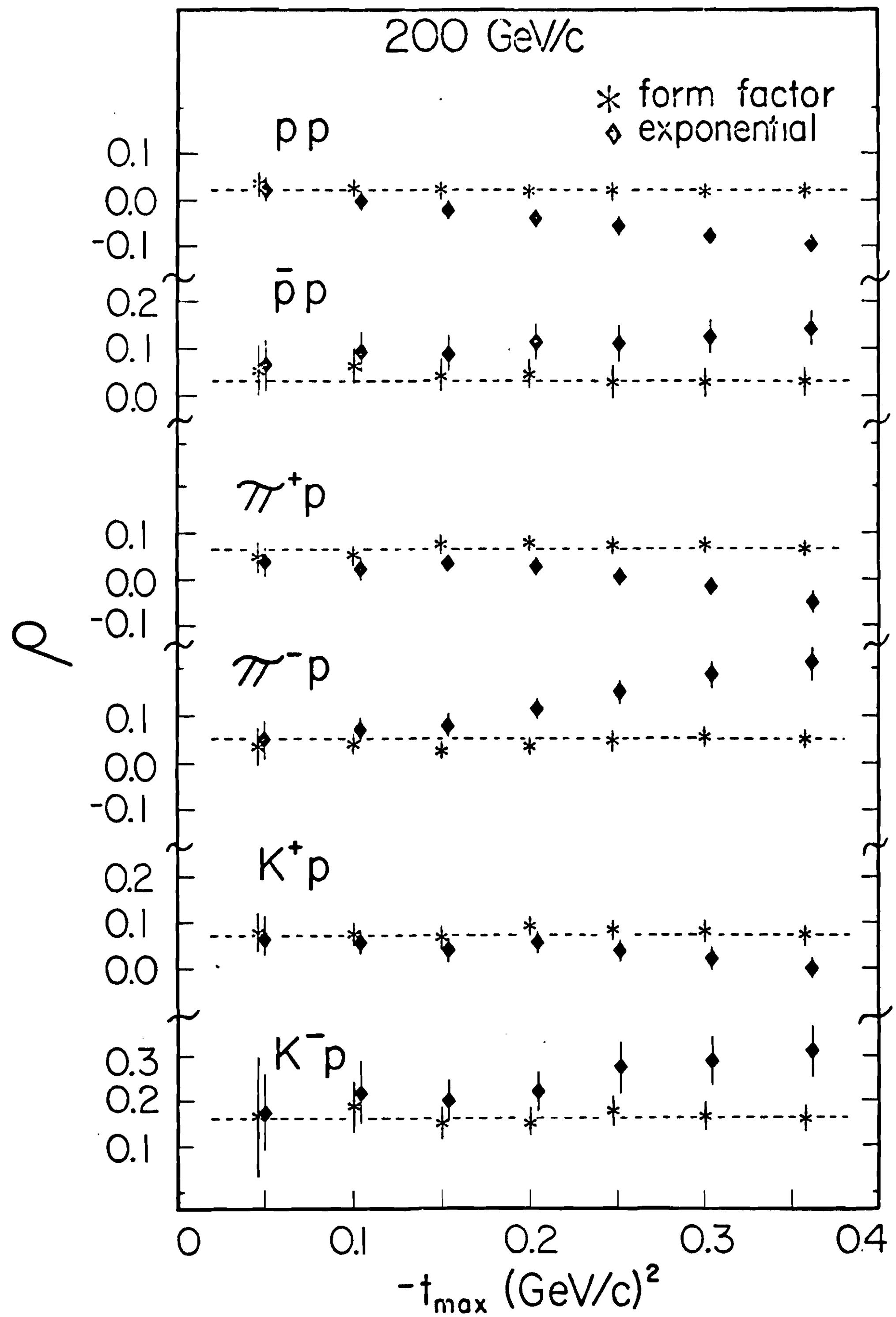
200 GeV/c
form factor
exponential
p p
p̄ p
π^+p
π^-p
K^+p
K^-p
ρ
0.1
0.0
-0.1
0.2
0.1
0.0
0.1
0.0
-0.1
0.1
0.0
-0.1
0.2
0.1
0.0
0.3
0.2
0.1
0
0.1
0.2
0.3
0.4
$-t_{max}$ $(GeV/c)^2$

LEGEND FOR TABLES 5.2a-f

Acronym	Description[a]	Units
MOMENTUM	p_{beam}	GeV/c
RHO	ρ ± total error	--
RSTAT,RSYS	statistical,systematic errors on ρ	--
U	u ± total error	$(GeV/c)^{-2}$
USTAT,USYS	statistical,systematic errors on u	$(GeV/c)^{-2}$
AN	A_n ± statistical error	--
SIGT	σ_{tot}	mb
CHI/D.F.	χ^2/degrees of freedom	--
D.F.	degrees of freedom	--
EVENTS (K)	number of events in thousands	--
MPTYERR	$\Delta R_s^{MT}/R_s^{MT}$	--
DR/DU	$d\rho/du$	$(GeV/c)^{2}$
DR/DAN	$d\rho/dA_n$	--
DR/DMPTY	$R_s^{MT}(d\rho/dR_s^{MT})$	--
DR/DSIGT	$d\rho/d\sigma_{tot}$	mb^{-1}
DR/DRA	$d\rho/dr_a$	fm^{-1}
DR/DRP	$d\rho/dr_p$	fm^{-1}
DR/DCMOM	$p_{beam}(d\rho/dp_{beam})$	--
DU/DAN	du/dA_n	$(GeV/c)^{-2}$
DU/DMPTY	$R_s^{MT}(du/dR_s^{MT})$	$(GeV/c)^{-2}$
DU/DSIGT	$du/d\sigma_{tot}$	$(GeV/c)^{-2}\ mb^{-1}$
DU/DRA	du/dr_a	$(GeV/c)^{-2}\ fm^{-1}$
DU/DRP	du/dr_p	$(GeV/c)^{-2}\ fm^{-1}$
DU/DCMOM	$p_{beam}(du/dp_{beam})$	$(GeV/c)^{-2}$
DAN/DMPTY	$R_s^{MT}(dA_n/dR_s^{MT})$	--
DAN/DSIGT	$dA_n/d\sigma_{tot}$	mb^{-1}
DAN/DRA	dA_n/dr_a	fm^{-1}
DAN/DRP	dA_n/dr_p	fm^{-1}
DAN/DCMOM	$p_{beam}(dA_n/dp_{beam})$	--
TMIN,TMAX	$-t_{min},-t_{max}$	$(GeV/c)^{2}$

[a]The parameters are defined as follows: ρ,u,σ_{tot} in Eq. 1.7; r_a,r_p in Eq. 1.3; R_s on page 83; A_n on page 86.

TABLE 5.2a

pp

RESULTS FOR P+ P SCATTERING

MOMENTUM	70	100	125	150	175	200
RHO	-0.115±0.015	-0.074±0.018	-0.024±0.014	0.008±0.012	-0.011±0.019	0.019±0.016
RSTAT,RSYS	0.013 0.008	0.016 0.007	0.013 0.005	0.010 0.006	0.017 0.007	0.014 0.009
U	0.460 --	1.035±0.142	1.247±0.092	1.369±0.059	1.539±0.087	1.839±0.049
USTAT,USYS	-- --	0.141 0.018	0.092 0.006	0.059 0.007	0.087 0.007	0.048 0.004
AN	1.006±0.008	1.037±0.011	1.031±0.007	1.035±0.005	1.038±0.008	1.106±0.005
SIGT	38.280	38.460	38.600	38.690	38.850	38.970
CHI/D.F.	0.703	1.003	0.769	1.065	1.150	1.015
D.F.	104	124	120	137	92	112
EVENTS (K)	157	178	229	385	124	282
MPTYERR	0.043	0.035	0.037	0.036	0.030	0.031
DR/DU	0.056	0.083	0.093	0.105	0.116	0.149
DR/DAN	1.436	1.300	1.455	1.534	1.588	1.471
DR/DMPTY	0.069	0.065	0.094	0.107	0.119	0.246
DR/DSIGT	-0.026	-0.029	-0.024	-0.020	-0.020	-0.016
DR/DRA	--	--	--	--	--	--
DR/DRP	1.366	0.100	0.145	0.202	0.274	0.465
DR/DCMOM	-2.068	-2.284	-1.881	-1.526	-1.568	-1.263
DU/DAN	--	11.247	11.029	10.653	9.357	8.087
DU/DMPTY	--	-0.259	-0.088	-0.012	0.027	0.060
DU/DSIGT	--	-0.073	-0.046	-0.029	-0.024	-0.013
DU/DRA	--	--	--	--	--	--
DU/DRP	--	-23.772	-22.885	-22.064	-21.405	-19.905
DU/DCMOM	--	-5.321	-3.383	-2.148	-1.836	-1.031
DAN/DMPTY	0.003	-0.019	-0.011	-0.010	0.000	-0.005
DAN/DSIGT	-0.062	-0.066	-0.060	-0.057	-0.058	-0.059
DAN/DRA	--	--	--	--	--	--
DAN/DRP	1.271	0.118	0.146	0.177	0.231	0.335
DAN/DCMOM	-1.802	-1.990	-1.586	-1.334	-1.395	-1.274
TMIN,TMAX	0.0018 0.0625	0.0016 0.1225	0.0015 0.1592	0.0015 0.2025	0.0016 0.2500	0.0016 0.3600

TABLE 5.2b $\pi^+ p$

RESULTS FOR PI+ P SCATTERING

MOMENTUM	70	100	125	150	175	200
RHO	-0.025±0.016	-0.003±0.020	0.052±0.014	0.058±0.014	0.035±0.018	0.053±0.017
RSTAT,RSYS	0.012 0.010	0.018 0.009	0.013 0.005	0.011 0.008	0.015 0.009	0.014 0.009
U	0.300 --	0.505±0.200	0.870±0.120	0.867±0.084	0.970±0.097	1.152±0.062
USTAT,USYS	-- --	0.198 0.026	0.119 0.011	0.083 0.013	0.096 0.012	0.062 0.007
AN	1.021±0.008	1.041±0.014	1.054±0.009	1.048±0.007	1.044±0.009	1.103±0.007
SIGT	23.220	23.330	23.430	23.500	23.710	23.840
CHI/D.F.	0.736	1.009	0.930	0.986	1.260	1.549
D.F.	104	124	120	137	92	112
EVENTS (K)	107	120	147	187	100	144
MPTYERR	0.051	0.035	0.037	0.039	0.029	0.031
DR/DU	0.048	0.075	0.079	0.091	0.106	0.131
DR/DAN	1.247	1.162	1.218	1.282	1.328	1.256
DR/DMPTY	0.059	0.064	0.062	0.094	0.100	0.193
DR/DSIGT	-0.055	-0.064	-0.053	-0.047	-0.047	-0.038
DR/DRA	0.509	0.064	0.080	0.111	0.158	0.234
DR/DRP	0.592	0.044	0.059	0.087	0.128	0.202
DR/DCMOM	-2.609	-2.992	-2.505	-2.159	-2.223	-1.777
DU/DAN	--	12.835	12.178	10.958	9.392	7.677
DU/DMPTY	--	-0.224	-0.172	0.008	0.038	0.049
DU/DSIGT	--	-0.208	-0.138	-0.093	-0.074	-0.041
DU/DRA	--	-9.495	-9.016	-8.538	-8.090	-7.337
DU/DRP	--	-11.756	-11.340	-10.912	-10.503	-9.776
DU/DCMOM	--	-8.279	-5.948	-4.061	-3.314	-1.855
DAN/DMPTY	-0.009	-0.025	-0.030	-0.014	-0.006	-0.015
DAN/DSIGT	-0.103	-0.113	-0.103	-0.098	-0.098	-0.097
DAN/DRA	0.506	0.080	0.092	0.113	0.151	0.208
DAN/DRP	0.587	0.064	0.075	0.094	0.128	0.183
DAN/DCMOM	-1.831	-2.196	-1.732	-1.508	-1.571	-1.378
TMIN,TMAX	0.0018 0.0625	0.0016 0.1225	0.0015 0.1592	0.0015 0.2025	0.0016 0.2500	0.0016 0.3600

RESULTS FOR K+ P SCATTERING

MOMENTUM	70	100	125	150	175	200
RHO	0.013±0.026	0.065±0.026	0.061±0.023	0.067±0.021	0.029±0.024	0.071±0.021
RSTAT,RSYS	0.023 0.011	0.025 0.009	0.023 0.005	0.020 0.009	0.022 0.009	0.019 0.009
U	0.400 --	1.291±0.309	1.070±0.219	1.209±0.155	1.246±0.140	1.784±0.090
USTAT,USYS	-- --	0.308 0.022	0.218 0.010	0.154 0.015	0.139 0.012	0.089 0.009
AN	0.998±0.017	1.068±0.021	1.026±0.016	1.043±0.013	1.005±0.014	1.096±0.010
SIGT	18.520	18.880	19.180	19.360	19.680	19.900
CHI/D.F.	0.807	0.928	1.316	0.865	1.272	1.301
D.F.	104	124	120	137	92	112
EVENTS (K)	25	51	45	54	44	64
MPTYERR	0.041	0.035	0.038	0.040	0.030	0.031
DR/DU	0.048	0.067	0.081	0.091	0.108	0.125
DR/DAN	1.217	1.102	1.215	1.241	1.317	1.200
DR/DMPTY	0.056	0.050	0.067	0.077	0.086	0.162
DR/DSIGT	-0.083	-0.078	-0.073	-0.063	-0.061	-0.051
DR/DRA	0.382	0.015	0.029	0.045	0.067	0.104
DR/DRP	0.588	0.034	0.059	0.088	0.128	0.191
DR/DCMOM	-3.080	-2.821	-2.728	-2.408	-2.395	-1.996
DU/DAN	--	14.071	12.095	10.713	8.872	7.652
DU/DMPTY	--	-0.332	-0.108	-0.073	-0.033	0.071
DU/DSIGT	--	-0.217	-0.171	-0.129	-0.088	-0.059
DU/DRA	--	-7.695	-7.445	-7.201	-6.966	-6.567
DU/DRP	--	-11.736	-11.276	-10.834	-10.415	-9.715
DU/DCMOM	--	-6.245	-5.582	-4.494	-3.122	-2.196
DAN/DMPTY	-0.009	-0.041	-0.024	-0.023	-0.013	-0.016
DAN/DSIGT	-0.126	-0.132	-0.123	-0.120	-0.115	-0.116
DAN/DRA	0.366	0.031	0.042	0.055	0.073	0.102
DAN/DRP	0.565	0.059	0.078	0.102	0.135	0.185
DAN/DCMOM	-1.810	-1.796	-1.714	-1.584	-1.594	-1.405
TMIN,TMAX	0.0018 0.0625	0.0016 0.1225	0.0015 0.1592	0.0015 0.2025	0.0016 0.2500	0.0016 0.3600

TABLE 5.2c

K^+p

TABLE 5.2d $p\bar{p}$

RESULTS FOR P- P SCATTERING

MOMENTUM	70	125	150	175	200
RHO	0.010±0.018	0.012±0.020	-0.001±0.028	0.067±0.039	0.029±0.030
RSTAT,RSYS	0.017 0.006	0.019 0.006	0.027 0.005	0.038 0.007	0.028 0.011
U	2.080 --	2.370±0.139	2.427±0.160	2.942±0.187	2.591±0.097
USTAT,USYS	-- --	0.138 0.011	0.160 0.007	0.187 0.006	0.097 0.004
AN	0.944±0.008	1.062±0.011	1.026±0.013	1.016±0.020	1.112±0.012
SIGT	43.050	41.710	41.790	41.650	41.440
CHI/D.F.	1.252	0.995	0.952	1.025	1.068
D.F.	104	120	137	92	112
EVENTS (K)	58	95	48	31	72
MPTYERR	0.064	0.042	0.054	0.031	0.030
DR/DU	-0.045	-0.087	-0.100	-0.119	-0.151
DR/DAN	-1.584	-1.455	-1.608	-1.658	-1.723
DR/DMPTY	-0.052	-0.073	-0.088	-0.120	-0.308
DR/DSIGT	0.017	0.021	0.017	0.020	0.017
DR/DRA	--	--	--	--	--
DR/DRP	-1.116	-0.137	-0.198	-0.268	-0.448
DR/DCMOM	1.464	1.727	1.435	1.688	1.358
DU/DAN	--	11.655	11.324	8.239	7.214
DU/DMPTY	--	-0.147	-0.123	0.012	0.022
DU/DSIGT	--	-0.039	-0.024	-0.023	-0.012
DU/DRA	--	--	--	--	--
DU/DRP	--	-22.984	-22.205	-21.811	-20.310
DU/DCMOM	--	-3.147	-1.977	-1.867	-1.043
DAN/DMPTY	-0.014	-0.019	-0.018	0.015	0.022
DAN/DSIGT	-0.047	-0.056	-0.052	-0.055	-0.057
DAN/DRA	--	--	--	--	--
DAN/DRP	0.866	0.138	0.167	0.234	0.351
DAN/DCMOM	-1.205	-1.531	-1.303	-1.549	-1.420
TMIN,TMAX	0.0018 0.0625	0.0015 0.1592	0.0015 0.2025	0.0016 0.2500	0.0016 0.3600

TABLE 5.2e $\pi^- p$

RESULTS FOR PI- P SCATTERING

MOMENTUM	70	125	150	175	200
RHO	0.027±0.016	0.035±0.017	0.027±0.018	0.054±0.016	0.064±0.020
RSTAT,RSYS	0.013 0.010	0.015 0.009	0.017 0.007	0.013 0.009	0.017 0.012
U	0.310 --	0.868±0.115	1.033±0.102	1.306±0.071	1.331±0.060
USTAT,USYS	-- --	0.114 0.016	0.102 0.006	0.071 0.010	0.059 0.007
AN	0.934±0.008	1.066±0.011	1.058±0.011	1.030±0.009	1.105±0.010
SIGT	24.000	24.070	24.110	24.230	24.330
CHI/D.F.	1.106	1.015	0.958	1.270	0.973
D.F.	104	120	137	92	112
EVENTS (K)	107	175	141	216	187
MPTYERR	0.063	0.041	0.052	0.024	0.028
DR/DU	-0.048	-0.098	-0.112	-0.126	-0.172
DR/DAN	-1.394	-1.211	-1.319	-1.351	-1.433
DR/DMPTY	-0.055	-0.066	-0.108	-0.091	-0.296
DR/DSIGT	0.051	0.057	0.050	0.051	0.045
DR/DRA	-0.521	-0.104	-0.145	-0.186	-0.314
DR/DRP	-0.606	-0.079	-0.116	-0.153	-0.273
DR/DCMOM	2.467	2.761	2.396	2.517	2.197
DU/DAN	--	9.361	8.451	7.291	5.125
DU/DMPTY	--	-0.133	-0.009	0.004	0.108
DU/DSIGT	--	-0.117	-0.081	-0.068	-0.038
DU/DRA	--	-8.963	-8.463	-8.142	-7.285
DU/DRP	--	-11.296	-10.849	-10.551	-9.734
DU/DCMOM	--	-4.913	-3.538	-2.998	-1.730
DAN/DMPTY	-0.010	-0.015	0.000	0.006	0.055
DAN/DSIGT	-0.090	-0.109	-0.104	-0.102	-0.106
DAN/DRA	0.469	0.119	0.151	0.185	0.300
DAN/DRP	0.545	0.097	0.125	0.157	0.263
DAN/DCMOM	-1.621	-2.148	-1.878	-1.961	-1.911
TMIN,TMAX	0.0018 0.0625	0.0015 0.1592	0.0015 0.2025	0.0016 0.2500	0.0016 0.3600

TABLE 5.2f K^-p

RESULTS FOR K- P SCATTERING

MOMENTUM	70	125	150	175	200
RHO	0.171±0.040	0.122±0.029	0.123±0.031	0.125±0.029	0.161±0.032
RSTAT,RSYS	0.039 0.012	0.027 0.009	0.030 0.008	0.027 0.010	0.029 0.014
U	1.400 --	1.610±0.170	1.909±0.153	2.095±0.126	1.959±0.084
USTAT,USYS	-- --	0.170 0.007	0.153 0.004	0.126 0.006	0.084 0.006
AN	0.863±0.027	1.026±0.022	1.013±0.023	1.008±0.020	1.054±0.021
SIGT	20.380	20.590	20.600	20.670	20.760
CHI/D.F.	1.016	1.043	1.079	1.349	1.147
D.F.	104	120	137	92	112
EVENTS (K)	23	97	73	75	95
MPTYERR	0.064	0.041	0.052	0.024	0.028
DR/DU	-0.064	-0.128	-0.142	-0.153	-0.221
DR/DAN	-1.372	-1.176	-1.256	-1.269	-1.309
DR/DMPTY	-0.072	-0.075	-0.119	-0.085	-0.332
DR/DSIGT	0.079	0.078	0.074	0.073	0.069
DR/DRA	-0.524	-0.061	-0.091	-0.106	-0.205
DR/DRP	-0.808	-0.118	-0.159	-0.199	-0.372
DR/DCMOM	2.986	2.906	2.906	2.929	2.839
DU/DAN	--	7.058	6.156	5.614	3.455
DU/DMPTY	--	-0.150	0.008	-0.042	0.111
DU/DSIGT	--	-0.070	-0.078	-0.064	-0.041
DU/DRA	--	-7.392	-7.141	-6.989	-6.494
DU/DRP	--	-11.176	-10.769	-10.452	-9.582
DU/DCMOM	--	-0.741	-2.182	-1.762	-1.321
DAN/DMPTY	0.011	0.001	0.026	0.013	0.131
DAN/DSIGT	-0.114	-0.133	-0.131	-0.129	-0.135
DAN/DRA	0.463	0.074	0.098	0.112	0.207
DAN/DRP	0.717	0.137	0.172	0.207	0.372
DAN/DCMOM	-1.941	-2.252	-2.331	-2.317	-2.488
TMIN,TMAX	0.0018 0.0625	0.0015 0.1592	0.0015 0.2025	0.0016 0.2500	0.0016 0.3600

Figure 5.5a

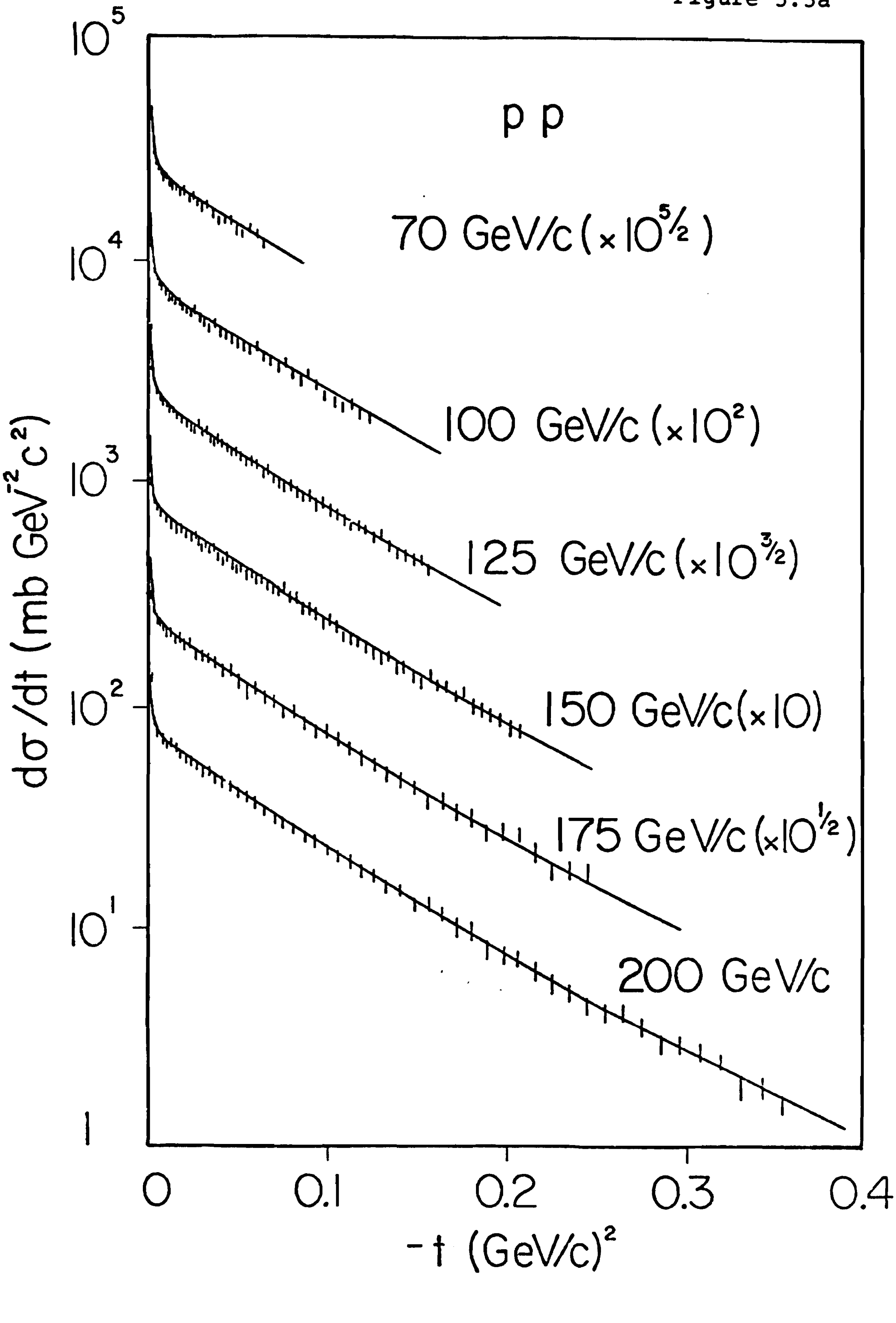
p p
70 GeV/c (×10^5/2)
100 GeV/c (×10^2)
125 GeV/c (×10^3/2)
150 GeV/c (×10)
175 GeV/c (×10^1/2)
200 GeV/c
10^5
10^4
10^3
10^2
10^1
1
dσ/dt (mb GeV^-2 c^2)
0
0.1
0.2
0.3
0.4
-t (GeV/c)^2

Figure 5.5b

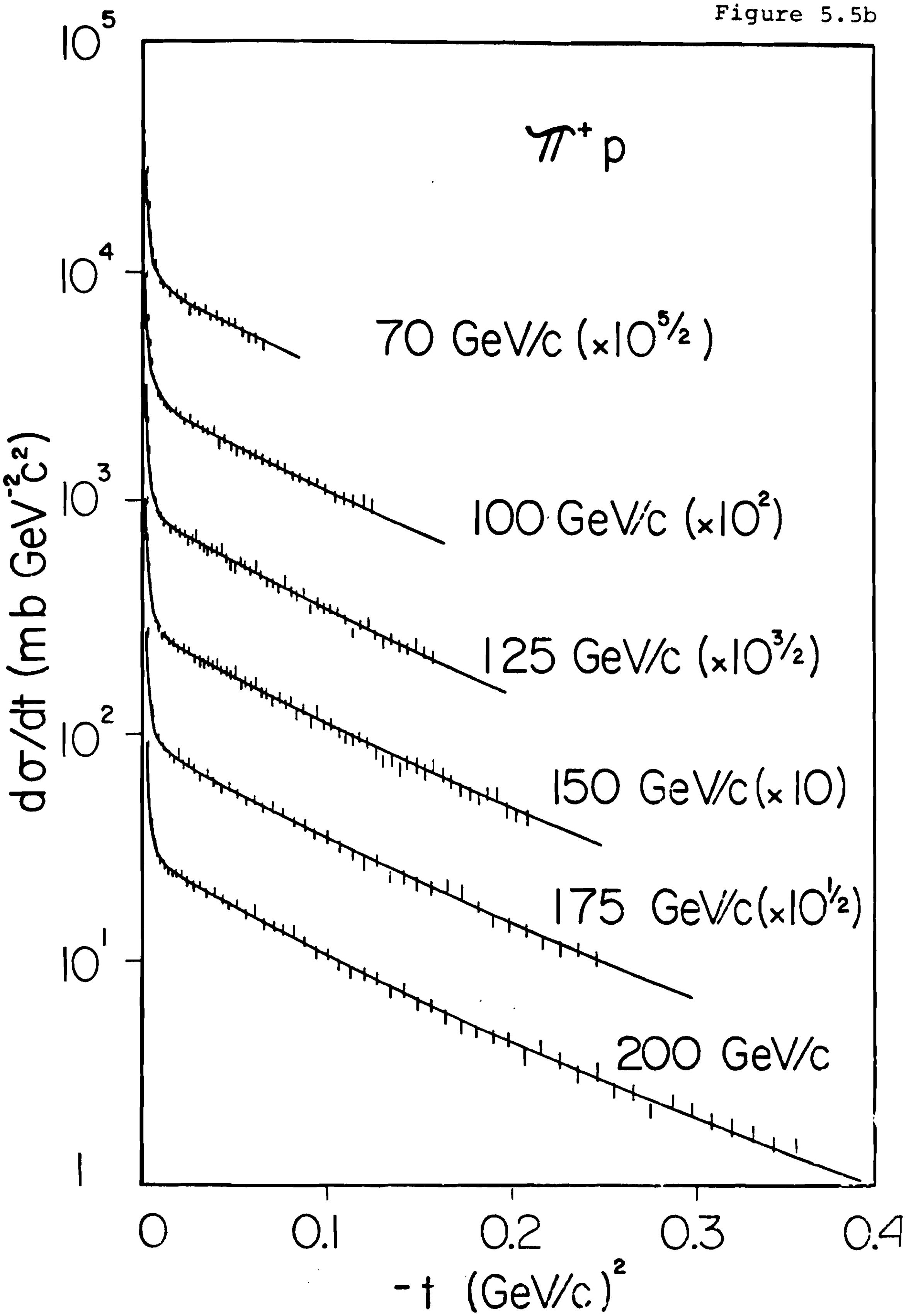
$\pi^+ p$
70 GeV/c ($\times 10^{5/2}$)
100 GeV/c ($\times 10^{2}$)
125 GeV/c ($\times 10^{3/2}$)
150 GeV/c ($\times$ 10)
175 GeV/c ($\times 10^{1/2}$)
200 GeV/c
$d\sigma/dt$ (mb GeV^{-2}c^{2})
$-t$ (GeV/c)^2
10^5
10^4
10^3
10^2
10^1
1
0
0.1
0.2
0.3
0.4

Figure 5.5c

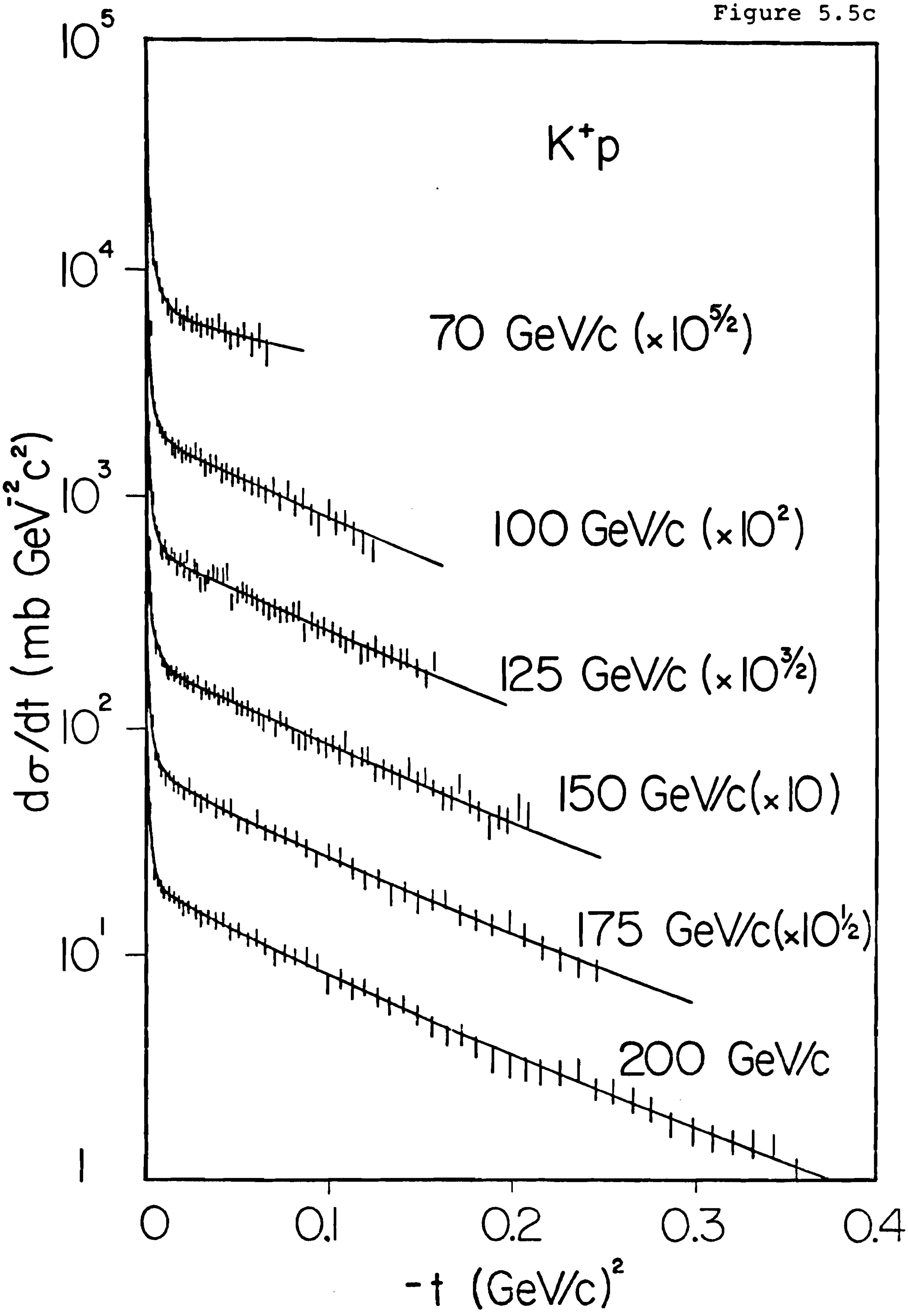
K⁺p
70 GeV/c ($\times 10^{5/2}$)
100 GeV/c ($\times 10^{2}$)
125 GeV/c ($\times 10^{3/2}$)
150 GeV/c($\times 10$)
175 GeV/c($\times 10^{1/2}$)
200 GeV/c
$d\sigma/dt$ (mb $GeV^{-2}c^{2}$)
$-t$ $(GeV/c)^2$
10^5
10^4
10^3
10^2
10^1
1
0
0.1
0.2
0.3
0.4

Figure 5.5d

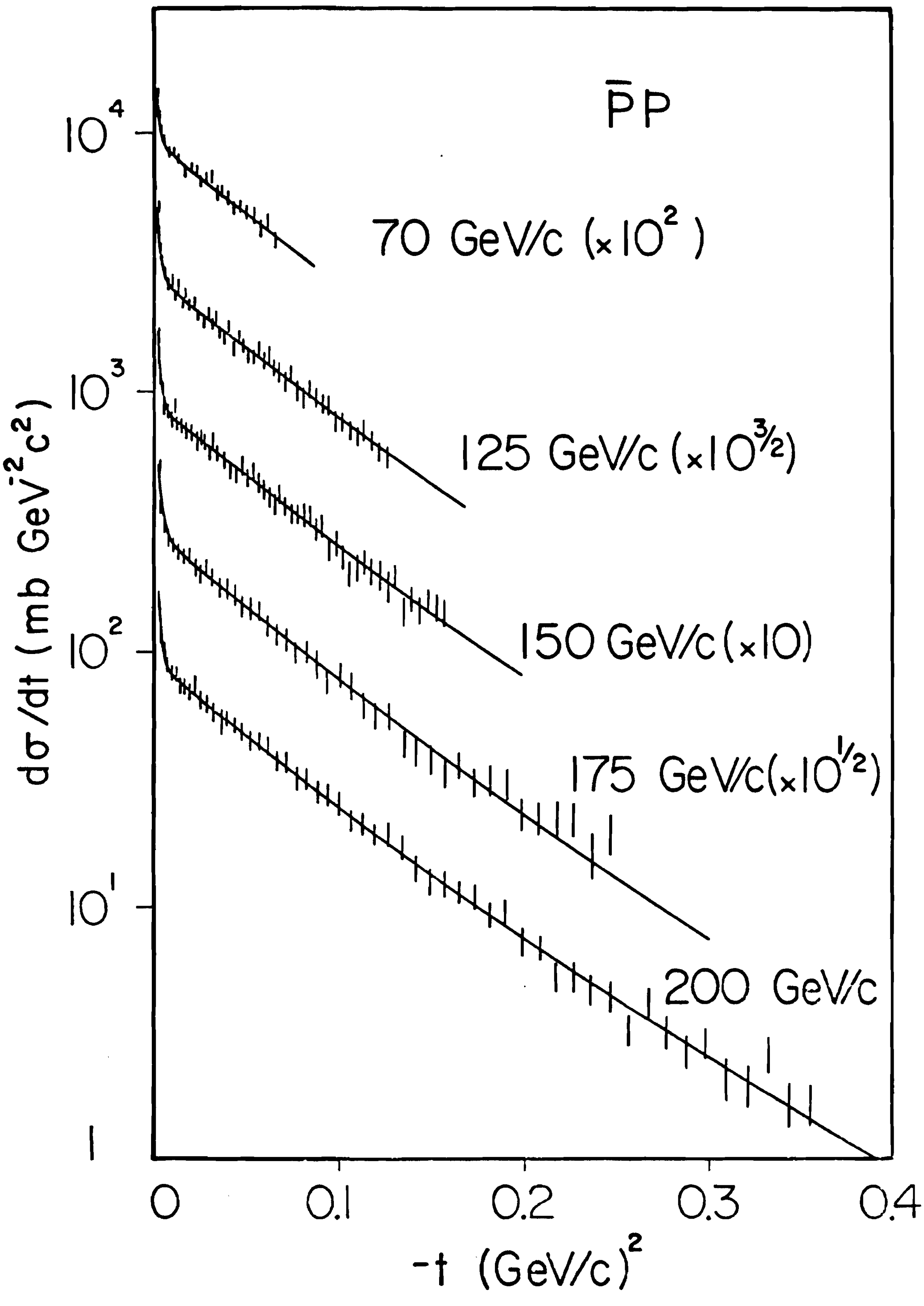

$\bar{P}P$
70 GeV/c ($\times 10^2$)
125 GeV/c ($\times 10^{3/2}$)
150 GeV/c ($\times 10$)
175 GeV/c ($\times 10^{1/2}$)
200 GeV/c
10^4
10^3
10^2
10^1
1
$d\sigma/dt$ (mb $GeV^{-2}c^2$)
0
0.1
0.2
0.3
0.4
$-t$ $(GeV/c)^2$

Figure 5.5e

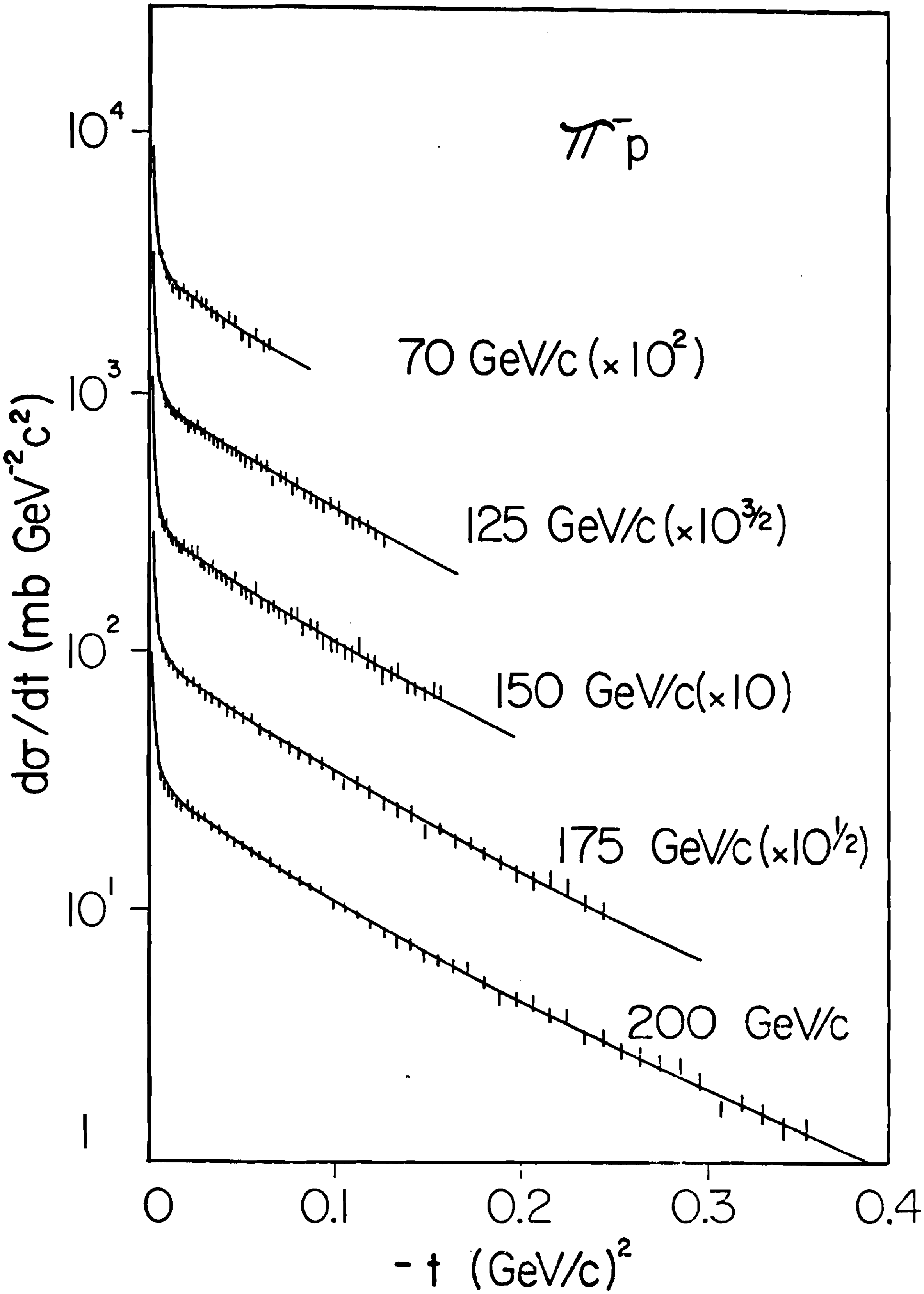

$\pi^- p$
70 GeV/c (×10²)
125 GeV/c (×10^{3/2})
150 GeV/c(×10)
175 GeV/c (×10^{1/2})
200 GeV/c
dσ/dt (mb GeV⁻²c²)
10⁴
10³
10²
10¹
1
0
0.1
0.2
0.3
0.4
-t (GeV/c)²

Figure 5.5f

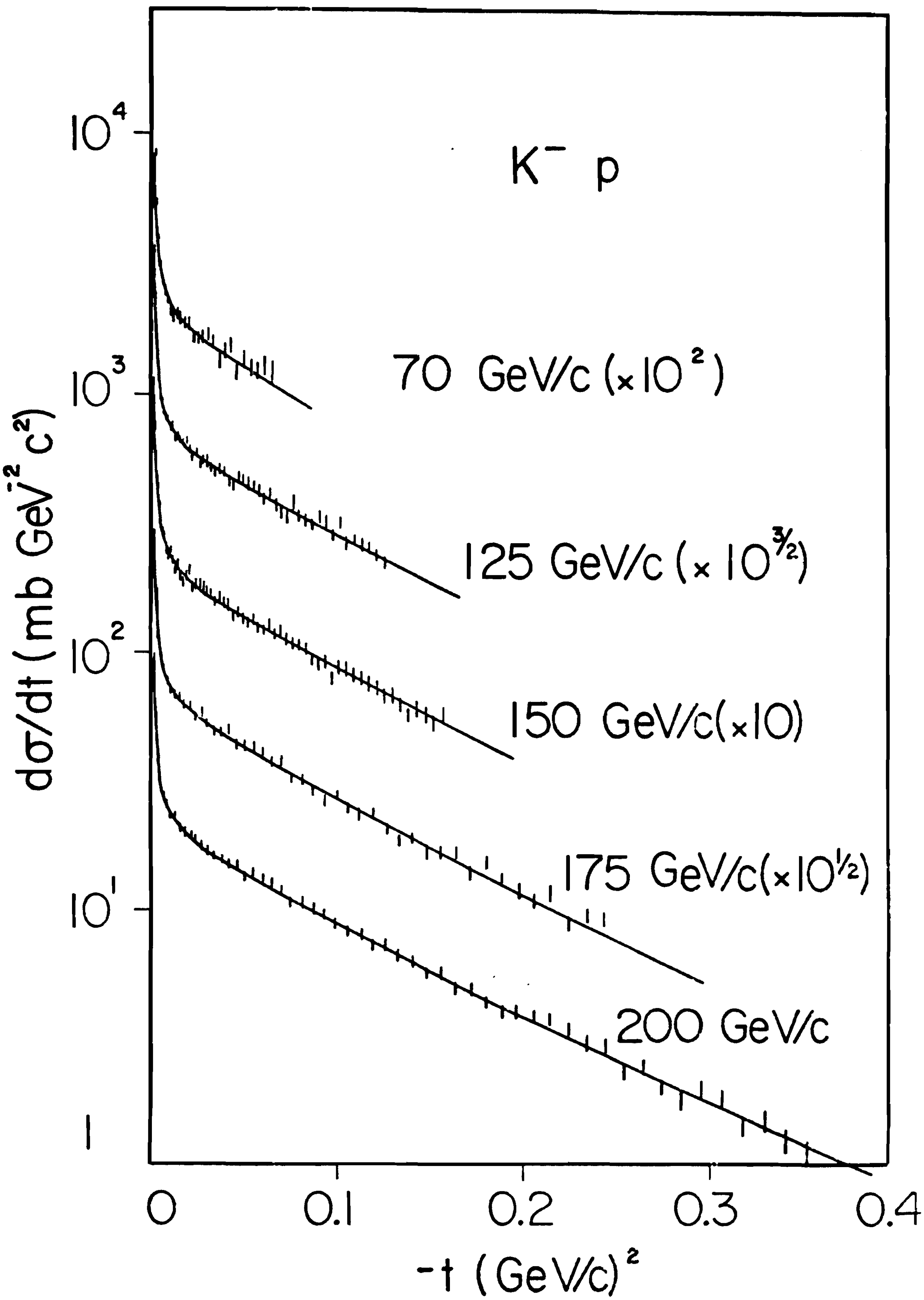

K⁻ p
70 GeV/c (×10²)
125 GeV/c (× 10^3/2)
150 GeV/c(×10)
175 GeV/c(×10^1/2)
200 GeV/c
dσ/dt (mb GeV⁻² c²)
10⁴
10³
10²
10¹
1
0
0.1
0.2
0.3
0.4
-t (GeV/c)²

at all six momenta. In Figs. 5.6a-f we compare the data and the fitted form factor cross sections divided by the fitted form factor cross section but with $\rho = 0$. With the parameters of Tables 5.2a-f the data cross sections were corrected per Eq. 4.2 and are found in Appendix C.

Systematics

The value of ρ was found to be insensitive to lower limit of the fitting range. This can be seen most readily in Figs. 5.6a-f, where the exclusion of a few points at small -t does not significantly alter the resulting fit. Studies were also made to determine the sensitivity of the results to variations of the more important cuts. Cuts 13 through 17 as described in Chapter 4 were applied one at a time to both data and Monte Carlo distributions. New fits were made for all particles at all energies and the resulting values of ρ, u, and A_n were all within the statistical errors of our final results. We emphasize that the data for three particles of like charge at a given momentum had the same cuts applied. In addition only the veto cut varied significantly between momenta due to the changing veto size.

We believe that the normalization parameter, A_n, was needed to compensate for losses of BEAM events due to PWC inefficiencies. Although the Monte Carlo simulated the t dependent effects of these inefficiencies (Cut 11 in Table 4.7), we had no reliable way of estimating these effects on the over all normalization. We expect that the values of A_n should then be the same for all three particles taken simultaneously. In Tables 5.1 and 5.2 we see that the values of A_n are in good agreement for the like charge particles at a given momentum.

Figure 5.6a

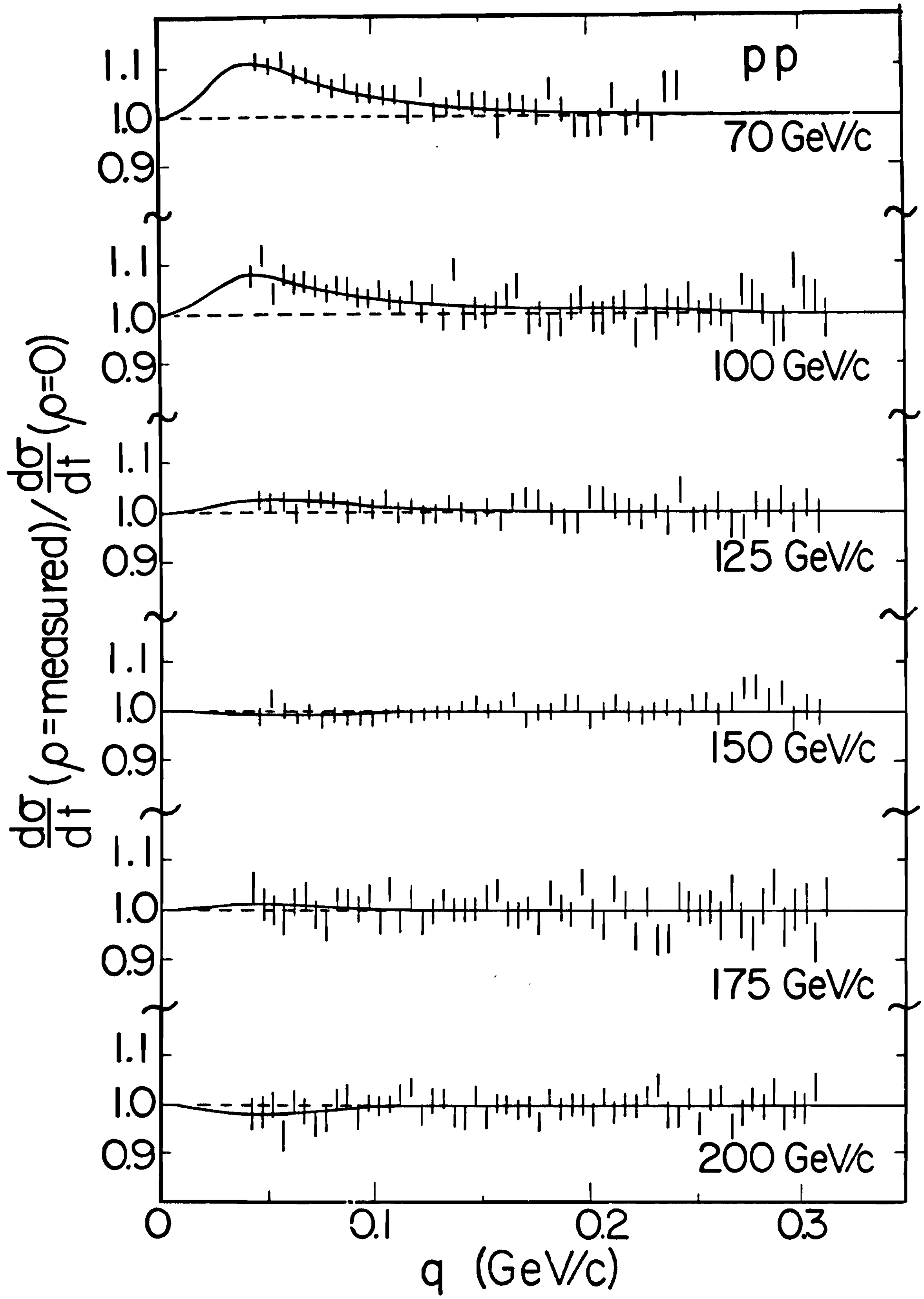
pp
1.1
1.0
0.9
70 GeV/c
100 GeV/c
125 GeV/c
150 GeV/c
175 GeV/c
200 GeV/c
$\frac{d\sigma}{dt}(\rho=\text{measured})/\frac{d\sigma}{dt}(\rho=0)$
0
0.1
0.2
0.3
q (GeV/c)

Figure 5.6b

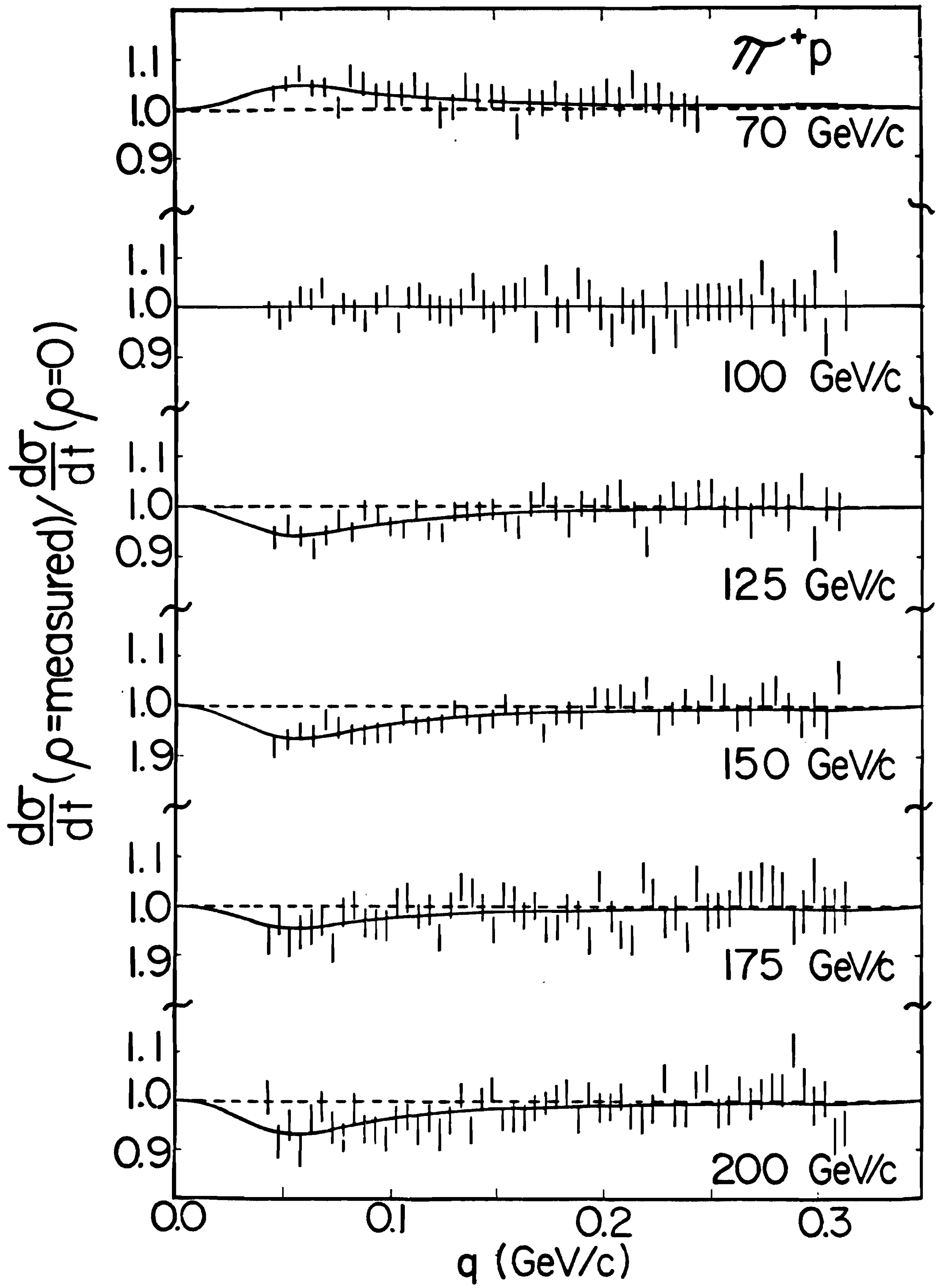
π^+p
70 GeV/c
100 GeV/c
125 GeV/c
150 GeV/c
175 GeV/c
200 GeV/c
1.1
1.0
0.9
$\frac{d\sigma}{dt}(\rho=\text{measured})/\frac{d\sigma}{dt}(\rho=0)$
0.0
0.1
0.2
0.3
q (GeV/c)

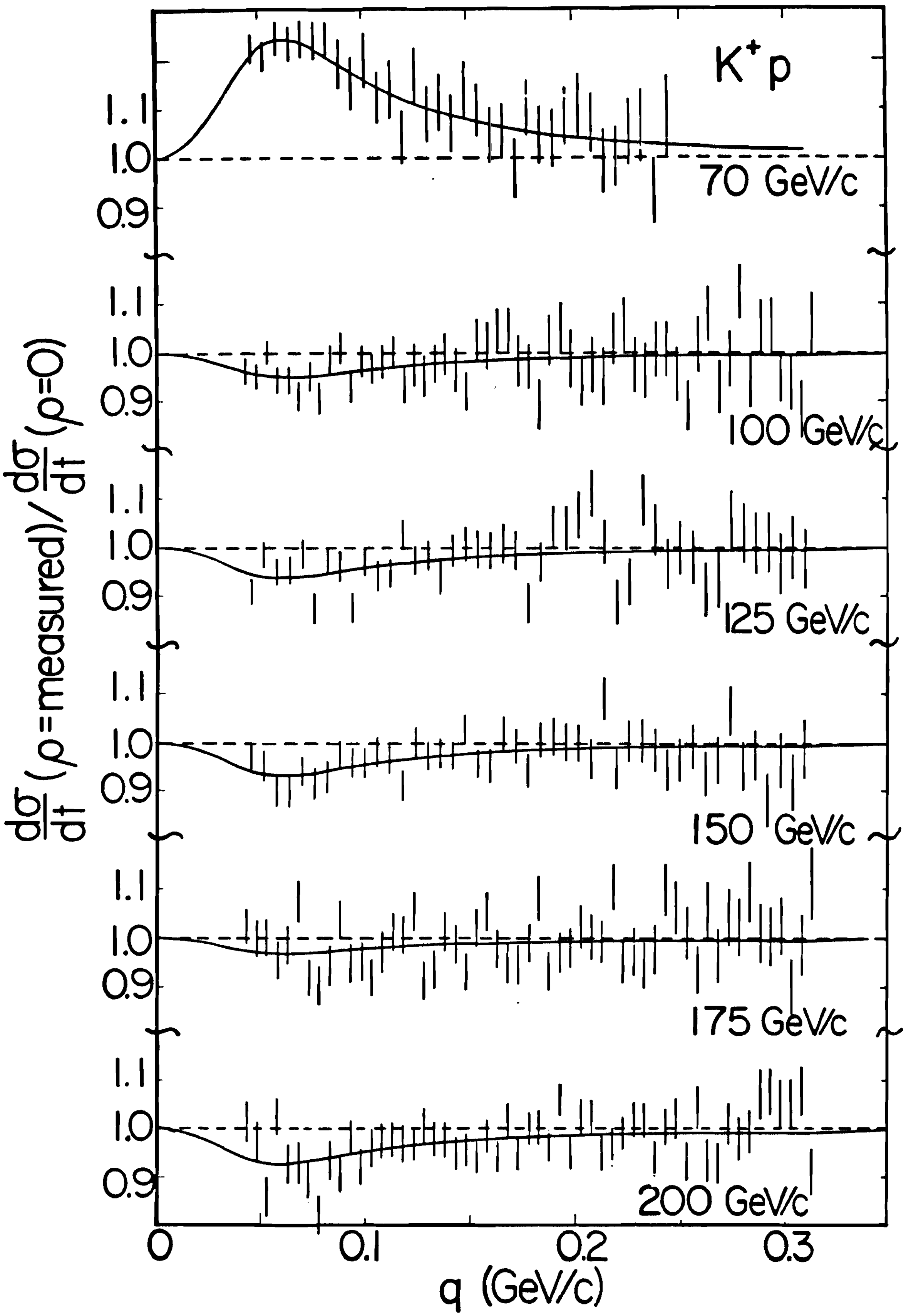
K+p
70 GeV/c
100 GeV/c
125 GeV/c
150 GeV/c
175 GeV/c
200 GeV/c
1.1
1.0
0.9
0
0.1
0.2
0.3
q (GeV/c)
dσ/dt (ρ=measured)/dσ/dt (ρ=0)

Figure 5.6d

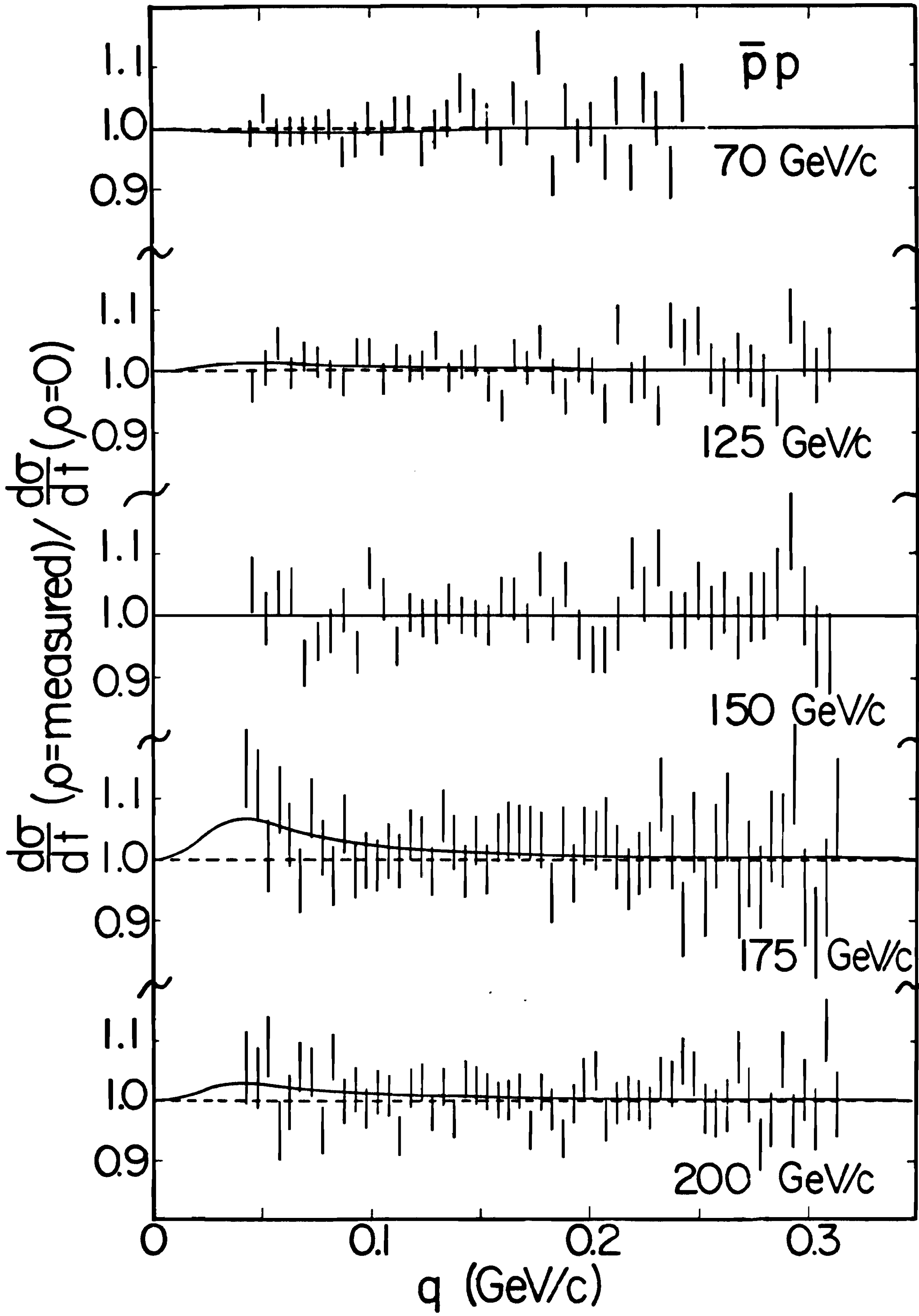

p̄p
70 GeV/c
125 GeV/c
150 GeV/c
175 GeV/c
200 GeV/c
1.1
1.0
0.9
0
0.1
0.2
0.3
q (GeV/c)
$\frac{d\sigma}{dt}(\rho\text{=measured})/\frac{d\sigma}{dt}(\rho\text{=0})$

Figure 5.6e

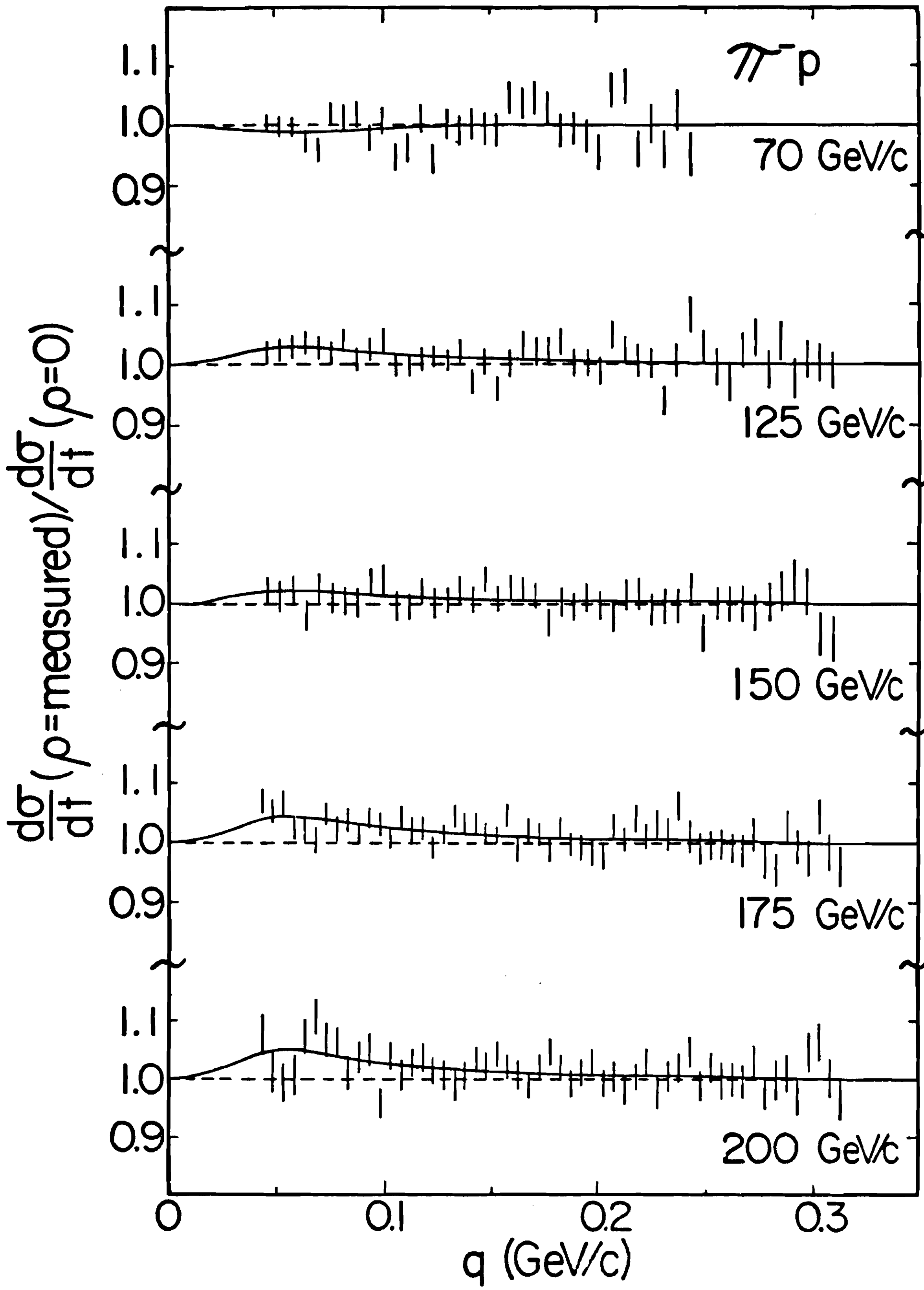
$\pi^- p$
70 GeV/c
125 GeV/c
150 GeV/c
175 GeV/c
200 GeV/c
1.1
1.0
0.9
0
0.1
0.2
0.3
q (GeV/c)
$\frac{d\sigma}{dt}(\rho=\text{measured})/\frac{d\sigma}{dt}(\rho=0)$

Figure 5.6f

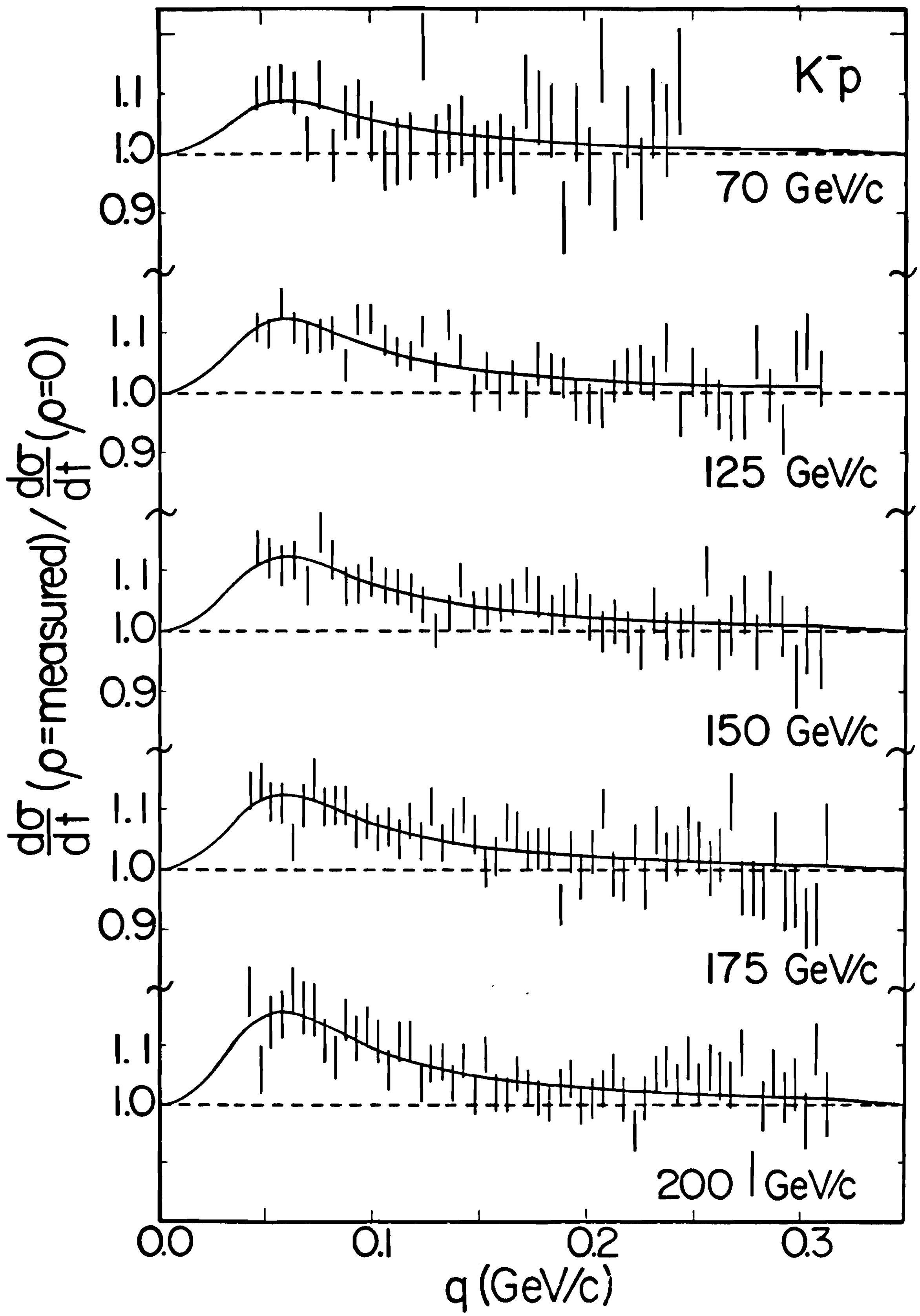

K⁻p
70 GeV/c
125 GeV/c
150 GeV/c
175 GeV/c
200 GeV/c
1.1
1.0
0.9
$\frac{d\sigma}{dt}(\rho=\text{measured})/\frac{d\sigma}{dt}(\rho=0)$
0.0
0.1
0.2
0.3
q (GeV/c)

At 200 GeV/c the beam area was smallest and, therefore, more sensitive to these corrections.

Measurements were also made at 100 GeV/c with negative charge particles. But because of problems during the data acquisition, we have not included them in our results.

In the fitting procedure we found that the statistical errors on ρ, u and A_n are symmetric and parabolic and that the χ^2 contours are smooth and ellipsoidal. The dependence of ρ , u, and A_n on each other and other quantities are given by the derivatives in Tables 5.2a-f. The derivatives $d\rho/du$, $d\rho/A_n$, and du/dA_n were determined by fixing the parameter in the denominator to a different value and allowing the other two parameters to vary. The derivatives with respect to other quantities were determined by allowing all three parameters to vary. We note that $(d\rho/du)\ \sigma_u$ and $(d\rho/dA_n)\ \sigma_{A_n}$ comprise about half of the statistical error of ρ.

The main contributions to the systematic errors come from the uncertainty of the absolute momentum ($\Delta p/p$ was about 0.3%) and the uncertainty of the target empty subtraction (about 3.0%). The largest error to ρ from the momentum uncertainty occurs at 70 GeV/c where it is 0.008. The largest error on ρ due to the target empty subtraction is 0.008 at 200 GeV/c. These two errors add in quadrature to a 0.01 error in ρ which is nearly independent of momentum. Since the total cross sections have uncertainties of 0.05 mb, they contribute very little to the systematic error. We believe the systematic errors are point to point, rather than scale shifts and are added quadratically with our statistical errors to give the total error. The statistical, systematic, and total errors for ρ and u are also included in Tables 5.2a-f.

DISCUSSION

In Figs. 5.7a-f we compare our values of ρ for all six reactions with previous measurements and with the dispersion relation predictions discussed in Chapter 1. For π^+p the values of ρ are quite consistent with the predictions of of Hendrick et. al. and of Hohler, while those of Lipkin are a little low. However for π^-p the values of ρ are more consistent with Lipkin, while those of Hendrick and Hohler seem a little high. For K^+p and K^-p the predictions of Hendrick et. al. and Lipkin fit the data well, while the results of Dumbrajs are somewhat low. The predictions of Lipkin and Hendrick et. al. are in very good agreement with the $\bar{p}p$ real parts.

Our pp results are higher than previous experimental results. We believe that this is due to the steeper slope we have measured in the forward direction. In order to verify this, we fit the data of Jenkins et al. with the form factor cross section. Since their t range is severely limited, we use the logarithmic fit of our values of u to fix the value of u in these fits. In Table 5.3 we present the results of the fits, in which the χ^2's are as good as with their exponential fits. In Fig. 5.8 we have plotted the refitted real parts of Jenkins et al. and see that they are in good agreement with our results.

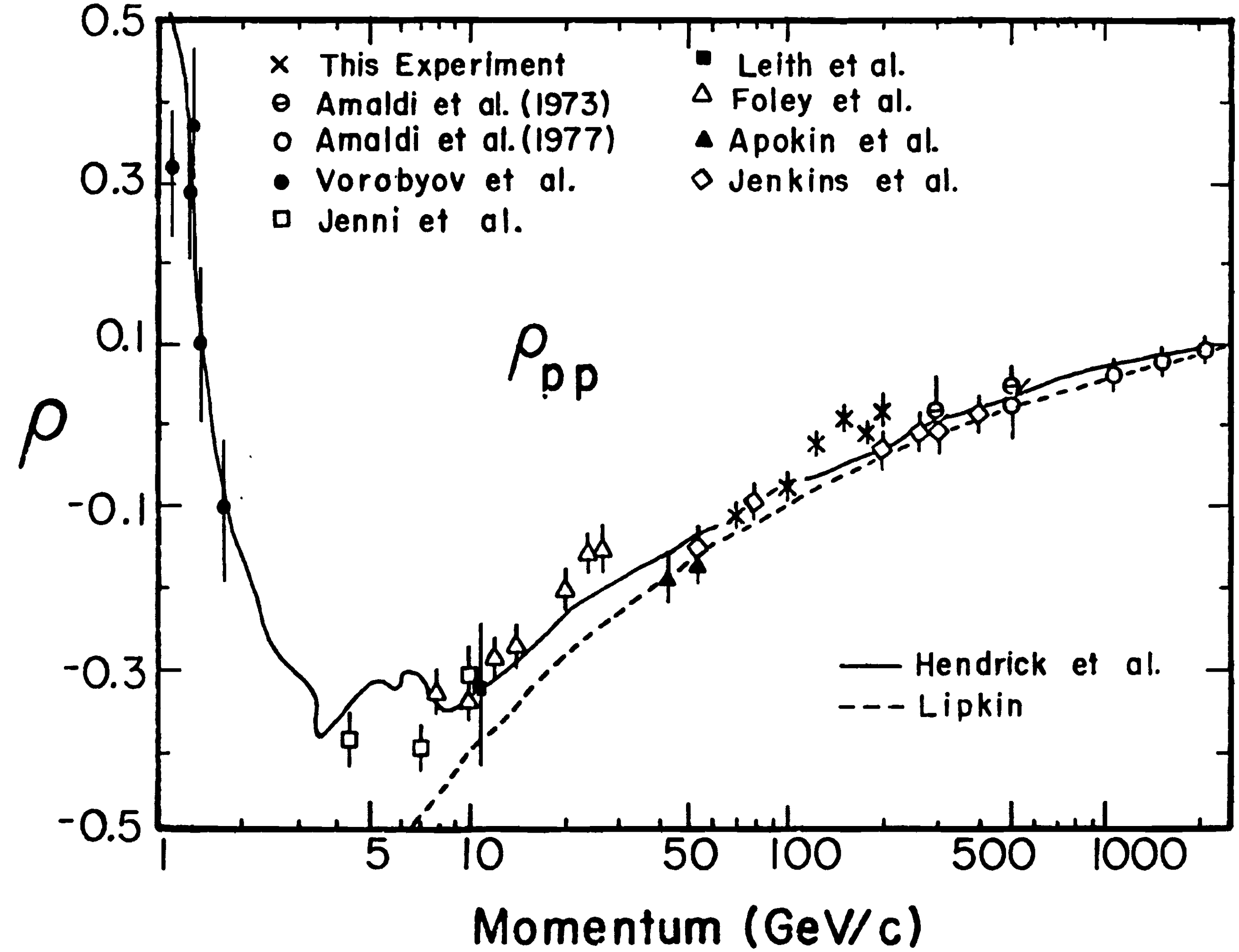
× This Experiment
⊖ Amaldi et al. (1973)
○ Amaldi et al. (1977)
● Vorobyov et al.
□ Jenni et al.
■ Leith et al.
△ Foley et al.
▲ Apokin et al.
◇ Jenkins et al.
Hendrick et al.
Lipkin
ρ_{pp}
ρ
0.5
0.3
0.1
-0.1
-0.3
-0.5
1
5
10
50
100
500
1000
Momentum (GeV/c)

Figure 5.7a

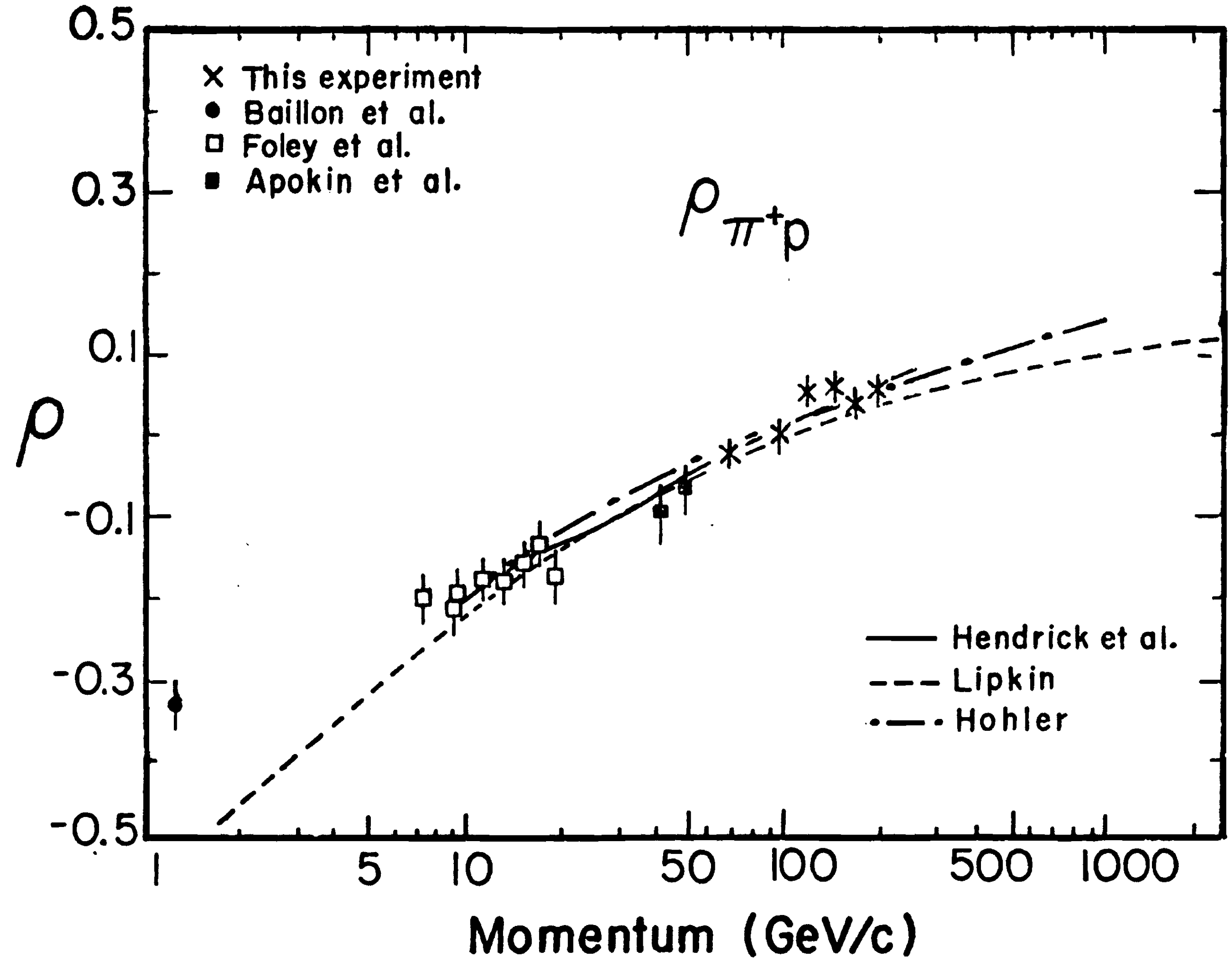
× This experiment
● Baillon et al.
□ Foley et al.
■ Apokin et al.
ρ_{π^+p}
ρ
0.5
0.3
0.1
-0.1
-0.3
-0.5
1
5
10
50
100
500
1000
Momentum (GeV/c)
Hendrick et al.
Lipkin
Hohler

Figure 5.7b

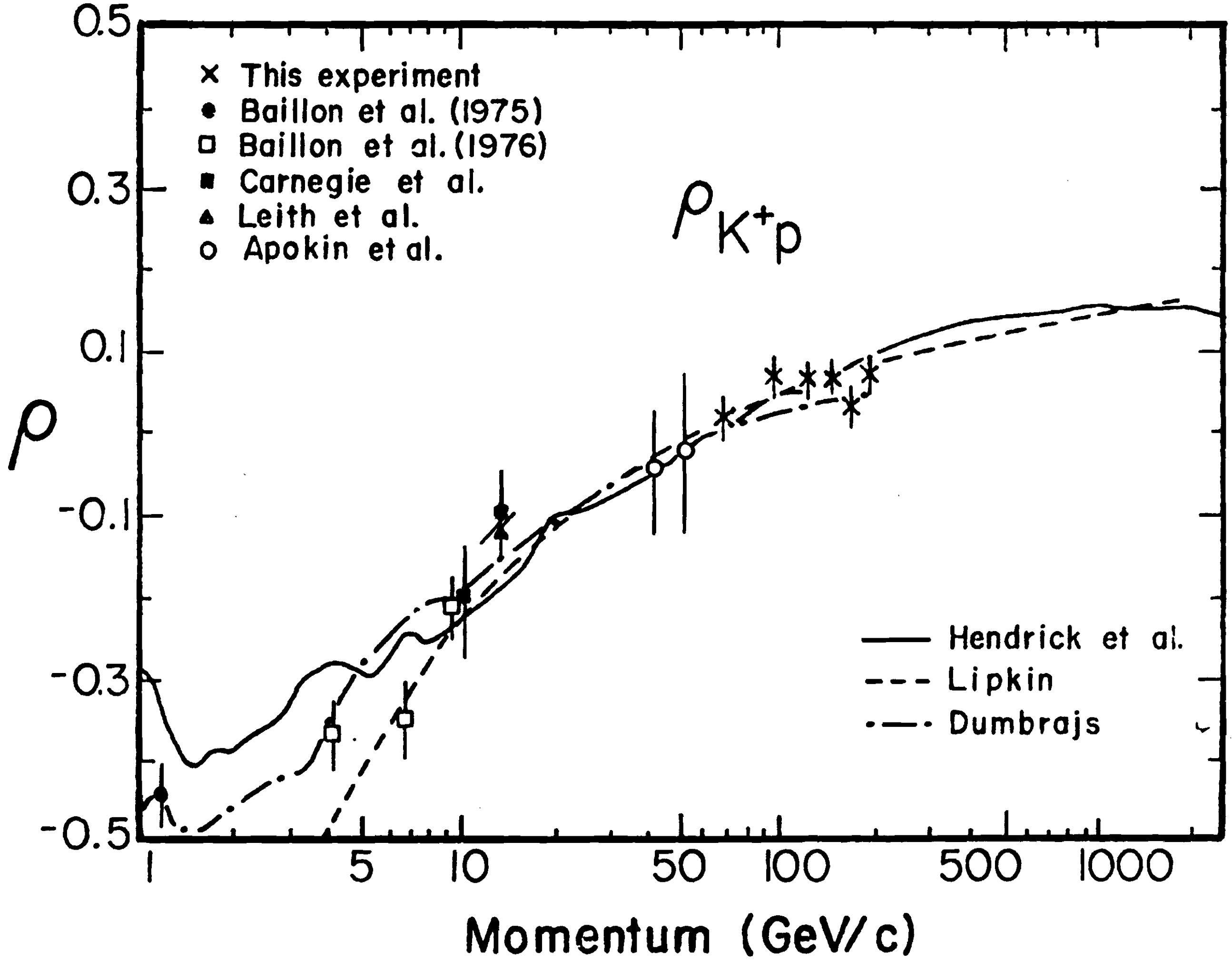
× This experiment
● Baillon et al. (1975)
□ Baillon et al. (1976)
■ Carnegie et al.
▲ Leith et al.
○ Apokin et al.
ρ_{K^+p}
Hendrick et al.
Lipkin
Dumbrajs
ρ
0.5
0.3
0.1
-0.1
-0.3
-0.5
1
5
10
50
100
500
1000
Momentum (GeV/c)

Figure 5.7c

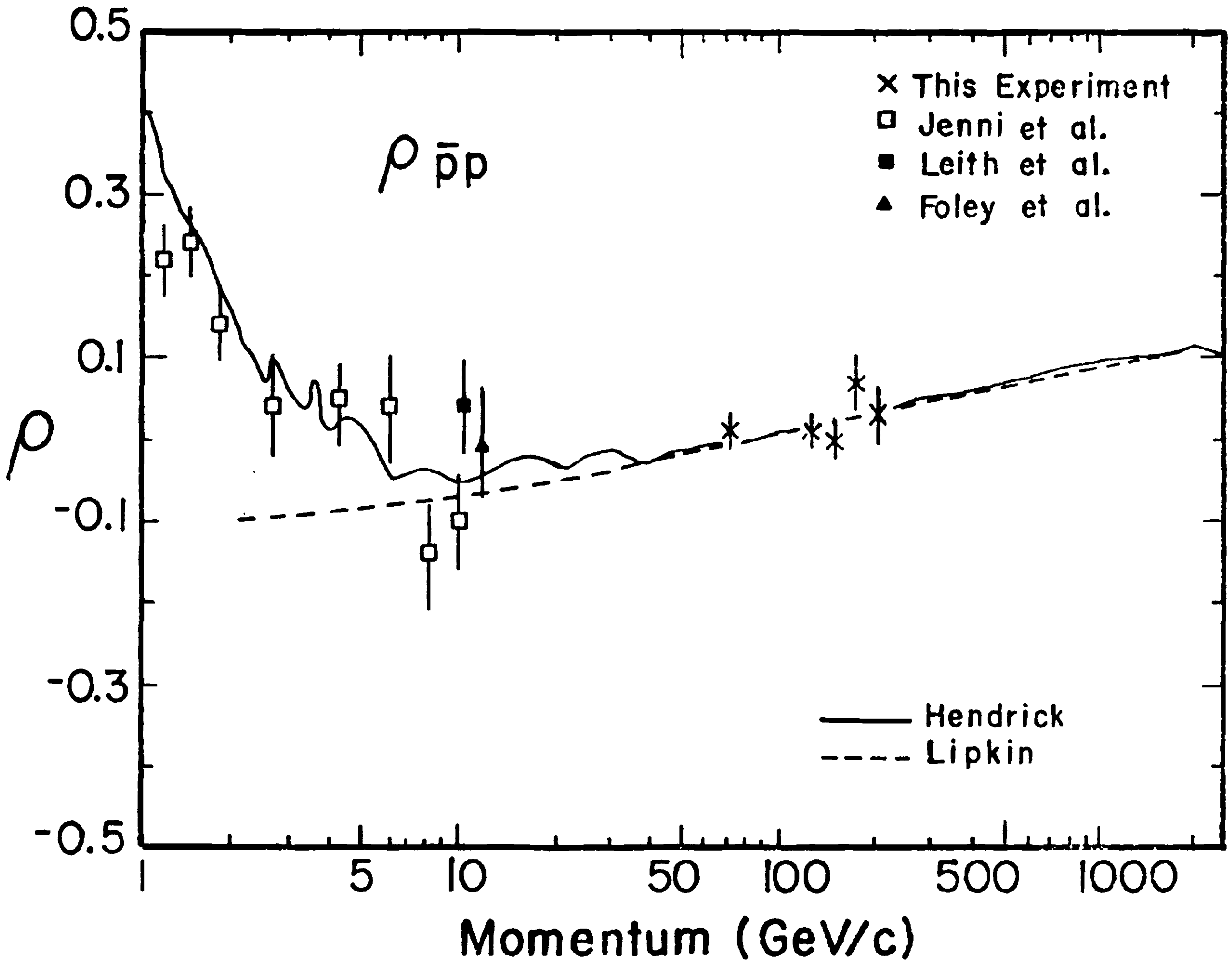
0.5
0.3
0.1
-0.1
-0.3
-0.5
ρ
ρ p̄p
× This Experiment
□ Jenni et al.
■ Leith et al.
▲ Foley et al.
Hendrick
Lipkin
1
5
10
50
100
500
1000
Momentum (GeV/c)

Figure 5.7d

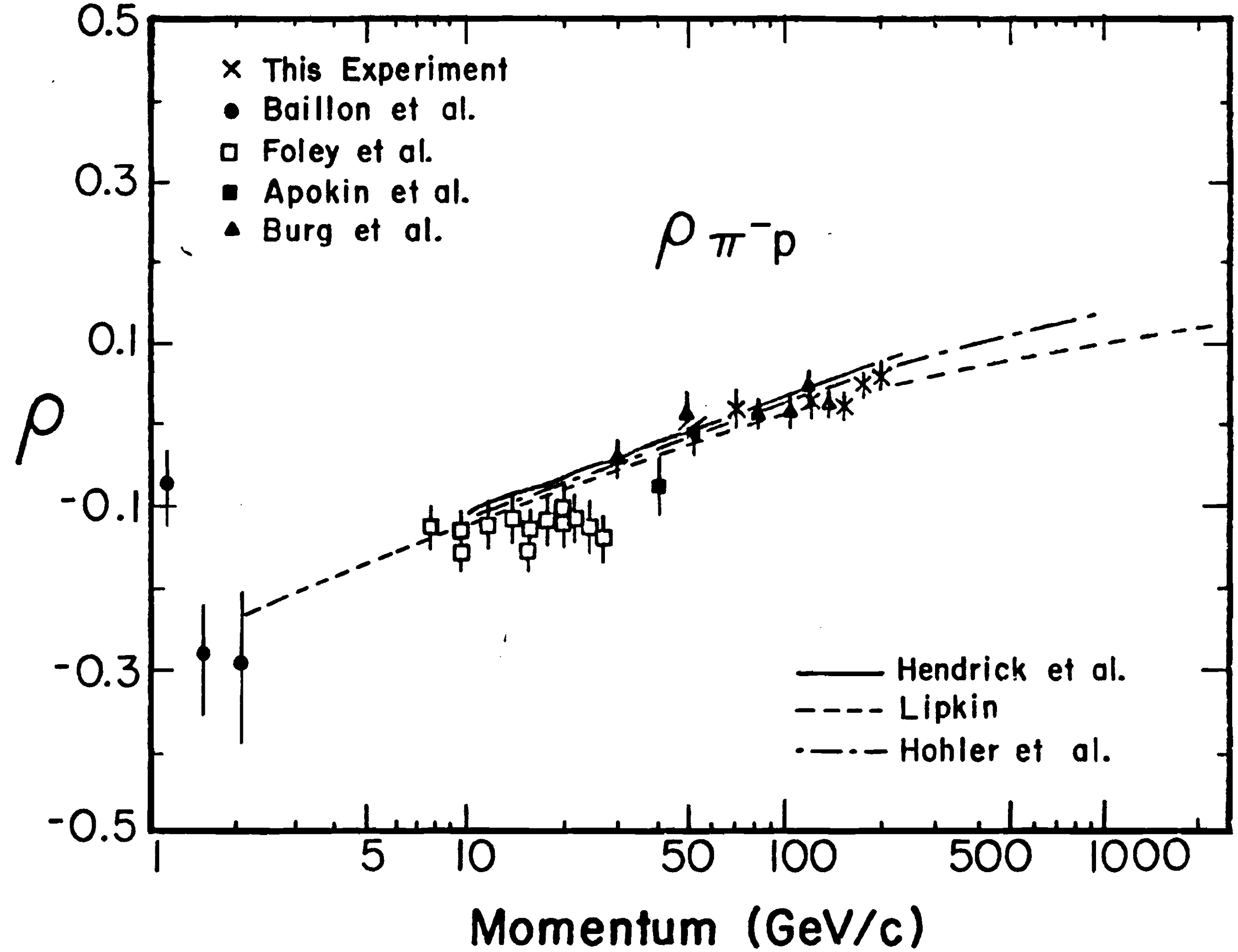

× This Experiment
● Baillon et al.
□ Foley et al.
■ Apokin et al.
▲ Burg et al.
$\rho_{\pi^- p}$
ρ
0.5
0.3
0.1
-0.1
-0.3
-0.5
1
5
10
50
100
500
1000
Momentum (GeV/c)
Hendrick et al.
Lipkin
Hohler et al.

Figure 5.7e

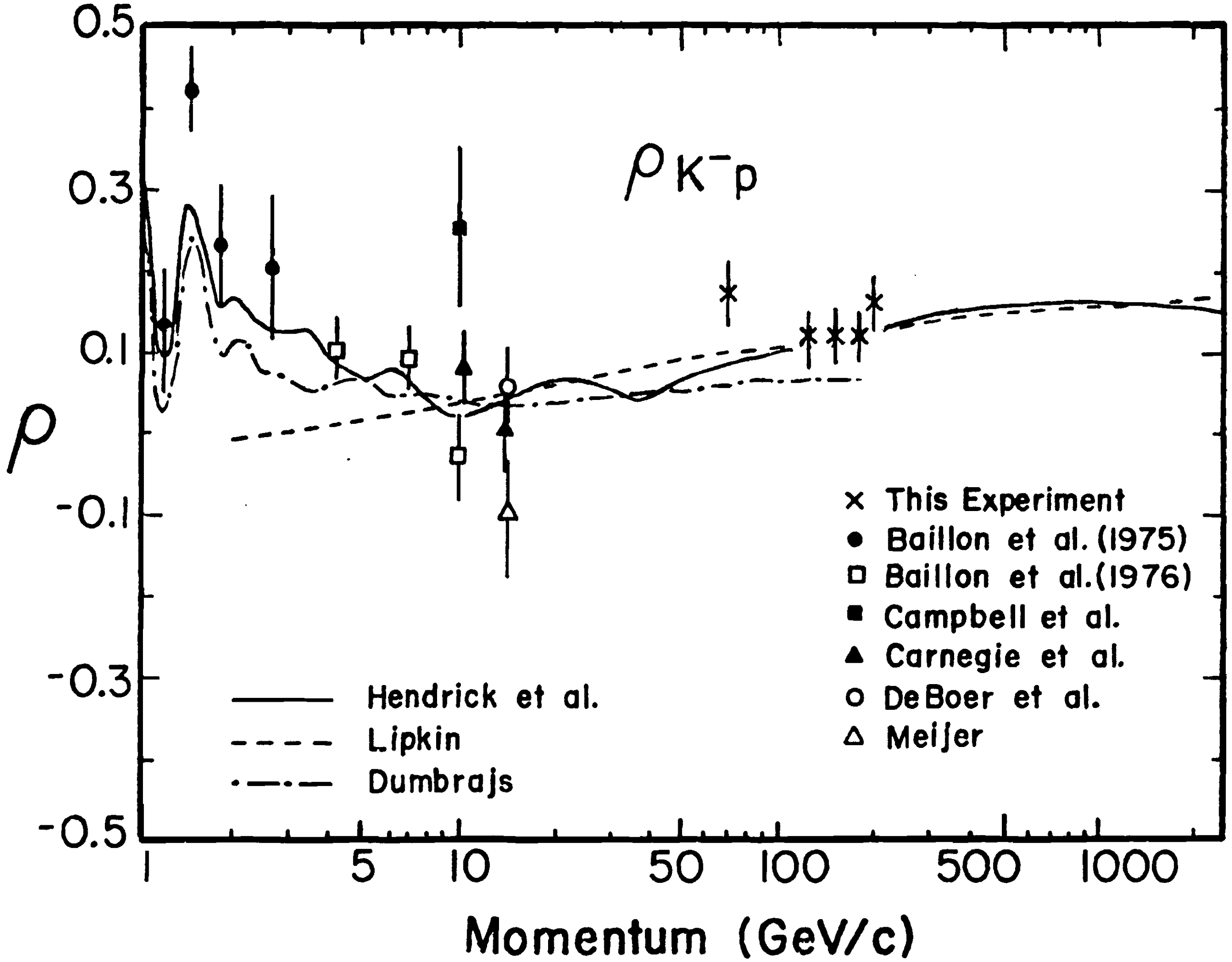

0.5
0.3
0.1
-0.1
-0.3
-0.5
ρ
ρ K⁻p
1
5
10
50
100
500
1000
Momentum (GeV/c)
Hendrick et al.
Lipkin
Dumbrajs
× This Experiment
● Baillon et al. (1975)
□ Baillon et al.(1976)
■ Campbell et al.
▲ Carnegie et al.
○ DeBoer et al.
△ Meijer

Figure 5.7f

TABLE 5.3

Results of Fitting the pp Cross Sections of Jenkins et al. with the Form Factor Formulation[a]

Momentum (GeV/c)	ρ_J	ρ_{ff}	u[b] $(GeV/c)^{-2}$	σ_{tot}[c] (mb)	A_n	χ^2/DF	$-t_{min}$ $(GeV/c)^2$	$-t_{max}$ $(GeV/c)^2$
50	-0.153 ± 0.012	-0.140 ± 0.013	0.08	38.33	1.01 ± 0.01	1.36	0.0016	0.0309
80	-0.096 ± 0.010	-0.075 ± 0.011	0.64	38.33	1.02 ± 0.01	0.97	0.0007	0.0293
199	-0.034 ± 0.009	0.023 ± 0.008	1.79	38.99	1.03 ± 0.01	1.11	0.0007	0.0315
261	-0.009 ± 0.009	0.026 ± 0.009	2.13	39.33	1.01 ± 0.02	0.96	0.0005	0.0298
303	-0.011 ± 0.008	0.028 ± 0.008	2.32	39.59	1.04 ± 0.01	1.26	0.0007	0.0316
398	0.012 ± 0.009	0.052 ± 0.008	2.66	40.80	1.04 ± 0.01	1.17	0.0005	0.0258

[a]The quantities ρ_J are from Jenkins et al., while ρ_{ff} are from these fits.

[b]The values of u were obtained from an a + b ln(momentum) fit to our values of u.

[c]The total cross sections used are those used by Jenkins et al.

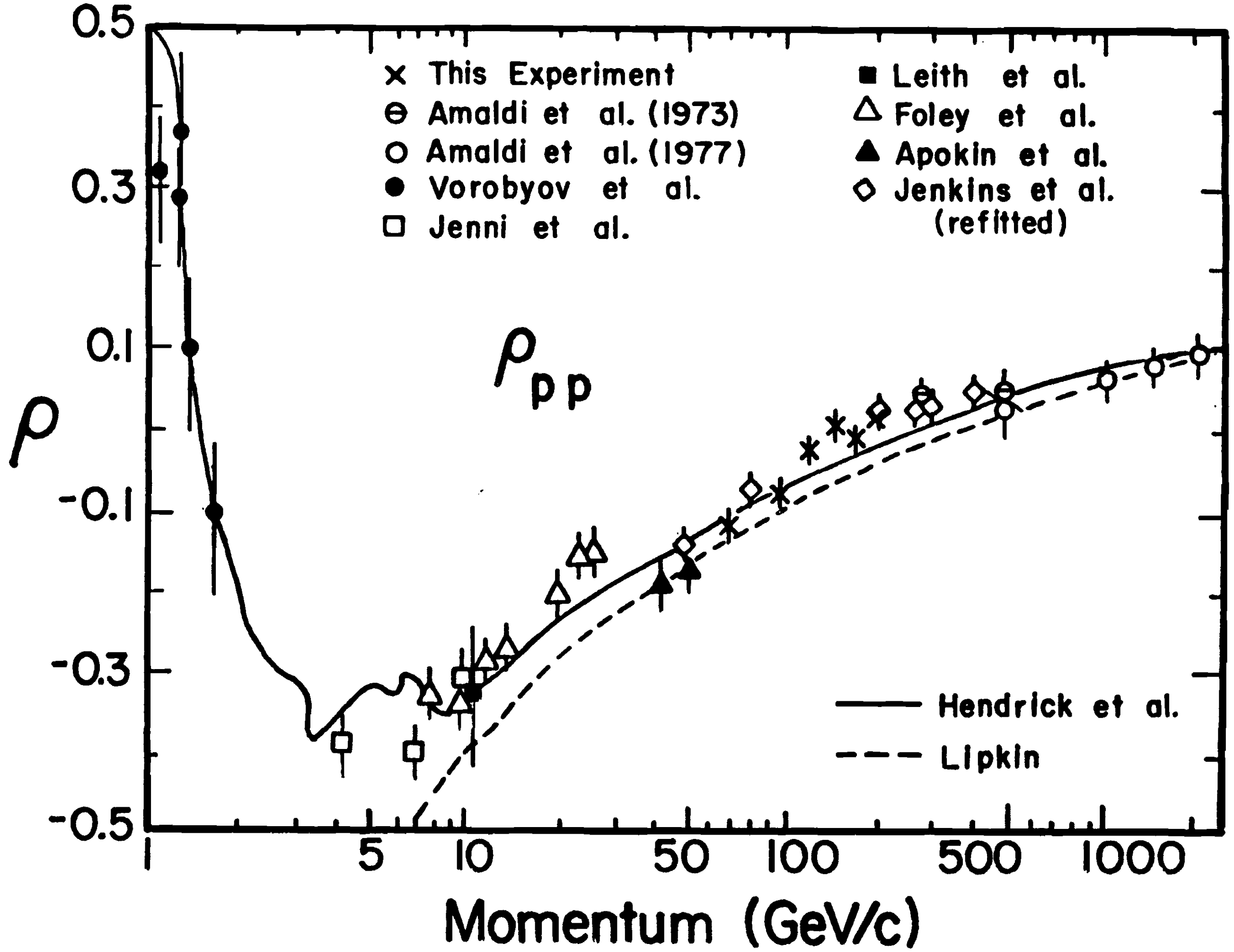

× This Experiment
⊖ Amaldi et al. (1973)
○ Amaldi et al. (1977)
● Vorobyov et al.
□ Jenni et al.
■ Leith et al.
△ Foley et al.
▲ Apokin et al.
◇ Jenkins et al. (refitted)
ρ_{pp}
Hendrick et al.
Lipkin
0.5
0.3
0.1
-0.1
-0.3
-0.5
ρ
1
5
10
50
100
500
1000
Momentum (GeV/c)

Figure 5.8

On the other hand, we can fit our data at 200 GeV/c using the exponential cross section and Jenkins et al.'s slope, $B = 11.56 \pm 0.12$ $(GeV/c)^{-2}$. Our values of ρ are then consistent with their published results, but only if we use the limited t range, $0.0016 \leq -t \leq 0.04$ $(GeV/c)^2$. If we extend the range of our fit to $-t_{max} = 0.09$ $(GeV/c)^2$, the steep fall off our data forces ρ to be inconsistent. The slopes that Jenkins et al. uses comes from a logarithmic fit to a previous measurement (Bartenev et. al.[5.2]) made in the range $0.005 < -t < 0.09$ $(GeV/c)^2$. To compare slopes we fit our data with the exponential cross section and $C = 0.0$ $(GeV/c)^{-4}$ and $-t_{max} = 0.09$ $(GeV/c)^2$. We obtain $B = 12.24 \pm 0.17$ $(GeV/c)^{-2}$, which still leaves a discrepancy in the slope of 0.73 $(GeV/c)^{-2}$.

CONCLUSIONS

We find that the real parts for $\bar{p}p$, π^+p, π^-p, K^+p, and K^-p are in good agreement with dispersion relations. The real parts for pp, however, are higher than dispersion relations and indicate that ρ_{pp} goes through zero near 175 GeV/c. Hendrick et al. point out that the contributions from pole terms and unphysical cuts for pp and $\bar{p}p$ scattering are still significant at these energies. Since the contributions are the same for both reactions, it is then puzzling to have such good agreement between our $\bar{p}p$ results and the dispersion relations of Hendrick et al. and Lipkin.

As derivative dispersion relations show, the real part at high energies becomes a local function of the total cross section. Specifically the real part is strongly correlated to the first derivative of the total cross section with respect to energy. This is reflected in the similarity of the different dispersion relations even when they differ in the extrapolation to higher energies. Our results are consistent with increasing total cross sections for all six reactions. In particular following the cross section predictions of Lipkin, we expect the $\bar{p}p$ total cross section to start increasing in the neighborhood of 300 GeV/c.

APPENDIX A

Multiple Scattering Distribution

In this appendix we extend the Moliere-Bethe[4.1] treatment of multiple scattering to the cross sections of interest Eqs. 1.6,1.7. To simplify notation throughout this appendix, the projections of q (where $-q^2$ is the four momentum transfer squared) are called x and y, such that $q^2 = x^2 + y^2$. We define the function $f(x,y,L)\,dx\,dy$ to be the probability of finding a particle in the q cell $(x, x+dx),(y, y+dy)$ after traversing a distance L in a homogeneous infinitely wide material. We define the incident distribution to be parallel, that is $f(x,y,L=0) = \delta(x)\,\delta(y)$. The steady state Boltzman transport equation with no absorption is given by:

scatter out

$$\partial f(x,y,L)/\partial L = -Nf(x,y,L) \iint dx'dy'\ R(x',y'|x,y)$$

scatter in

$$+N \iint dx'dy'\ f(x',y',L)\ R(x',y'|x,y)$$

where N is the atomic density and $R(x',y'|x,y)$ is the cross section for going from x,y to x',y'. Thus the number of particles in a given q cell is decreased by the number of particles that scatter out but increased by those that scatter into the cell.

In general the cross section R is energy dependent and $R(x',y'|x,y) \neq R(x,y|x',y')$ because of kinematic constraints. In this treatment we assume that the total energy loss is small enough that:

$$\sigma(x-x',y-y') = R(x',y'|x,y)$$

$$\frac{d\sigma}{d\tau} \simeq \frac{\sigma(x)-\sigma(x')}{x - x'}$$

where σ is the single scatter differential cross section. We also assume that the cross section decreases rapidly at large q so the limits of integration can be conveniently set to infinity. Then by change of variables, the dependence of σ on x and y is removed and we write:

$$\partial f(x,y,L)/\partial L = -Nf(x,y,L)\iint_{-\infty}^{\infty} dx'dy' \; \sigma(x',y') + N\iint_{-\infty}^{\infty} dx'dy' \; f(x-x',y-y') \; \sigma(x',y') \qquad (A.1)$$

The first intergral is the total cross section and the difference between the two integrals is the effective cross section. We now define the Fourier transform of f:

$$g(u,v,L) = (1/2\pi) \iint_{-\infty}^{\infty} dx \, dy \; e^{-iux-ivy} \; f(x,y,L)$$

Applying the Fourier transform to both sides of the transport equation gives:

$$\partial g(u,v,L)/\partial L = -NK(u,v) \; g(u,v,L) \; ,$$

where

$$K(u,v) = \iint_{-\infty}^{\infty} dx'dy' \; \sigma(x',y') \; (1 - e^{-iux'-ivy'}). \qquad (A.2)$$

Since K is independent of L, the differential equation of the variable L is a first order differential equation with the following solution for g:

$$g(u,v,L) = e^{-NLK(u,v)}$$

The solution of f is then the Fourier transform of g:

$$f(x,y,L) = (1/2\pi) \iint_{-\infty}^{\infty} du\, dv\, e^{iux+ivy}\, e^{-NLK(u,v)} \qquad (A.3)$$

Thus Eq.(A.3) is the exact solution of Eq.(A.1) for any cross section, σ. We note that for $L = 0$, $f(x,y,0)$ equals $\delta(x)\,\delta(y)$ by the definition of the Dirac delta function.

Fun Time

To explore the implications of Eq.(A.3), we assume for the moment that the cross section has a finite total cross section, σ_0, and that $NL\,\sigma_0$ is less than one. Then we can write:

$$f(x,y,L) = e^{-NL\sigma_0} \iint_{-\infty}^{\infty} du\, dv\, e^{iux+ivy}$$

$$\times \quad \exp[+NL \iint_{-\infty}^{\infty} dx'dy'\, e^{-iux'-iuy'} \quad \sigma(x',y')]$$

Expanding the exponential braced in square brackets, we have:

$$f(x,y,L) = e^{-NL\,\sigma_0} \quad \iint_{-\infty}^{\infty} du\, dv\, e^{+iux+ivy}$$

$$\times\ [\ 1 + NL \iint_{-\infty}^{\infty} dx'dy'\ \sigma(x',y')\, e^{-iux'-ivy'}$$

$$+ (1/2!)(NL)^2 \iiiint_{-\infty}^{\infty} dx'dy'dx''dy'' \quad \sigma'\,\sigma''\, e^{-iux'-iux''-ivy'-ivy''}$$

$$+ (1/3!)(NL)^3 \cdot \cdot \cdot\ ] \qquad .$$

Integrating over u, v, x', and y' gives:

$$f(x,y,L) = e^{-NL\sigma_o} \; [\, \delta(x) \;\; \delta(y) + (NL) \;\; \sigma(x,y)$$

$$+ (1/2!)(NL)^2 \iint dx''dy'' \;\; \sigma(x-x'',y-y'') \;\; \sigma(x'',y'')$$

$$+ (1/3!)(NL)^3 \iiiint dx''dy''dx'' \; dy'' \;\; \sigma(x-x''-x'' \;,y-y''-y'' \;) \;\; \sigma'' \;\; \sigma''$$

$$+ (1/4!)(NL)^4 \cdot \cdot \cdot \,] \, . \qquad \text{(A.4)}$$

The factor $\exp(-NL\,\sigma_0)$ is the attenuation of the parallel beam. The higher order terms in NL describe how those particles were distributed. The first order term gives the single scatter cross section, but attenuated by multiple scattering. The second term gives double scattering, the third term gives triple scattering, and so on. The integrals convolute over all possible permutations of individual scatters that sum to the appropriate x and y. Since a particle undergoes only one set of scatters, the factorials divide out the overcounting. Integrating Eq.(A.4) over all x and y, we verify that f(x,y,L) normalizes to one to conserve probablity.

As a concrete example, we let $\sigma = \sigma_0 \; B \;\; e^{-Bq^2}$ be the elastic nuclear scattering distribution. Then f becomes:

$$f(x,y,L) = e^{-NL\;\sigma_0} \;\; [\, \delta(x) \; \delta(y) \;\; + (NL\;\sigma_0) \; B \; e^{-Bq^2}$$

$$+ (1/2!)(NL\,\sigma_0)^2 \;\; (B/2) \; e^{-(Bq^2)/2}$$

$$+ (1/3!)(NL\,\sigma_0)^3 \;\; (B/3) \; e^{-(Bq^2)/3} \quad + \cdots].$$

$$\text{(A.5)}$$

The double scattering distribution decreases with only half the slope of the single scatter. Thus if the recoil particle is not detected, a substantial fraction of large angle deflections are in reality the sum of two scatters of smaller angle. For this experiment NL σ_0 is 0.003 for protons and with a B of 10 $(GeV/c)^{-2}$, the double scattering is an 11% correction at $q^2 = 1$ $(Gev/c)^2$, but only .5% at $q^2 = 0.4$ $(GeV/c)^2$.

Brass Tacks

The Coulomb cross section is too singular at q = 0 and NL $_0$ is much greater than one, making the direct expansion of Eq.(A.4) unproductive. The cross section allows no particle to traverse unperturbed: the $\delta(x)\,\delta(y)$ term in the expansion of f(x,y,L) in Eq.(A.4) is replaced by a gaussian distribution. This gaussian function is due to the central limit theorem of statistics for a large number of independent collisions, $NL\,\sigma_{effective}$. Qualitatively the width of the distribution is given by the statistical fluctuation of the number of collisions times the average q of the scatters, <q>:

$$w = [\,N\,L\,\sigma_{effective}\,]^{1/2}\,\langle q\rangle.$$

Below we make quantitative calculation of w for a specific Coulomb scattering cross section. After the Coulomb term is made manageable, the interference and nuclear terms will be amenable to the expansion method.

We write σ as follows:

$$\sigma = \sigma_C + \sigma_I + \sigma_n ,$$

where

$$\sigma_C = (4\pi e^4/c^2)\,(Z^2 + Z)\,(q^2+q_m{}^2)^{-2} \qquad \text{(A.6a)}$$

$$\sigma_I = \alpha\, \sigma_{tot}\, \exp[(-Bq^2)/2]\, (z_a \rho \cos\Omega + \sin\Omega)\, (q^2+q_m{}^2)^{-1} \qquad \text{(A.6b)}$$

$$\sigma_n = (\sigma_{tot}{}^2/16\pi\hbar^2)\, (1 + \rho^2)\, \exp(-Bq^2) \qquad \text{(A.6c)}$$

The first term, σ_C, describes elastic Coulomb scattering off a screened atom with Z protons, using a Fermi-Thomas potential. By quantum mechanical arguments, Moliere obtained an expression for the screening angle for the Fermi-Thomas potential. This screening angle becomes q_m under our q formulation and is given by:

$$q_m = (h/0.885\, a_\infty)\, [1.13 + 3.76\, \alpha^2\, Z^2\,]^{1/2}\ ,$$

where a_∞ is the Bohr radius and α is the fine structure constant. For hydrogen q_m is 4.48 MeV/c. Even though q_m is the only parameter of Moliere's theory, the results are very weakly dependent on its precise value. This model dependent cross section yields the same results as Bethe's model independent method and is computationally more straight forward. For simplicity we set the electromagnetic form factors to one. The second term, σ_I, is the Coulomb-nuclear interference term and the last term, σ_n, is the pure nuclear term using the exponential formulation with C = 0.

In σ_C the Z^2 contribution is due to coherent elastic scattering off the nucleus, while the Z contribution is due to incoherent elastic scattering off the electrons. Even though the apparatus can distinguish a single scatter off an electron wiht $q > 7$ Mev/c, this has a negligible effect on the multiple scattering width. The 7 MeV/c cutoff is more than a thousand times larger than the single impacts, approximately q_m, that comprise the bulk of the multiple scatters. Our measurements of the multiple scattering width w are in excellent agreement with our calculation, where the proton and electron contributions are equal.

Basic Tricks

Since the cross section of interest has no azimuthal dependence, we integrate over the azimuthal angles. Let $x = q\cos(\phi)$, $y = q\sin(\phi)$, $u = h\cos(\psi)$, and $v = h\sin(\psi)$. The definition of the Bessel function J_0 is given by:

$$J_0(hq) = (1/2\pi)\int_0^{2\pi} d\phi\, e^{ihq\cos(\phi-\psi)}$$

Thus we can write Eqs.(A.2,A.3) as:

$$K(h) = 2\int_0^\infty q'dq'\ \sigma(q')\,[1 - J_0(hq')]$$

and

$$f(q,L) = \int_0^\infty h\,dh\, J_0(hq)\, e^{-NLK(h)}.$$

We first solve for the pure Coulomb contribution. We define and evaluate $K_C(h)$ as follows:

$$NLK_C(h) = NL\int_0^\infty 2q'dq'\ \sigma_C(q')\,[1 - J_0(hq')]$$

$$= (q_C^2/q_m^2)\,[1 - hq_mK_1(hq_m)]\ ,$$

where $q_C^2 = (4\pi e^4/c^2)\,Z(Z+1)\,NL$ and K_1 is the modified Bessel function of order one. The integral, Number 6.532.4, in Gradshteyn and Ryzhik (G.R.)[A.1] was useful. The quantity q_C represents the minimum scattering impact all particles receive in traversing the target. For

52.7 cm of LH_2 the value of q_c is 1.077 MeV/c. Since the contribution to $f(q,L)$ is maximum where $K_c(h)$ is minimum, we expand K_1 to second order about h equal to zero. K_c is then approximated by:

$$NLK_c(h) = (hw/2)^2 \, [1 - V^{-1} \ln(h^2w^2/4)] \; ,$$

where $w^2 = Vq_c{}^2$ and where V is given by the transcendental equation:

$$V - \ln V = 1 - 2E + \ln(q_c{}^2/q_m{}^2) \; ,$$

and E = 0.577 is Euler's constant. For this experiment V is 13.40 and w is 3.94 MeV/c. The width of the multiple scattering distribution, as we see below, is given by w. We note that even if q_m changed by a factor of 2, the change in w is only 6%.

We then define the Coulomb distribution function, f_c, and evaluate it as:

$$\begin{aligned} f_c(q,L) &= \int_0^\infty hdh \; J_0(hq) \exp[-NLK_c(h)] \\ &= \int_0^\infty hdh \; J_0(hq) \exp[-(hw/2)^2 + (hw/2)^2 V^{-1} \ln(h^2w^2/4)]. \end{aligned}$$

Let Q = q/w and U = hw, then we can write:

$$f_c = w^{-2} \int_0^\infty UdU \; J_0(UQ) \exp(-U^2/4) \exp[V^{-1} (U^2/4) \ln(U^2/4)] \; .$$

Expanding the second exponential we have:

$$\begin{aligned} f_c = w^{-2} \int_0^\infty UdU \; J_0(UQ) \exp(-U^2/4) \\ \times \, [\, 1 + V^{-1} (U^2/4) \ln(U^2/4) \\ + (1/2!) \, V^{-2} (U^2/4)^2 (\ln(U^2/4))^2 \end{aligned}$$

$$+ (1/3!)\, V^{-3}\, (U^2/4)^3\, (\ln(U^2/4))^3 + \cdots] .$$

We define the integral of each term as the functions, $w^{-2}V^{-n}\, f^{(n)}$, which correspond exactly with Bethe's $f^{(n)}$ given by his Eqs.(25,26). We write $f_C(q,L)$ as follows:

$$f_C = w^{-2}\, [f^{(0)}(Q) + V^{-1}\, f^{(1)}(Q) + V^{-2}\, f^{(2)}(Q) + V^{-3}\, f^{(3)}(Q) + \cdots]$$

The function $f^{(0)}$ is easily evaluated (See G.R. 6.633.2) as:

$$f^{(0)}(q/w) = 2\, \exp(-q^2/w^2)$$

The function $f^{(0)}$ describes 99% of the beam in which the mean scatter has $q = w$. The remaining $f^{(n)}$ functions give the distribution of scatters with larger q. However, these functions are extremely cumbersome. We gratefully accept Bethe's approximation for $q > 3w$ and write $f_C(q,L)$ as;

$$f_C = 2w^{-2}\, \exp(-q^2/w^2) + NL\, \sigma_C\, [1-(4w^2/q^2)(1+2V^{-1}\ln(2q/5w)))]^{-1} \tag{A.7}$$

At $q = 40$ MeV/c, the function f_C is given solely by the Coulomb cross section with a 4% correction.

All at Once

We now solve $f(q,L)$ for all three terms. We write $f(q,L)$ as:

$$f = \int_0^\infty hdh\, J_0(qh)\, \exp(-NLK_C)\, \exp[-NL\ \ 2q'dq'(\ \sigma_I + \sigma_n)(1-J_0(hq'))]$$

The total cross sections of the interference and nuclear terms, $\sigma_{I,o}$ and $\sigma_{n,o}$ are very small and $NL\,\sigma_{I,o}$ and $NL\,\sigma_{n,o}$ are both much less than one. Then f(q,L) becomes:

$$f = A\int_0^\infty hdh\ J_0(hq)\ \exp(-NLK_C)\ \exp[NL \int 2q'dq'\ (\sigma_I+\sigma_n)\ J_0(hq')],$$

where $A = \exp[-NL(\sigma_{I,o} + \sigma_{n,o})]$ is the depletion of the forward beam by the interference and nuclear terms. Since A is an overall normalization and greater than 0.99, we set it to 1.0. We now expand f(q,L) as follows:

$$f = \int_0^\infty hdh\ J_0(hq)\ \exp(-h^2w^2/4)$$
$$\times\ [1 + V^{-1}\ (h^2w^2/4)\ \ln(h^2w^2/4) + (1/2!) \cdots]$$
$$\times\ [1 + NL \int 2q'dq'\ \sigma_I(q')\ J_0(hq') + (1/2!) \cdots]$$
$$\times\ [1 + NL \int 2q'dq'\ \sigma_n(q')\ J_0(hq') + (1/2!) \cdots]$$

Since the overlap of the different terms is very small the cross terms are unimportant. We approximate f by:

$$f = \int_0^\infty hdh\ J_0(hq)\ \exp(-h^2w^2/4)$$
$$\times\ [\ 1 + V^{-1}\ (h^2w^2/4)\ \ln(h^2w^2/4) + (1/2!) \cdots$$
$$+\ 2NL \int q'dq'\ \sigma_I\ J_0(hq')$$
$$+\ 2NL \int q'dq'\ \sigma_n(q')\ J_0(hq')$$
$$+\ 2N^2L^2 \int\int q'dq'q''dq''\ \sigma_n'\ \sigma_n''\ J_0'\ J_0''\ ]$$

Thus we can express f as the sum of three functions:

$$f(q,L) = f_C + f_I + f_n\ ,$$

where f_C is given by Eq.(A.7) and f_I and f_n are given below. Since the region where the interference term is important is small, the plural interference scattering terms are ignored and we write $f_I(q,L)$ as:

$$f_I = 2NL \int_0^\infty q'dq' \ \sigma_I(q') \ hdh \ J_0(hq) \exp(-h^2w^2/4) \ J_0(hq')$$

Integrating over h (see G.R. 6.633.2) and approximating the modified Bessel function I_0 for $q >> w$, we have:

$$f_I(q,L) = NLw^{-1}\pi^{-1/2} \int_0^\infty dq' \ \sigma_I(q') \exp[-(q'-q)^2/w^2]$$

Thus the function f_I gives the convolution of the interference term with the multiple Coulomb scattering distribution. Since only the q^{-2} variation is significant, we expand $(q')^{-2}$ about $q' = q$. Extending the limits of integration to infinity, we obtain f_I to second order as:

$$f_I(q,L) = NL \ \sigma_I(q) \ [1 + (3w^2/2q^2) + (15w^4/8q^4)] \qquad (A.9)$$

At q = 40 MeV/c, the interference term has a 1.5% correction.

For the nuclear function we retain the double scattering term and define $f_n(q,L)$ as:

$$f_n = 2NL \int_0^\infty hdh \ J_0(hq) \exp(-h^2w^2/4)$$
$$\times \left[\int_0^\infty q'dq' \ \sigma_n(q') \ J_0(hq') \right.$$
$$\left. \times \left(1 + NL \int_0^\infty q''dq'' \ \sigma_n(q'') \ J_0(hq'') \right) \right]$$

The integral representation of J_0 makes the evaluation of f_n straight foward, although laborious. In essence, the multiple Coulomb scattering smears the nuclear cross section: B is changed to

$B/(1 + Bw^2)$. This correction, however, is 0.1% and is ignored. Thus f_n is similar to Eq.(A.5) and is given by:

$$f_n(q,L) = NL\,\sigma_n(q)\,[1 + NL\,\sigma_{tot}^2\,(64\pi\hbar^2\,B)^{-1}\,\exp((B/2)q^2)\,]\,.$$

In our q range the exponential cross section and form factor cross sections are sufficiently similar to σ_n that we extend the result of f_n to both cross sections. We define $f_n^{\,e}(q,L)$ and $f_n^{\,ff}(q,L)$ as follows:

$$f_n^{\,e} = NL\,\sigma_n^{\,e}(q)\,[1 + NL\,\sigma_{tot}^2\,(64\pi\hbar^2\,b^e(0))^{-1}\,\exp((B/2)q^2)\,]$$

and

$$f_n^{\,ff} = NL\,\sigma_n^{\,ff}(q)\,[1 + NL\,\sigma_{tot}^2\,(64\pi\hbar^2\,b^{ff}(0)\,G_aG_p\,\exp(-uq^2/2))^{-1}\,]$$

where $\sigma_n^{\,e}$ and $\sigma_n^{\,ff}$ are the nuclear cross sections defined by Eqs.(1.6,1.7) and where b^e and b^{ff} are the local nuclear slopes defined in Eqs.(1.8,1.9).

The Corrected Cross Sections

The multiple scattering corrected cross sections, $\sigma_{MS}^{\,e}$ and $\sigma_{MS}^{\,ff}$, are given as follows:

$$\sigma_{MS} = (\,f_C + f_I + f_n)\,/\,NL$$

$$\sigma_{MS}^{\,e}(q) = \sigma_C(q)\,[1 - (4w^2/q^2)(1+2V^{-1}\,\ln(2q/5w))]^{-1}$$

$$+\ \sigma_I^{\,e}(q)\,[1 + (3w^2/2q^2) + (15w^4/8q^4)\,]$$

$$+\ \sigma_n^{\,e}(q)\,[1 + NL\,\sigma_{tot}^2(64\pi\hbar^2 b^e(0))^{-1}\,\exp((-Bq^2+Cq^4)/2)]$$

and

$$\sigma_{MS}^{ff}(q) = \sigma_C(q)\,[1 - (4w^2/q^2)(1+2V^{-1}\ \ln(2q/5w))]^{-1}$$

$$+\ \sigma_I^{ff}(q)\,[1 + (3w^2/2q^2) + (15w^4/8q^4)\,]$$

$$+\ \sigma_n^{ff}(q)\,[1+NL\sigma_{tot}^{\ 2}\,(64\pi\hbar^2\ b^{ff}(0)G_aG_p\ \exp(-uq^2/2))^{-1}],$$

where σ_C, $\sigma_I^{\ e}$, $\sigma_n^{\ e}$, $\sigma_I^{\ ff}$, and $\sigma_n^{\ ff}$ are given in Eqs.(1.6,1.7).

APPENDIX B

Expanded Cross Sections

In this appendix we give a detailed prescription for expanding the multiple scattering corrected cross sections, $S_{MS}{}^{ff}$ and $S_{MS}{}^{e}$. The expansions take the form:

$$S_{MS}{}^{ff}(t, \rho, u, r_a, r_p, \sigma_{tot}) = \sum_m g_m(\rho,u,r_a,r_p,\sigma_{tot})\, h_m(t) ,$$

where g_m is a function only of the parameters to be varied in the fitting procedure, while h_m depends only on t. We seek expansions that are numerically accurate and simple to program. To simplify notation we define the operator $DZ_i\langle\, u(y)\, \rangle$ as

$$DZ_i\langle\, u(y)\, \rangle = d^i(\, u\,)/dy^i\big|_{y=0} \quad .$$

Using Liebniz's theorem for differentiation of a product of functions, say u, v, w, we can write

$$DZ_j\langle\, uv\, \rangle = \sum_{i=0}^{j} (j!/i!(j-i)!)\, DZ_i\langle u\rangle\, DZ_{j-i}\langle v\rangle$$

$$DZ_k\langle\, uvw\, \rangle = \sum_{j=0}^{k} (k!/j!(k-j)!)\, DZ_j\langle uv\rangle\, DZ_{k-j}\langle w\rangle .$$

The Taylor series expansion of u can then be written as:

$$u(y) = \sum_{m=0}^{\infty} (m!)^{-1}\, DZ_m\langle u\rangle\, y^m \quad .$$

Form Factor Expansion

We write the multiple scattering corrected form factor cross section, $S_{MS}{}^{ff}$ (Eq. 1.7) as:

$$S_{MS}^{ff} = S_{MS,C}^{ff} + S_{MS,Ic}^{ff} + S_{MS,Is}^{ff} + S_{MS,n}^{ff} + S_{MS,nd}^{ff} ,$$

where

$$S_{MS,C}^{ff} = (4\pi e^4/c^2)\ t^{-2}\ (1-\varepsilon_C)^{-1}\ [G_a^2\ G_p^2]$$

$$S_{MS,Ic}^{ff} = \alpha\sigma_{tot}(z_a\rho\cos\beta + \sin\beta)\cos\mu\ t^{-1}\ (1+\varepsilon_I) \times [G_a^2 G_p^2 \exp(ut/2)]$$

$$S_{MS,Is}^{ff} = \alpha\ \sigma_{tot}(-z_a\rho\sin\beta + \cos\beta)\sin\mu\ t^{-1}\ (1+\varepsilon_I) \times [G_a^2 G_p^2 \exp(ut/2)]$$

$$S_{MS,n}^{ff} = (\sigma_{tot}^2/16\pi\hbar^2)\ (1+\rho^2)\ [G_a^2\ G_p^2\ \exp(ut)\ ]$$

$$S_{MS,nd}^{ff} = (\sigma_{tot}^4/1024\pi^2\hbar^4 b^{ff}(0))\ [G_a\ G_p\ \exp(ut/2)\ ]$$

and where the Coulomb phase shift angle, Ω, is given by:

$$\Omega = \beta + \mu(t) \tag{B.1a}$$

$$\beta = \alpha\ \ln(B_z/(b_{ff}(0) + 4v_p + 4v_a)) \tag{B.1b}$$

$$\mu(t) = \alpha\ \ln(1.123\ /\ |t|\ B_z) \tag{B.1c}$$

$$B_z = 10\ (\text{GeV}/c)^{-2} \tag{B.1d}$$

In the above terms of S_{MS}^{ff}, we are interested in expanding only the functions within the square brackets to fully decouple t from the remaining parameters.

The form factor functions are of the type $(1 + x)^{-1}$, which has a series expansion of $1 - x + x^2 - x^3 + \cdots$. This series converges only for $|x| < 1$. In the pion case x equals $2v_\pi\ |t|$, where $2v_\pi$ is about 2.5 $(\mathrm{GeV}/c)^{-2}$. Thus the series diverges for $|t| > 0.40$ $(\mathrm{GeV}/c)^2$. To bypass this problem we expand the form factors about $y = 0$, where

$$y = |t| - y_0$$

and y_0 was set to 0.3 $(\mathrm{GeV}/c)^2$. The form factors can then be written as:

$$G_a(t) = G_a(y_0)\; F_a(y) \;,$$

where

$$F_p(y) = (1 + u_p y)^{-2}$$

$$F_a(y) = (1 + u_a y)^{-1} \qquad \text{for } a = \pi \text{ or } K$$

$$u_p = v_p\;(1 + v_p y_0)^{-1}$$

$$u_a = 2v_a\;(1 + 2v_a y_0)^{-1} \qquad \text{for } a = \pi \text{ or } K$$

For pions u_π is then about 1.4 $(\mathrm{GeV}/c)^{-2}$. Thus the radius of convergence of F_π is $|y| < 0.70$ $(\mathrm{GeV}/c)^2$ or $0.0 \leq -t < 1.0$ $(\mathrm{GeV}/c)^2$. The series expansions of F_a converge easily within our t range. To increase the accuracy of our expansions which have a limited number of terms, a convergence function, $V(y)$, was used:

$$V(y) = (1 + u_c\; y)^{-4} \;,$$

where u_c was set to 1.4 $(\mathrm{GeV}/c)^{-2}$. We can then write:

$$G_a(t)G_p(t) = G_a(y_0)G_p(y_0)V(y)\;[F_a(y)F_p(y)/V(y)] \;\;.$$

While $G_a^{\,2}(t)G_p^{\,2}(t)$ varies about a factor of 1000 in our t range, the expression in the square brackets squared varies only by a factor of 4. Thus its expansion with only 25 terms is accurate to one part in 10^{10} in the range $0.0 \leq -t \leq 0.70$ $(GeV/c)^2$. We define $H_a(y)$ and $W_a(y)$ as:

$$H_a(y) = F_a(y)\ F_p(y)\ /\ V(y)$$

$$W_a(y) = G_a(y_0)\ G_p(y_0)\ .$$

We now specify the g^{ff} and h^{ff} functions for the different terms of $S_{MS}{}^{ff}$:

$$g_{C,m}{}^{ff} = (4\pi e^4/c^2)\ W_a{}^2\ DZ_m\langle H_a{}^2(y)\rangle$$

$$h_{C,m}{}^{ff} = (m!)^{-1}\ t^{-2}\ (1-\varepsilon_C)^{-1}\ V(y)\ y^m$$

$$g_{Ic,m}{}^{ff} = \alpha\,\sigma_{tot}(z_a\rho\cos\beta + \sin\beta)W_a{}^2\ \exp(-uy_0/2)\ DZ_m\langle H_a{}^2\exp(-uy/2)\rangle$$

$$h_{Ic,m}{}^{ff} = (m!)^{-1}\ t^{-1}\ \cos\mu\ (1+\varepsilon_I)\ V^2(y)\ y^m$$

$$g_{Is,m}{}^{ff} = \alpha\,\sigma_{tot}(-z_a\rho\sin\beta + \cos\beta)W_a{}^2\ \exp(-uy_0/2)DZ_m\langle H_a{}^2\exp(-uy/2)\rangle$$

$$h_{Is,m}{}^{ff} = (m!)^{-1}\ t^{-1}\ \sin\mu\ (1+\varepsilon_I)\ V^2(y)\ y^m$$

$$g_{n,m}{}^{ff} = (\sigma_{tot}{}^2/16\pi\hbar^2)\ (1+\rho^2)\ W_a{}^2\ \exp(-uy_0)\ DZ_m\langle H_a{}^2\exp(-uy)\rangle$$

$$h_{n,m}{}^{ff} = (m!)^{-1}\ V^2(y)\ y^m$$

$$g_{nd,m}{}^{ff} = (\sigma_{tot}{}^4(1+\rho^2)^2 NL/1024\pi^2\hbar^4 b^{ff}(0))\ W_a\ \exp(-uy_0/2)$$
$$\times\ DZ_m\langle H_a\exp(-uy_0/2)\rangle$$

$$h_{nd,m}{}^{ff} = (m!)^{-1}\ V(y)\ y^m$$

Thus $S_{MS}{}^{ff}$ is given by

$$S_{MS}{}^{ff} = \sum_{m=0}^{24} [g_{C,m}{}^{ff}\, h_{C,m}{}^{ff}(t) + g_{Ic,m}{}^{ff}\, h_{Ic,m}{}^{ff}(t) + g_{Is,m}{}^{ff}\, h_{Is,m}{}^{ff}(t) + g_{n,m}{}^{ff}\, h_{n,m}{}^{ff}(t) + g_{nd,m}{}^{ff}\, h_{nd,m}{}^{ff}(t)] \ .$$

Now all that remains is to specify the algorithms for the derivatives. Since we can use Liebniz's theory for the products, we need to specify the derivatives of each function:

$$DZ_m\langle F_p(y)\rangle = (1+m)!\ (-u_p)^m$$

$$DZ_m\langle F_a(y)\rangle = m!\ (-u_a)^m \qquad \text{for } a = \pi \text{ or } K$$

$$DZ_m\langle V^{-1}(y)\rangle = 4!/(4-m)!\ (-u_c)^m \qquad \text{for } 0 \leq m \leq 4$$
$$= 0 \qquad m > 4$$

$$DZ_m\langle \exp(-uy/2)\rangle = (-u/2)^m$$

To save computer time the function squared algorithms were also used:

$$DZ_m\langle F_p{}^2(y)\rangle = (3+m)!\ (-u_p)^m$$

$$DZ_m\langle F_a{}^2(y)\rangle = (1+m)!\ (-u_a)^m \qquad \text{for } a = \pi \text{ or } K$$

$$DZ_m\langle V^{-2}(y)\rangle = 8!/(8-m)!\ (-u_c)^m \qquad \text{for } 0 \leq m \leq 8$$
$$= 0 \qquad m > 8$$

$$DZ_m\langle \exp(-uy)\rangle = (-u)^m$$

Voila! At least the derivatives are easy to program!

Exponential Expansion

The series expansion of the multiple scattering corrected exponential cross section, $S_{MS}{}^{e}$ (Eq. 1.6) is somewhat simpler. We write the cross section as follows:

$$S_{MS}{}^{e} = S_{MS,C}{}^{e} + S_{MS,Ic}{}^{e} + S_{MS,Is}{}^{e} + S_{MS,n}{}^{e} + S_{MS,nd}{}^{e} \quad ,$$

where

$$S_{MS,C}{}^{e} = (4\pi e^{4}/c^{2})\ t^{-2}\ (1-\varepsilon_{C})^{-1}\ \exp[B_{z}t]$$

$$S_{MS,Ic}{}^{e} = \alpha\,\sigma_{tot}(z_{a}\rho\cos\beta + \sin\beta)\cos\mu\ t^{-1}\ (1+\varepsilon_{I}) \times \exp[(B_{c}t+Bt+Ct^{2})/2]$$

$$S_{MS,Is}{}^{e} = \alpha\,\sigma_{tot}(-z_{a}\rho\sin\beta + \cos\beta)\sin\mu\ t^{-1}\ (1+\varepsilon_{I}) \times \exp[(B_{c}t+Bt+Ct^{2})/2]$$

$$S_{MS,n}{}^{e} = (\sigma_{tot}{}^{2}/16\pi h^{2})\ (1+\rho^{2})\ \exp[Bt+Ct^{2}]$$

$$S_{MS,nd}{}^{e} = (\sigma_{tot}{}^{4}(1+\rho^{2})^{2}NL/1024\pi^{2}\ h^{4}B)\ \exp[(Bt+Ct^{2})/2]$$

where β and μ were defined in Eq.(B.1). The Coulomb form factors were approximated as

$$G_{a}(t)G_{p}(t) = \exp(B_{c}t) \quad ,$$

where $B_{c} = 4v_{a} + 4v_{p}$ and where v_{a} and v_{p} were defined in Eq.(1.00). In the limited t range where the Coulomb term is significant, this approximation is good to 0.01%. Since $\exp(Ct^{2})$ varies little in our t range and its expansion is rather complicated, it was not expanded but was included in the g_m functions. We expand about $t = 0$ with a convergence function $V(t) = \exp(B_z t)$, where $B_z = 10\ (\mathrm{GeV}/c)^{-2}$.

The g_m^e and h_m^e functions are easily and explicitly specified as follows:

$$g_{C,m}^e = (4\pi e^4/c^2)\ [B_c - B_z]^m$$

$$h_{C,m}^e = (m!)^{-1}\ (1-\varepsilon_C)^{-1}\ t^{m-2}\ \exp(B_z t)$$

$$g_{Ic,m}^e = \alpha\, \sigma_{tot}(z_a \rho\cos\beta + \sin\beta)\ \exp(Ct^2/2)\ [(B_c + B - 2B_z)/2]^m$$

$$h_{Ic,m}^e = (m!)^{-1}\ \cos\mu\ (1+\varepsilon_I)\ t^{m-1}\ \exp(B_z t)$$

$$g_{Is,m}^e = \alpha\, \sigma_{tot}(-z_a \rho\sin\beta + \cos\beta)\ \exp(Ct^2/2)\ [(B_c + B - 2B_z)/2]^m$$

$$h_{Is,m}^e = (m!)^{-1}\ \sin\mu\ (1+\varepsilon_I)\ t^{m-1}\ \exp(B_z t)$$

$$g_{n,m}^e = (\sigma_{tot}^2/16\pi\hbar^2)\ (1+\rho^2)\ \exp(Ct^2)\ [B - B_z]^m$$

$$h_{n,m}^e = (m!)^{-1}\ t^m\ \exp(B_z t)$$

$$g_{nd,m}^e = (\sigma_{tot}^4 (1+\rho^2)^2 NL/1024\pi^2\hbar^4 B)\ \exp(Ct^2/2)\ [(B - 2B_z)/2]^m$$

$$h_{nd,m}^e = (m!)^{-1}\ t^m\ \exp(B_z t)$$

Thus the function S_{MS}^e is given by:

$$S_{MS}^e = \sum_{m=0}^{24} [g_{C,m}^e\ h_{C,m}^e(t) + g_{Ic,m}^e\ h_{Ic,m}^e(t) + g_{Is,m}^e\ h_{Is,m}^e(t) + g_{n,m}^e\ h_{n,m}^e(t) + g_{nd,m}^e\ h_{nd,m}^e(t)\ ]\ .$$

C'est tout!

APPENDIX C

Tables of Differential Cross Sections

The measured differential cross sections for pp, π^+p, K^+p, $\bar{p}p$, π^-p, and K^-p elastic scattering between 70 and 200 GeV/c are presented in the following tables. The cross sections have been normalized and corrected as specified by Eq. 4.2. The values of -t are give at the middle of the bin and in units of $(GeV/c)^2$. The differential cross section, $d\sigma/dt$, and its statistical error are in units of microbarns/$(GeV/c)^2$.

MOMENTUM = 70 GEV/C

-T IN (GEV/C)**2; S = DSIGMA/DT AND E = ERROR IN MICROBARNS/(GEV/C)**2

	P+ P		PI+ P		K+ P	
-T	S	E	S	E	S	E
0.001849	159000	3547	101600	2408	106000	3914
0.002025	147800	3362	89970	2154	98640	3556
0.002209	137300	3118	80080	1929	87820	3215
0.002401	123800	2881	71590	1790	76190	2929
0.002601	119300	2738	66350	1651	63720	2760
0.002809	116400	2688	61270	1604	59950	2593
0.003025	112200	2612	57620	1505	54900	2396
0.003249	106300	2481	53830	1422	52250	2231
0.003481	100400	2384	48540	1293	47470	2211
0.003721	94400	2341	45730	1277	45300	2045
0.003969	95860	2347	44620	1247	39000	2078
0.004225	93290	2315	39780	1165	39790	1903
0.004489	90520	2218	38670	1154	37810	1923
0.004761	88200	2219	38330	1164	33660	1883
0.005041	86520	2193	37890	1140	35410	1888
0.005329	84860	2195	34640	1082	30970	1906
0.005625	83860	2150	34390	1081	33810	1983
0.005929	80830	2140	31790	1099	30640	1881
0.006241	80080	2232	33730	1090	28730	1815
0.006561	79960	2121	34560	1113	30700	1833
0.006889	78720	2226	31300	1087	28440	1861
0.007225	77850	2239	31530	1120	26630	1912
0.007569	79040	2211	31590	1118	26410	1949
0.007921	76810	2223	29880	1115	25520	1799
0.008281	72770	2207	29000	1124	23470	1732
0.008649	75620	2245	28940	1121	25670	1937
0.009025	75380	2282	29270	1119	23080	1917
0.009409	71970	2194	27530	1086	24600	1945
0.009801	74760	2285	28760	1109	25080	2017
0.010201	72630	2260	28280	1127	22580	1779
0.010609	70870	2230	25740	1051	20500	1842
0.011025	71140	2397	28040	1103	25590	1988
0.011449	71560	2254	28010	1120	19600	1689
0.011881	68960	2199	26690	1104	24190	1791
0.012321	71840	2244	27370	1093	20790	1840
0.012769	68240	2196	27410	1162	20330	1847
0.013225	65080	2153	26990	1085	22060	1902
0.013689	67930	2261	25710	1118	18080	1818
0.014161	66840	2219	25030	1040	18170	1716
0.014641	69100	2231	24010	1085	21620	1861
0.015129	67680	2167	24120	1007	21560	1746
0.015625	67500	2184	25310	1074	21140	1785
0.016129	64390	2095	24100	1042	21700	1867
0.016641	64120	2190	24960	1088	19490	1688
0.017161	63020	2118	24040	1029	17860	1654
0.017689	65440	2120	26570	1085	22210	1974
0.018225	59610	2089	24110	1028	17130	1565
0.018769	63490	2142	24010	1090	20110	1946
0.019321	64680	2093	23170	1024	17640	1842
0.019881	65450	2148	24580	1048	19460	1703
0.020449	57360	1989	24060	1012	19370	1739
0.021025	62240	2085	23430	991	19720	1825
0.021609	60380	2070	23860	1005	20100	1674
0.022201	60510	2059	23110	1019	19500	1708
0.022801	60460	2055	22710	975	19870	1703
0.023409	59450	2044	25030	1047	17500	1559
0.024025	60210	2025	21210	985	19220	1700
0.024649	58500	2002	20330	960	17970	1640
0.025281	58430	1954	21480	970	18460	1811
0.025921	56690	1958	22010	961	17020	1600
0.026569	55170	1958	22000	970	19850	1678
0.027225	58390	2019	22270	953	16150	1688
0.027889	57520	2022	21530	965	17320	1551
0.028561	56500	1972	22010	980	17390	1557
0.029241	55790	1975	21400	954	16720	1599
0.029929	54000	1920	20880	926	15000	1713
0.030625	54310	1955	21570	955	15790	1565
0.031329	51840	1843	21000	956	20530	1695
0.032041	54880	1900	21730	992	18120	1661

MOMENTUM = 70 GEV/C CONTINUED

-T IN (GEV/C)**2, S = DSIGMA/DT AND E = ERROR IN MICROBARNS/(GEV/C)**2

	P+ P		PI+ P		K+ P	
-T	S	E	S	E	S	E
0.032761	53810	1909	21280	926	17450	1632
0.033489	56660	1957	20330	941	17350	1653
0.034225	53420	1898	19870	912	16510	1726
0.034969	49710	1883	20560	947	17520	1724
0.035721	53670	1931	20620	908	17420	1579
0.036481	50870	1848	19430	914	15480	1641
0.037249	46980	1803	19300	905	17380	1582
0.038025	50540	1861	19990	962	17900	1681
0.038809	47820	1820	20240	950	16760	1631
0.039601	45310	1759	18800	903	19660	1788
0.040401	46540	1828	20170	926	16580	1787
0.041209	49500	1830	19990	917	16540	1657
0.042025	45970	1809	19800	939	17480	1623
0.042849	45450	1782	18120	921	15240	1519
0.043681	47470	1858	18980	950	17590	1745
0.044521	47820	1854	18930	924	14730	1622
0.045369	48170	1905	18950	923	17560	1693
0.046225	45720	1820	19710	951	14120	1601
0.047089	44840	1870	17330	929	14330	1536
0.047961	43920	1823	19160	973	16050	1640
0.048841	42290	1827	18280	928	15860	1654
0.049729	42790	1839	18110	953	15090	1646
0.050625	42990	1940	18130	984	14750	1862
0.051529	43470	1958	17080	967	18070	1857
0.052441	39830	1854	16430	972	16510	1791
0.053361	40360	1892	17120	959	15380	1749
0.054289	41390	1927	17570	1020	16310	1950
0.055225	44400	2056	16880	1011	13400	1707
0.056169	41320	2032	17490	1078	15300	1878
0.057121	42070	2097	15170	985	12920	1763
0.058081	42570	2137	14430	1019	16950	2049
0.059049	40720	2146	16980	1088	13110	2215
0.060025	40970	2216	16540	1175	17680	2253
0.061009	41090	2288	14500	1049	14870	2068
0.062001	40320	2288	15440	1126	17390	2331
0.063001	37460	2281	14840	1157	14810	2188
0.064009	38420	2350	13760	1237	14290	2505
0.065025	40370	2487	16380	1305	11830	2093
0.066049	33390	2323	14610	1229	12230	2199
0.067081	39290	2670	15330	1329	15000	2576
0.068121	36010	2615	11450	1243	14400	2589
0.069169	28190	2458	14000	1337	10320	2251
0.070225	32230	2733	12150	1375	11710	2497
0.071289	38180	3126	15060	1569	12630	2823
0.072361	32410	3151	12600	1500	10410	2686
0.073441	35310	3397	13270	1664	13800	3345
0.074529	37500	3657	15400	1875	15070	3654
0.075625	33190	3688	15670	2032	11260	3393
0.076729	28990	3671	15710	2168	11650	3681
0.077841	32290	4561	13760	2188	4078	2351
0.078961	34750	4704	13280	2329	11190	4224
0.080089	28390	4953	12430	2628	4353	3073
0.081225	35580	6508	17150	3625	15020	6709
0.082369	29050	7050	13470	3850	21610	9650
0.083521	38470	8612	11380	3754	19480	9729

MOMENTUM = 70 GEV/C

-T IN (GEV/C)**2, S = DSIGMA/DT AND E = ERROR IN MICROBARNS/(GEV/C)**2

	P- P		PI- P		K- P	
-T	S	E	S	E	S	E
0.001849	162700	5861	102700	2717	107000	4053
0.002025	136100	5219	86990	2358	91160	3601
0.002209	150200	5358	80560	2174	75220	3193
0.002401	141800	4997	72610	2027	72080	3118
0.002601	123400	4631	64040	1793	61220	2779
0.002809	127000	4699	58410	1694	59180	2728
0.003025	118400	4267	54620	1594	53970	2585
0.003249	112500	4384	53180	1551	49580	2313
0.003481	104900	4140	46110	1410	43430	2223
0.003721	112100	4285	46640	1407	43510	2113
0.003969	95950	4059	40800	1356	40050	2259
0.004225	102900	4165	39330	1286	34980	1914
0.004489	101300	4086	37980	1279	30860	2008
0.004761	96090	3970	35450	1222	30920	1930
0.005041	96450	3987	37030	1252	32930	2080
0.005329	92220	3994	35520	1225	32970	2005
0.005625	99370	4048	36430	1227	30190	1926
0.005929	91060	3918	34900	1221	29100	1955
0.006241	94590	3963	34350	1197	23720	1988
0.006561	95690	3947	33300	1162	26480	1781
0.006889	85710	3930	31840	1141	25420	1859
0.007225	90740	3913	31870	1131	26480	1810
0.007569	82210	3824	31630	1198	27000	1780
0.007921	83910	4069	31380	1165	22530	1898
0.008281	89920	4172	29710	1168	23550	1769
0.008649	86660	4248	27900	1116	24660	1839
0.009025	79500	3892	29700	1129	24360	1926
0.009409	80130	3893	30460	1183	22610	1866
0.009801	87230	4437	28040	1209	20710	1899
0.010201	91260	4142	28390	1166	23870	1793
0.010609	82730	4144	26550	1153	20320	1700
0.011025	82010	4008	26680	1141	20340	1867
0.011449	80770	4068	26010	1157	21030	1763
0.011881	86100	4268	25250	1122	21510	1872
0.012321	80590	4268	25610	1111	18240	1983
0.012769	82780	4129	27610	1131	20990	1992
0.013225	84680	4227	25760	1142	18010	1888
0.013689	81390	3996	28310	1152	20060	1916
0.014161	78690	4040	26490	1116	21580	1770
0.014641	78250	3961	23360	1090	23330	1849
0.015129	72590	3838	24830	1088	22360	1871
0.015625	74630	3797	25240	1090	21960	1805
0.016129	76650	4059	25200	1069	19060	1887
0.016641	70280	3873	23820	1088	17480	1699
0.017161	81690	4072	27250	1140	20170	1677
0.017689	76580	3909	25870	1096	18200	1832
0.018225	74000	3873	24540	1110	18940	1757
0.018769	76420	4080	23490	1083	19010	1856
0.019321	78150	4030	26190	1102	18640	1792
0.019881	74430	4092	23900	1094	17410	1802
0.020449	78670	4040	23070	1082	19510	1669
0.021025	68050	3984	24760	1143	19450	1763
0.021609	70940	3889	22630	1043	14530	1593
0.022201	80880	4167	23620	1112	17750	1702
0.022801	70520	4079	22960	1028	16590	1713
0.023409	71410	3843	23570	1083	18470	1648
0.024025	68110	3720	22870	1037	16100	1524
0.024649	67800	3799	24110	1087	17100	1584
0.025281	62250	3751	23780	1039	17280	1595
0.025921	67020	3800	23720	1095	16300	1650
0.026569	66590	3690	23060	1048	16040	1615
0.027225	66190	3720	23780	1056	15730	1622
0.027889	72990	4004	22600	1043	16610	1824
0.028561	66860	3679	22890	1043	18400	1743
0.029241	60590	3656	23130	1048	17110	1592
0.029929	67320	3681	22580	1036	17340	1625
0.030625	68320	3735	21180	1001	16640	1669
0.031329	75990	3968	22890	1041	17380	1828
0.032041	66410	3940	21860	1007	16430	1582

MOMENTUM = 70 GEV/C CONTINUED

-T IN (GEV/C)**2, S = DSIGMA/DT AND E = ERROR IN MICROBARNS/(GEV/C)**2

	P- P		PI- P		K- P	
-T	S	E	S	E	S	E
0.032761	54900	3391	19180	954	14720	1581
0.033489	57660	3424	21190	995	12710	1585
0.034225	55350	3573	21740	1020	20930	1803
0.034969	65870	3662	20250	995	13940	1669
0.035721	60930	3616	21340	998	11790	1451
0.036481	56630	3528	19210	959	14130	1660
0.037249	55600	3422	19680	998	14640	1617
0.038025	59050	3512	19820	949	13810	1665
0.038809	53620	3289	19120	929	17360	1709
0.039601	58610	3414	19460	958	11750	1446
0.040401	56430	3409	17920	998	15980	1699
0.041209	52780	3268	18360	929	13860	1783
0.042025	56620	3500	19950	983	17910	1700
0.042849	50180	3212	21130	1003	14730	1645
0.043681	47140	3167	19030	941	15270	1558
0.044521	51900	3344	19020	932	12920	1437
0.045369	55160	3502	19610	972	11970	1526
0.046225	56090	3451	20410	1008	12870	1572
0.047089	44770	3311	19020	986	11460	1374
0.047961	49050	3301	17470	943	15960	1628
0.048841	47270	3213	15410	905	13580	1604
0.049729	51660	3407	18030	987	13510	1538
0.050625	52440	3427	17930	951	11750	1429
0.051529	49060	3316	16760	936	11430	1555
0.052441	44940	3464	16680	928	14700	1624
0.053361	46410	3478	16050	903	11330	1440
0.054289	51750	3552	16340	963	13660	1616
0.055225	40600	3218	18660	1030	11150	1451
0.056169	39770	3304	15860	981	14380	1713
0.057121	45610	3424	16500	981	11990	1561
0.058081	46940	3569	16180	1019	12460	1637
0.059049	41900	3423	15170	1029	12300	1656
0.060025	49830	3849	14610	1014	14540	2050
0.061009	48220	3860	16400	1071	13310	1809
0.062001	39580	3561	15720	1074	11940	1754
0.063001	41550	3903	15800	1068	13250	1888
0.064009	34710	4084	15030	1101	16250	2151
0.065025	38630	3819	17700	1205	7455	1887
0.066049	42320	4363	14330	1111	12880	2047
0.067081	38650	4269	15120	1162	12030	2014
0.068121	36040	4405	13990	1166	13120	2112
0.069169	39210	4338	16020	1284	13150	2265
0.070225	41290	4706	16010	1420	10830	2170
0.071289	45240	5562	14640	1430	11880	2382
0.072361	32290	4831	13930	1321	16760	2846
0.073441	36440	4957	17390	1585	8238	2129
0.074529	34540	4876	15030	1484	10100	2383
0.075625	34130	5182	11650	1649	12860	2881
0.076729	35620	5814	16420	1819	14770	3392
0.077841	30430	5579	13430	1704	8407	2659
0.078961	40620	7328	14550	2013	7601	2872
0.080089	28410	6534	14060	2113	14880	4296
0.081225	30340	7374	11060	2041	8877	3622
0.082369	26750	7731	12400	2415	7396	3694
0.083521	28880	9635	10990	2725	7988	4607
0.084681	18250	8162	8336	3879	6058	4279

MOMENTUM = 100 GEV/C

-T IN (GEV/C)**2; S = DSIGMA/DT AND E = ERROR IN MICROBARNS/(GEV/C)**2

	P+ P		PI+ P		K+ P	
-T	S	E	S	E	S	E
0.001702	174100	3844	114500	2541	101000	2971
0.001914	149500	3514	92640	2173	82990	2510
0.002139	141200	3128	79210	1878	67410	2253
0.002377	129700	2985	69250	1728	60050	1951
0.002627	112700	2698	60720	1596	54860	1782
0.002889	106500	2563	56740	1448	46040	1618
0.003164	103800	2500	52620	1338	40290	1495
0.003452	99760	2348	47690	1261	35730	1411
0.003752	94180	2183	44690	1165	32570	1256
0.004064	91420	2186	41410	1168	30730	1240
0.004389	87980	2128	40320	1104	25830	1093
0.004727	88330	2053	38300	1052	27080	1105
0.005077	84870	1961	34740	981	25220	1062
0.005439	83020	1896	33650	982	24270	1088
0.005814	80430	1821	32270	912	23180	962
0.006202	79320	1821	33030	935	20160	989
0.006602	80250	1845	31580	894	21260	942
0.007014	77590	1802	29500	838	22410	950
0.007439	79460	1779	29480	837	22490	940
0.007877	73670	1775	27940	814	19880	886
0.008327	72750	1687	29310	825	18230	851
0.008789	75030	1664	28140	819	19090	914
0.009264	70720	1616	28360	793	19330	860
0.009752	73840	1661	28140	793	18590	843
0.010252	72160	1640	27270	813	17620	852
0.010764	72280	1595	24840	736	18580	779
0.011289	70290	1610	27850	789	18430	841
0.011827	69080	1646	25670	794	17190	831
0.012377	70680	1636	26380	777	17830	767
0.012939	64730	1609	26490	768	17590	838
0.013514	69080	1634	25590	786	16800	915
0.014102	67980	1746	25090	841	15690	870
0.014702	66030	1747	25220	852	17490	885
0.015314	63660	1772	24230	855	15630	944
0.015939	64940	1789	24080	838	15710	997
0.016577	66370	1800	24190	864	15940	888
0.017227	62450	1728	24740	833	15030	837
0.017889	60900	1789	23740	888	16790	930
0.018564	68270	1839	24760	894	16130	901
0.019252	65230	1871	24240	910	15880	993
0.019952	59900	1827	23170	894	14360	1022
0.020664	60090	1913	23540	892	16150	1053
0.021389	60700	1860	23600	867	14480	871
0.022127	58660	1732	21130	846	14150	829
0.022877	58510	1809	22150	868	16700	914
0.023639	57340	1838	23300	896	14790	893
0.024414	57190	1763	22110	875	15930	933
0.025202	58940	1808	22770	880	14680	953
0.026002	56290	1733	21840	885	15520	886
0.026814	59380	1810	22530	918	15450	948
0.027639	58350	1849	20810	832	14890	913
0.028477	57650	1851	20170	837	15620	941
0.029327	53440	1780	23230	942	13540	983
0.030189	52350	1740	20760	885	14720	1049
0.031064	53780	1834	20260	889	14560	907
0.031952	51230	1781	20420	882	12760	919
0.032852	51510	1789	20610	906	12390	928
0.033764	49060	1797	19100	856	12520	959
0.034689	48620	1717	20290	932	13570	973
0.035627	51160	1826	21010	933	14420	992
0.036577	51640	1917	20100	958	12680	948
0.037539	48250	1768	19410	876	15520	1034
0.038514	52600	1852	20490	926	12890	1044
0.039502	46820	1781	17130	866	13260	972
0.040502	48260	1831	17590	878	12520	992
0.041514	45620	1801	18030	916	11880	889
0.042539	47310	1818	18710	917	12330	956
0.043577	44330	1739	18080	896	12560	978
0.044627	46300	1836	18420	883	12430	1017

MOMENTUM = 100 GEV/C CONTINUED

-T IN (GEV/C)**2; S = DSIGMA/DT AND E = ERROR IN MICROBARNS/(GEV/C)**2

	P+ P		PI+ P		K+ P	
-T	S	E	S	E	S	E
0.045689	44330	1828	16750	866	11380	936
0.046764	44160	1784	16920	824	12960	935
0.047852	45200	1768	18190	910	12300	963
0.048952	42280	1737	16420	895	13330	988
0.050064	40510	1680	16110	843	12110	888
0.051189	43470	1721	16480	818	11060	849
0.052327	42540	1697	17650	888	12030	1030
0.053477	39400	1597	15960	811	10750	825
0.054639	40890	1635	15640	790	11630	865
0.055814	39640	1587	16980	811	10860	866
0.057002	41210	1645	15180	804	12010	914
0.058202	37050	1549	15620	765	10470	838
0.059414	40470	1544	16210	782	12030	856
0.060639	39520	1522	15750	774	10280	778
0.061877	38220	1497	15350	764	10730	837
0.063127	36660	1472	15360	750	9256	765
0.064389	36200	1449	15050	706	9862	781
0.065664	35830	1424	14910	716	11260	828
0.066952	35830	1429	14670	706	10070	818
0.068252	34490	1434	14370	682	10880	770
0.069564	34500	1353	14910	730	11320	778
0.070889	32690	1323	14270	682	9472	742
0.072227	33040	1368	13450	707	9281	739
0.073577	33680	1350	14890	715	9642	716
0.074939	34500	1374	14020	661	9831	718
0.076314	32090	1307	13430	675	10580	744
0.077702	33510	1356	13340	653	11050	772
0.079102	30320	1259	12530	660	8351	692
0.080514	31600	1287	12910	636	9372	742
0.081939	29520	1234	12830	658	9687	709
0.083377	28270	1226	12890	646	9627	747
0.084827	30190	1279	12660	647	9325	780
0.086289	26360	1182	11700	599	9579	705
0.087764	31610	1309	11740	608	8337	665
0.089252	29090	1248	13150	694	8330	671
0.090752	28740	1258	11400	619	8352	671
0.092264	27650	1221	10630	602	7851	697
0.093789	26200	1249	12930	672	7537	650
0.095327	27790	1235	12390	683	7241	739
0.096877	26120	1188	10750	618	9397	729
0.098439	24230	1193	11300	636	7956	674
0.100014	23350	1144	11300	646	8638	760
0.101602	22670	1135	11880	668	7700	679
0.103202	23620	1213	9031	588	7196	658
0.104814	22090	1179	10110	614	8264	723
0.106439	22680	1174	10020	616	7163	677
0.108077	20440	1123	8682	578	8465	744
0.109727	21980	1248	11520	695	7649	803
0.111389	22570	1245	10910	683	6365	752
0.113064	23490	1338	9800	692	7159	739
0.114752	18810	1235	8942	630	7244	739
0.116452	21320	1326	10690	719	6964	756
0.118164	19810	1242	9007	696	6776	835
0.119889	18820	1245	9769	746	5349	684
0.121627	18610	1322	8451	676	5533	713
0.123377	19960	1359	10150	809	6205	781
0.125139	18900	1435	9958	787	5503	762
0.126914	19360	1388	8785	740	5630	773
0.128702	19580	1497	8511	781	7465	955
0.130502	18300	1541	8870	803	7209	946
0.132314	17150	1471	7549	772	4874	810
0.134139	16820	1541	8818	884	6971	1230
0.135977	13390	1399	8877	903	6453	1007
0.137827	13970	1519	9066	970	6399	1065
0.139689	14760	1633	8530	984	4477	932
0.141564	14320	1702	8251	1025	5018	1044
0.143452	10950	1565	9719	1170	6765	1276
0.145352	16080	1968	8109	1107	6491	1296
0.147264	14570	2276	6355	1029	4289	1105
0.149189	14660	2530	6877	1161	5051	1301
0.151127	12820	2078	6138	1141	4012	1207

MOMENTUM = 125 GEV/C

-T IN (GEV/C)**2; S = DSIGMA/DT AND E = ERROR IN MICROBARNS/(GEV/C)**2

	P+ P		PI+ P		K+ P	
-T	S	E	S	E	S	E
0.001640	169400	4032	116700	2592	109600	3745
0.001892	146200	3388	90420	2086	79470	2857
0.002162	128500	3023	75740	1790	65790	2515
0.002450	117400	2683	64710	1552	59740	2134
0.002756	105500	2498	57260	1411	48980	1882
0.003080	99910	2286	49070	1240	40030	1656
0.003422	95440	2169	45300	1151	38850	1508
0.003782	89080	2044	40480	1036	32450	1378
0.004160	85410	1923	37240	976	31490	1283
0.004556	85090	1884	35860	936	30370	1246
0.004970	82730	1778	34110	870	26140	1182
0.005402	79280	1713	33180	863	22480	1049
0.005852	79990	1719	32660	837	22070	1068
0.006320	78410	1674	31030	807	23410	1011
0.006806	75640	1608	28900	754	21710	975
0.007310	75440	1569	30550	752	21870	936
0.007832	71600	1517	28620	744	19710	883
0.008372	69770	1483	28050	709	17760	849
0.008930	74750	1500	28070	708	18280	823
0.009506	70290	1454	27020	691	18010	819
0.010100	70070	1436	26100	671	20070	854
0.010712	70240	1438	25210	647	17780	825
0.011342	69740	1402	26070	647	17860	802
0.011990	65420	1369	25690	653	18150	822
0.012656	68620	1376	26140	649	16490	742
0.013340	66560	1340	24330	619	18010	770
0.014042	65460	1332	24130	620	18540	780
0.014762	64580	1319	23660	609	16620	765
0.015500	63150	1276	23640	598	17320	739
0.016256	61950	1265	24340	604	17740	757
0.017030	63380	1297	23870	609	15760	736
0.017822	63170	1295	23860	599	15100	708
0.018632	61540	1281	23410	601	16120	737
0.019460	60870	1296	23530	620	16810	786
0.020306	59800	1300	22800	625	15650	758
0.021170	58080	1294	22850	629	15200	777
0.022052	58530	1342	22680	647	17080	842
0.022952	59410	1368	22090	634	17120	845
0.023870	56810	1328	21360	638	14200	829
0.024806	56670	1348	20830	651	15400	807
0.025760	54490	1328	21200	642	15290	826
0.026732	55350	1383	21380	667	15980	863
0.027722	56420	1388	21750	676	14580	829
0.028730	58440	1411	21910	667	16130	900
0.029756	51940	1325	21080	661	13410	795
0.030800	54480	1368	20490	649	13120	809
0.031862	52710	1359	20530	655	12760	776
0.032942	51190	1339	19780	647	13780	799
0.034040	50150	1306	19000	629	13940	827
0.035156	48710	1293	19700	656	13960	822
0.036290	48580	1289	19770	653	15200	887
0.037442	47740	1276	18920	633	13710	817
0.038612	46730	1277	19110	631	14770	855
0.039800	48600	1305	19150	634	14590	877
0.041006	47980	1308	18950	642	14110	842
0.042230	47130	1294	19570	652	14660	847
0.043472	46200	1278	17940	626	14620	847
0.044732	43830	1276	17810	648	14180	870
0.046010	45740	1300	17160	634	11800	795
0.047306	42010	1229	16230	614	10480	740
0.048620	44080	1274	16080	619	11840	837
0.049952	41150	1247	16400	613	11740	848
0.051302	41380	1251	17250	633	11090	782
0.052670	41010	1265	16580	642	13090	880
0.054056	40290	1268	16970	647	13230	888
0.055460	38300	1241	16400	632	11500	860
0.056882	38620	1263	15560	629	12750	887
0.058322	39020	1266	15580	641	11000	824
0.059780	39530	1291	16290	650	11120	822

MOMENTUM = 125 GEV/C CONTINUED

-T IN (GEV/C)**2; S = DSIGMA/DT AND E = ERROR IN MICROBARNS/(GEV/C)**2

	P+ P		PI+ P		K+ P	
-T	S	E	S	E	S	E
0.061256	36430	1247	16090	648	11230	838
0.062750	35250	1212	14910	622	11110	838
0.064262	34390	1204	15430	643	10440	809
0.065792	35340	1232	13630	608	10860	864
0.067340	35060	1231	14650	635	9894	800
0.068906	33820	1225	14020	624	9515	809
0.070490	32060	1185	13830	623	10970	851
0.072092	32130	1208	13120	614	8331	788
0.073712	30900	1195	13260	616	11580	912
0.075350	30460	1193	13950	628	9679	811
0.077006	30450	1187	13750	637	9811	838
0.078680	31070	1189	12640	598	10350	845
0.080372	29450	1174	12820	615	9526	809
0.082082	28960	1157	12160	589	9714	808
0.083810	28730	1136	12410	588	10460	841
0.085556	28840	1113	12780	598	8310	735
0.087320	26430	1054	11770	566	8016	766
0.089102	27310	1072	10140	529	9415	765
0.090902	26830	1060	11110	553	8722	776
0.092720	26110	1033	11820	550	8823	750
0.094556	24250	975	10480	526	8167	715
0.096410	25430	1017	11400	544	8422	712
0.098282	24820	988	10550	513	8979	743
0.100172	22270	941	10660	510	7939	679
0.102080	24830	979	10590	516	8516	701
0.104006	24580	951	10350	494	8383	704
0.105950	20890	880	10760	497	7401	633
0.107912	22030	899	9739	471	7315	642
0.109892	20660	849	9677	466	7194	635
0.111890	20600	851	7927	422	7654	647
0.113906	20140	828	8889	434	7151	622
0.115940	20190	827	9484	456	6259	568
0.117992	20060	833	8536	430	6581	614
0.120062	20040	847	8905	450	6427	574
0.122150	18520	816	9407	451	6929	603
0.124256	19380	813	8211	421	6040	590
0.126380	16720	751	8225	418	8098	644
0.128522	19060	799	7613	405	6269	565
0.130682	17330	757	7715	405	6525	586
0.132860	16620	752	7677	403	6209	570
0.135056	16220	750	8109	427	6723	596
0.137270	15480	723	7391	399	6459	577
0.139502	15080	707	7606	401	6046	569
0.141752	15170	736	7489	399	7172	611
0.144020	14550	713	6851	381	5220	537
0.146306	14240	711	7077	404	5760	555
0.148610	14800	725	7905	423	5478	559
0.150932	14020	701	6630	380	5863	577
0.153272	14240	700	7383	405	4366	482
0.155630	12920	677	6594	388	5765	574
0.158006	13060	699	6645	391	6303	597
0.160400	13650	715	6757	423	5551	594
0.162812	12310	657	6608	399	4868	539
0.165242	12250	667	5987	375	4343	495
0.167690	11220	633	6332	387	5383	572
0.170156	11950	683	6207	397	4431	543
0.172640	12040	690	5766	381	4521	545
0.175142	11350	685	5429	393	4769	554
0.177662	10140	645	5775	392	4392	536
0.180200	9418	626	5587	395	5329	589
0.182756	9550	662	4887	379	3602	494
0.185330	10940	703	4547	366	4219	574
0.187922	9257	664	5071	390	4381	569
0.190532	8889	686	5278	401	3772	532
0.193160	8802	665	4215	364	4306	580
0.195806	9089	704	4715	410	4081	588
0.198470	9848	778	4607	414	4157	665
0.201152	9632	768	3958	389	4587	661
0.203852	7021	657	4847	440	4299	655
0.206570	7347	709	4197	435	3589	613
0.209306	7161	694	3681	402	4057	666

MOMENTUM = 125 GEV/C

-T IN (GEV/C)**2; S = DSIGMA/DT AND E = ERROR IN MICROBARNS/(GEV/C)**2

	P- P		PI- P		K- P	
-T	S	E	S	E	S	E
0.001640	185400	6355	129200	2745	125900	3232
0.001892	150100	5452	98110	2231	101300	2646
0.002162	134000	4919	84920	1894	82650	2174
0.002450	127000	4352	71460	1643	70540	1908
0.002756	116400	3874	62160	1453	57530	1631
0.003080	112700	3789	57740	1331	52370	1518
0.003422	110900	3531	48810	1186	49790	1365
0.003782	99730	3294	46550	1125	42220	1265
0.004160	96910	3117	43800	1061	38890	1172
0.004556	97860	3144	41330	995	35610	1095
0.004970	93070	3021	37840	955	33180	1051
0.005402	91320	2934	36060	924	30800	956
0.005852	89770	2788	35720	883	31030	985
0.006320	87130	2646	34040	813	28060	918
0.006806	84460	2617	34440	820	29210	898
0.007310	82510	2508	30810	775	25950	855
0.007832	82280	2571	32240	777	25260	804
0.008372	85600	2530	31950	752	26530	811
0.008930	82790	2466	29550	729	25660	775
0.009506	83860	2452	29860	706	25740	757
0.010100	81230	2360	30470	711	24460	750
0.010712	74820	2334	27880	666	22930	685
0.011342	80390	2324	28240	685	24090	717
0.011990	79230	2289	27580	666	23730	720
0.012656	76900	2290	27250	662	21230	675
0.013340	77460	2226	27130	640	21670	657
0.014042	72980	2153	26810	654	21810	683
0.014762	71940	2104	26720	629	21770	658
0.015500	75730	2125	26310	618	22220	662
0.016256	74650	2119	26300	627	20700	659
0.017030	74420	2154	25340	605	20040	628
0.017822	68890	2084	25820	640	21460	667
0.018632	70130	2078	25540	619	21140	656
0.019460	69790	2105	24520	606	20300	652
0.020306	68840	2088	23250	618	19880	649
0.021170	67970	2159	23920	622	19280	677
0.022052	68040	2216	24340	660	17720	677
0.022952	61020	2165	22750	644	18410	683
0.023870	66430	2226	22550	631	18830	693
0.024806	60300	2205	23440	667	18240	670
0.025760	60200	2155	22910	670	17300	679
0.026732	62460	2207	24000	657	17490	688
0.027722	64940	2281	22740	642	18200	682
0.028730	60330	2173	22370	646	16800	670
0.029756	61070	2225	22830	661	16940	661
0.030800	59540	2215	22210	641	18310	755
0.031862	63650	2256	22080	636	16420	667
0.032942	57010	2150	21600	639	17050	661
0.034040	56370	2155	22320	669	16550	699
0.035156	52690	2110	20530	626	15660	696
0.036290	54250	2131	20940	645	17070	695
0.037442	52140	2052	20340	620	15080	651
0.038612	56340	2193	20100	636	15810	654
0.039800	55110	2160	20440	641	16040	664
0.041006	48680	2052	18530	600	13950	654
0.042230	46850	2073	21120	640	15310	650
0.043472	49190	2091	19240	614	13790	633
0.044732	52490	2113	19240	638	14700	667
0.046010	52880	2178	19070	631	14950	667
0.047306	46020	2050	18750	618	15220	673
0.048620	47150	2058	18080	616	14360	660
0.049952	43760	1972	17650	601	14990	680
0.051302	47220	2098	17940	646	13980	677
0.052670	40140	1925	16060	590	14510	669
0.054056	43270	2037	16510	602	13280	649
0.055460	48500	2191	17220	637	14540	698
0.056882	43210	2098	16780	631	13930	704
0.058322	41780	2061	18230	645	12750	683
0.059780	44390	2102	17330	631	12170	650

MOMENTUM = 125 GEV/C CONTINUED

-T IN (GEV/C)**2; S = DSIGMA/DT AND E = ERROR IN MICROBARNS/(GEV/C)**2

	P- P		PI- P		K- P	
-T	S	E	S	E	S	E
0.061256	41460	2132	15830	620	13120	695
0.062750	42940	2222	16930	656	12830	704
0.064262	36970	1974	15720	613	12760	670
0.065792	39780	2065	15140	606	11770	649
0.067340	37050	2053	14320	602	11810	659
0.068906	35170	1950	14800	620	11460	664
0.070490	34270	2034	15010	615	10960	655
0.072092	37730	2103	14830	616	11340	655
0.073712	34990	1988	15030	624	10150	641
0.075350	32600	1908	14510	621	11530	666
0.077006	31290	1980	13090	578	12160	690
0.078680	32610	1931	14060	602	11200	641
0.080372	28840	1783	13990	599	10450	608
0.082082	30580	1868	13610	575	10680	659
0.083810	32760	1900	12570	557	9898	592
0.085556	32330	1853	12550	546	9495	579
0.087320	29370	1763	13010	556	10400	605
0.089102	29960	1774	12080	529	10850	628
0.090902	27320	1707	11960	515	10110	578
0.092720	27130	1674	12160	531	10890	612
0.094556	29150	1703	11020	515	9640	575
0.096410	24670	1573	12000	515	9647	547
0.098282	24390	1543	11370	481	8458	515
0.100172	24770	1526	12440	529	10230	578
0.102080	23330	1511	10810	478	9784	544
0.104006	22360	1402	10060	463	8270	511
0.105950	22650	1445	10860	474	8571	503
0.107912	21550	1366	10540	474	9030	511
0.109892	21720	1378	9510	428	8262	481
0.111890	22530	1411	9750	439	8440	517
0.113906	21500	1411	10180	464	8177	484
0.115940	21620	1389	9262	431	8532	494
0.117992	19580	128[illegible]	10130	442	7471	457
0.120062	17460	1266	8907	418	7546	479
0.122150	19300	1368	9152	418	7634	476
0.124256	18680	1246	8443	405	7384	472
0.126380	16900	1234	8479	394	6658	437
0.128522	19450	1274	8542	408	6554	426
0.130682	18590	1243	8556	403	7055	442
0.132860	17910	1232	8689	420	7178	451
0.135056	17060	1189	7775	385	6624	449
0.137270	16580	1182	7884	395	6342	433
0.139502	15590	1186	7679	388	6998	468
0.141752	13460	1053	7354	388	6913	438
0.144020	15670	1162	7387	377	6653	438
0.146306	13490	1110	7543	385	6109	419
0.148610	13620	1098	7862	401	6069	425
0.150932	14040	1140	7508	381	5860	413
0.153272	14390	1140	7280	389	5968	425
0.155630	13150	1119	7197	378	5943	421
0.158006	11810	1071	6652	378	6050	427
0.160400	13230	1172	7056	389	4767	379
0.162812	10050	963	6241	385	6081	434
0.165242	11840	1101	6775	384	5351	410
0.167690	11690	1065	6171	372	5607	427
0.170156	11150	1050	6633	389	5331	450
0.172640	9219	1020	5398	348	5521	448
0.175142	11340	1092	6752	398	4621	403
0.177662	10860	1075	5648	374	4295	410
0.180200	11140	1108	4902	355	4923	426
0.182756	8715	989	5017	363	4323	423
0.185330	10290	1100	5043	383	4958	443
0.187922	8657	1029	5012	401	4759	442
0.190532	10380	1156	5032	391	3929	462
0.193160	7687	1002	4966	379	4081	449
0.195806	7185	1120	5008	413	3667	421
0.198470	7601	1065	5174	414	4517	476
0.201152	8548	1154	5006	416	3822	446
0.203852	7593	1132	4435	407	3639	454
0.206570	8407	1255	4610	437	3653	525
0.209306	6658	1110	3933	401	3428	461

MOMENTUM = 150 GEV/C

-T IN (GEV/C)**2, S = DSIGMA/DT AND E = ERROR IN MICROBARNS/(GEV/C)**2

	P+ P		PI+ P		K+ P	
-T	S	E	S	E	S	E
0.001640	169700	4130	114100	3014	110500	4639
0.001892	139500	3416	88170	2375	84240	3465
0.002162	125700	2872	75640	1931	71550	2833
0.002450	117000	2589	64030	1647	53820	2378
0.002756	107300	2312	55350	1433	51480	2027
0.003080	95050	2017	50180	1257	38920	1797
0.003422	96430	1960	45530	1173	36590	1530
0.003782	87780	1796	41510	1072	31920	1405
0.004160	84660	1676	38280	978	29100	1359
0.004556	82370	1691	37150	907	30030	1294
0.004970	81400	1612	35430	911	24450	1108
0.005402	78120	1513	33570	841	24490	1084
0.005852	75500	1454	31430	796	22880	1016
0.006320	76220	1455	29840	766	20910	997
0.006806	73350	1391	30080	756	22850	991
0.007310	72240	1342	28550	712	21490	933
0.007832	72170	1325	28250	694	21380	868
0.008372	70830	1281	27750	671	20190	850
0.008930	70380	1261	26900	655	19720	824
0.009506	69610	1238	25910	615	19360	834
0.010100	67380	1220	26700	626	18870	814
0.010712	67850	1213	26810	622	19580	804
0.011342	67350	1188	26050	600	18150	763
0.011990	67600	1174	25520	588	17690	756
0.012656	66100	1156	25010	581	18280	735
0.013340	64500	1117	24800	574	16800	733
0.014042	65330	1134	24470	568	16420	715
0.014762	63450	1094	24000	546	18160	750
0.015500	63960	1091	24380	556	17250	716
0.016256	63580	1093	24440	547	16710	676
0.017030	61960	1064	24380	557	17110	694
0.017822	62600	1066	23760	552	17130	716
0.018632	60220	1042	23330	536	16120	660
0.019460	60880	1044	22630	521	16630	663
0.020306	60340	1030	22740	521	15760	664
0.021170	60460	1029	22500	517	16750	667
0.022052	59280	1014	22420	513	16680	667
0.022952	58980	1011	22450	513	15790	657
0.023870	56530	984	22670	512	14860	628
0.024806	57310	994	22150	521	15240	663
0.025760	56260	1000	21320	515	14680	654
0.026732	56940	1009	21620	514	15750	666
0.027722	55670	1008	20900	517	15600	710
0.028730	53590	1005	20160	511	15480	706
0.029756	51910	996	20000	513	14560	688
0.030800	52050	1021	20640	538	13730	699
0.031862	52030	1021	19940	537	14210	699
0.032942	50380	1025	19550	542	14830	736
0.034040	51260	1035	20430	552	14300	740
0.035156	49810	1021	18920	543	14660	731
0.036290	50220	1039	19810	550	14100	711
0.037442	50280	1041	19590	554	14030	739
0.038612	47630	1012	19700	558	13830	748
0.039800	45870	1002	19230	555	13070	726
0.041006	46100	996	19050	556	14130	742
0.042230	44970	991	18990	555	12450	734
0.043472	46100	1008	18670	550	13370	728
0.044732	45210	998	17780	540	13700	762
0.046010	44910	984	18380	541	14740	758
0.047306	42430	968	17940	545	12400	696
0.048620	43510	988	18270	553	11660	691
0.049952	40760	940	17050	522	13270	717
0.051302	41500	953	15990	528	11690	701
0.052670	41310	954	16500	534	12210	722
0.054056	39120	931	16170	523	12240	710
0.055460	38540	929	15990	520	11680	699
0.056882	39810	938	16650	528	11700	742
0.058322	37210	900	15380	509	10910	696
0.059780	37150	917	15710	519	10930	673

MOMENTUM = 150 GEV/C CONTINUED

-T IN (GEV/C)**2, S = DSIGMA/DT AND E = ERROR IN MICROBARNS/(GEV/C)**2

	P+ P		PI+ P		K+ P	
-T	S	E	S	E	S	E
0.061256	36970	918	16490	533	11380	701
0.062750	36850	913	15090	519	10390	677
0.064262	36400	921	14850	514	10290	690
0.065792	35200	893	15330	539	11480	732
0.067340	33570	877	13900	497	10340	697
0.068906	33900	897	14080	508	9771	668
0.070490	33020	885	14120	515	9741	676
0.072092	33650	895	13550	500	10400	692
0.073712	32240	885	13990	515	10910	728
0.075350	33650	931	13540	516	10770	751
0.077006	33030	914	13360	520	9719	698
0.078680	30760	881	13720	533	9110	675
0.080372	30150	895	12860	510	9303	701
0.082082	29600	871	12480	508	9430	702
0.083810	30160	901	11690	495	7800	669
0.085556	28040	867	12240	516	8725	694
0.087320	26160	851	12440	513	8662	714
0.089102	27070	841	11130	485	8832	724
0.090902	26030	849	11090	490	8772	726
0.092720	26180	863	11220	511	7507	677
0.094556	25110	844	12650	535	9161	723
0.096410	24550	846	10900	515	7789	673
0.098282	22590	807	11030	505	8409	697
0.100172	25150	866	10550	522	7758	685
0.102080	22400	823	10410	504	8864	730
0.104006	23440	832	10460	505	7935	723
0.105950	21170	771	9606	472	7159	679
0.107912	20830	782	9385	473	7862	698
0.109892	20670	778	9772	484	9032	744
0.111890	20350	780	9170	468	7430	694
0.113906	19360	756	9302	478	7226	706
0.115940	19210	743	8504	457	7369	683
0.117992	18640	744	10170	502	7226	699
0.120062	17830	718	8856	449	6530	645
0.122150	18390	728	8953	451	8049	687
0.124256	17730	717	8024	426	6565	621
0.126380	16270	674	8375	429	5960	577
0.128522	15940	643	7618	402	6266	633
0.130682	16870	670	7484	412	6592	606
0.132860	16510	665	7863	410	6087	576
0.135056	16170	640	7016	375	6333	574
0.137270	14990	604	7044	378	5438	552
0.139502	14530	604	6704	367	6367	570
0.141752	15590	622	7392	391	6555	588
0.144020	13900	579	7107	376	6369	569
0.146306	13010	561	7569	383	5448	518
0.148610	13740	577	6665	359	5978	542
0.150932	12830	528	6665	351	5811	523
0.153272	12500	524	6876	357	6183	552
0.155630	14180	564	7220	368	5333	505
0.158006	12680	525	6870	354	5407	538
0.160400	12190	514	6720	344	5020	492
0.162812	12590	529	6290	341	4858	472
0.165242	12150	511	5962	326	4261	451
0.167690	11890	495	6232	328	5438	490
0.170156	11540	505	5621	314	5918	516
0.172640	10610	464	5555	309	5089	471
0.175142	11760	486	5085	292	4192	424
0.177662	10720	471	5690	321	5278	489
0.180200	10330	474	5642	314	4737	459
0.182756	9326	433	4643	287	3973	418
0.185330	9454	434	5732	321	3331	382
0.187922	9747	449	4621	280	4122	423
0.190532	8681	430	4971	297	4060	423
0.193160	9274	440	5705	313	3989	423
0.195806	9141	436	4765	285	4055	447
0.198470	8311	416	4330	274	3978	433
0.201152	8464	426	4165	272	4357	464
0.203852	7434	395	4346	272	4631	448
0.206570	7915	409	4522	278	4301	439
0.209306	7524	390	3890	262	3899	418

MOMENTUM = 150 GEV/C

-T IN (GEV/C)**2; S = DSIGMA/DT AND E = ERROR IN MICROBARNS/(GEV/C)**2

	P- P		PI- P		K- P	
-T	S	E	S	E	S	E
0.001640	181200	11740	130700	4264	123600	5241
0.001892	150100	10220	104500	3342	109000	3976
0.002162	155800	8759	79850	2681	80460	3300
0.002450	125000	7017	71150	2239	71370	2914
0.002756	117300	6185	61410	1993	59300	2298
0.003080	110700	5665	55070	1762	52370	2069
0.003422	112000	5404	50720	1568	46580	1860
0.003782	102600	5461	42680	1465	41800	1721
0.004160	103600	5165	42830	1377	39880	1569
0.004556	88830	4752	40140	1296	35330	1354
0.004970	84270	4512	39120	1243	32610	1448
0.005402	90250	4351	36340	1179	32450	1281
0.005852	81550	4052	34980	1127	33430	1245
0.006320	83940	4242	33320	1035	26680	1155
0.006806	84880	4098	33030	1016	31520	1173
0.007310	82770	4046	31680	1015	26770	1126
0.007832	86960	3827	31050	947	25770	1055
0.008372	79240	3762	30650	937	24710	976
0.008930	75670	3514	31620	912	25480	971
0.009506	83430	3740	30570	889	23240	967
0.010100	89530	3675	30130	868	25490	968
0.010712	79220	3342	27840	847	24180	915
0.011342	81450	3508	28410	814	22350	843
0.011990	73770	3312	27540	823	23620	856
0.012656	72470	3377	27000	779	21400	833
0.013340	75700	3203	27410	797	21490	837
0.014042	75780	3051	27220	794	21960	858
0.014762	73010	3208	26000	762	21210	804
0.015500	72840	3007	26620	748	20310	788
0.016256	70990	3018	25790	726	20150	746
0.017030	70950	2902	25730	717	18810	748
0.017822	70830	3041	25570	716	19260	739
0.018632	72210	2951	25840	732	20170	755
0.019460	66690	2786	24550	681	19640	724
0.020306	70850	2949	25010	695	20920	754
0.021170	66770	2766	24580	677	20250	742
0.022052	66630	2716	25470	696	17750	694
0.022952	63730	2763	23510	656	18570	683
0.023870	65140	2768	24020	685	18840	731
0.024806	63300	2692	23300	647	17770	682
0.025760	67920	2802	24090	672	18990	703
0.026732	63520	2739	23740	669	17830	675
0.027722	64020	2769	22460	651	18500	696
0.028730	56880	2644	22480	657	18470	707
0.029756	62370	2833	22260	660	17850	715
0.030800	63320	2863	21240	671	17220	702
0.031862	62650	2894	20550	665	17620	729
0.032942	56430	2784	21060	681	17010	734
0.034040	57470	2829	21230	684	16170	749
0.035156	60430	2871	20850	688	15860	757
0.036290	56310	2869	20080	691	17100	748
0.037442	54400	2970	20440	687	16610	754
0.038612	50260	2882	20210	687	16230	750
0.039800	50110	2670	19590	686	15510	737
0.041006	49210	2674	19560	669	15480	726
0.042230	49180	2801	19060	666	15550	732
0.043472	46620	2635	18420	666	13930	688
0.044732	48990	2705	18070	650	14440	692
0.046010	47650	2704	19640	671	14790	722
0.047306	53110	2884	19230	666	13960	696
0.048620	49890	2730	17680	634	14040	720
0.049952	45810	2671	17670	639	13630	677
0.051302	49210	2860	17340	637	13050	701
0.052670	46870	2737	17200	637	13600	685
0.054056	50130	2794	17130	635	14030	738
0.055460	41190	2564	15580	606	13180	682
0.056882	43750	2635	17780	667	12740	705
0.058322	43480	2632	16890	636	12680	682
0.059780	38330	2472	16400	616	12680	671

MOMENTUM = 150 GEV/C CONTINUED

-T IN (GEV/C)**2; S = DSIGMA/DT AND E = ERROR IN MICROBARNS/(GEV/C)**2

	P- P		PI- P		K- P	
-T	S	E	S	E	S	E
0.061256	43400	2665	14970	615	12160	663
0.062750	39290	2573	15120	598	12580	693
0.064262	36800	2618	15710	643	13450	726
0.065792	39620	2624	14890	611	12990	682
0.067340	39760	2530	15390	609	10880	648
0.068906	35440	2383	14390	597	12000	670
0.070490	38060	2535	14960	620	12330	696
0.072092	31330	2267	13900	594	10610	676
0.073712	36990	2578	13280	597	11900	701
0.075350	31910	2530	14270	615	11040	693
0.077006	35290	2517	13780	600	10890	689
0.078680	30920	2428	13390	597	10160	654
0.080372	34880	2751	14780	650	11480	752
0.082082	30820	2486	12030	591	10430	662
0.083810	34810	2587	13080	616	10580	674
0.085556	33330	2722	13250	645	9763	691
0.087320	26280	2418	12310	610	9321	691
0.089102	31940	2622	12730	669	8794	710
0.090902	27810	2472	11800	645	9360	700
0.092720	24380	2404	10750	574	9291	691
0.094556	24320	2314	11130	600	9268	720
0.096410	24920	2401	10480	598	8245	702
0.098282	26530	2664	11150	663	7739	645
0.100172	22240	2303	10840	629	9786	725
0.102080	24140	2462	10440	634	7928	722
0.104006	19130	2156	10170	616	9358	716
0.105950	20280	2217	9852	581	7889	708
0.107912	21520	2326	10880	636	8908	709
0.109892	19940	2311	8894	555	7313	647
0.111890	23610	2458	10600	632	7591	688
0.113906	19030	2143	10740	619	8303	671
0.115940	22370	2366	9718	597	6491	662
0.117992	18230	2041	8843	535	8663	668
0.120062	23190	2354	9167	567	7399	628
0.122150	15550	1884	9235	558	7311	638
0.124256	18020	2006	8362	525	6736	631
0.126380	17230	2094	7740	526	6939	587
0.128522	19510	2030	8801	544	6367	572
0.130682	18680	1975	7878	482	7397	611
0.132860	14470	1682	8767	504	5960	556
0.135056	13890	1647	8224	487	6527	535
0.137270	16830	1809	7477	463	6462	552
0.139502	14660	1671	7430	457	5014	486
0.141752	14180	1760	7481	447	6682	533
0.144020	14710	1599	7030	433	5288	473
0.146306	16680	1745	6843	438	5822	528
0.148610	13830	1568	7256	437	5766	499
0.150932	15230	1675	7002	436	5809	510
0.153272	13820	1575	7247	438	4974	446
0.155630	14070	1664	6648	410	6118	486
0.158006	13890	1652	7606	431	5429	477
0.160400	11100	1344	6265	380	5226	455
0.162812	12300	1421	6353	393	4395	421
0.165242	11420	1374	6338	385	5671	459
0.167690	11250	1404	7244	424	5672	472
0.170156	10480	1460	5626	404	6022	501
0.172640	9015	1210	5666	369	4806	439
0.175142	10430	1282	4949	349	4197	404
0.177662	10470	1296	5585	355	4732	431
0.180200	9139	1238	5734	378	4781	423
0.182756	10700	1314	6101	382	4518	424
0.185330	11340	1383	5855	373	4756	444
0.187922	8260	1288	4878	344	4906	443
0.190532	8748	1230	5149	354	4287	407
0.193160	8032	1140	5098	350	4232	392
0.195806	9334	1242	5313	361	4051	408
0.198470	8842	1209	4592	335	4459	407
0.201152	6305	1012	4353	315	4001	403
0.203852	6834	1070	4560	337	4500	433
0.206570	7690	1137	4453	334	3802	401
0.209306	8645	1226	4731	340	3705	379

MOMENTUM = 175 GEV/C

-T IN (GEV/C)**2; S = DSIGMA/DT AND E = ERROR IN MICROBARNS/(GEV/C)**2

	P+ P		PI+ P		K+ P	
-T	S	E	S	E	S	E
0.001806	156300	4770	96940	2673	98470	3345
0.002256	123200	3686	74100	2025	68020	2469
0.002756	105500	2962	55760	1573	51830	1927
0.003306	93710	2595	47470	1333	39740	1588
0.003906	89670	2420	41770	1147	34300	1325
0.004556	86300	2206	37570	1027	32760	1244
0.005256	79770	2026	32770	927	25240	1024
0.006006	75410	1892	32920	896	22810	937
0.006806	76930	1870	31810	838	22320	902
0.007656	74870	1725	29400	786	23130	892
0.008556	72230	1702	28330	750	20360	813
0.009506	72720	1647	27340	702	19690	783
0.010506	67740	1528	27870	703	18440	760
0.011556	71120	1546	27580	680	18860	721
0.012656	65490	1477	25950	641	19280	703
0.013806	67630	1466	25720	640	18710	690
0.015006	63020	1390	23920	610	19240	703
0.016256	63470	1410	25060	613	16410	636
0.017556	63910	1357	25560	601	16510	624
0.018906	61600	1350	24740	598	17480	656
0.020306	60260	1289	23720	570	16850	626
0.021756	59360	1286	22250	540	15580	605
0.023256	59460	1270	23420	562	16810	611
0.024806	59190	1277	22720	566	17060	621
0.026406	55470	1232	21680	543	15580	592
0.028056	54030	1237	21710	551	14910	584
0.029756	53680	1215	20350	537	14610	596
0.031506	50990	1184	20030	528	15010	596
0.033306	53010	1234	20420	538	16180	615
0.035156	50510	1206	19760	532	13700	580
0.037056	48590	1190	18320	513	14020	575
0.039006	50480	1195	20140	540	13870	583
0.041006	46600	1171	18570	524	14250	591
0.043056	44120	1118	17510	502	13700	592
0.045156	46240	1174	16910	502	13280	575
0.047306	43820	1151	18800	539	14550	610
0.049506	40030	1103	17800	522	12260	574
0.051756	41550	1151	16510	511	12340	586
0.054056	37620	1090	16400	517	11750	577
0.056406	36510	1098	15220	512	11880	584
0.058806	38840	1146	16580	537	13090	618
0.061256	36920	1120	15270	522	12400	607
0.063756	35590	1118	15000	515	11550	601
0.066306	34850	1094	14690	507	10450	562
0.068906	33010	1085	14820	528	11580	613
0.071556	33740	1117	14490	520	10330	590
0.074256	30880	1070	14330	523	10900	607
0.077006	29040	1053	13840	509	10460	583
0.079806	29680	1062	13350	505	10930	612
0.082656	29950	1071	12120	484	9860	568
0.085556	26700	1004	12180	489	9585	567
0.088506	26840	1042	12580	504	9523	567
0.091506	26140	1011	11530	483	8168	538
0.094556	23360	965	11160	477	8718	562
0.097656	24750	993	11040	483	9605	599
0.100806	23540	980	10840	476	8488	561
0.104006	23050	988	10090	478	9020	581
0.107256	21960	970	9869	460	8087	564
0.110556	21400	925	9376	444	7395	518
0.113906	19920	932	9051	439	8080	549
0.117306	20840	966	8704	450	7340	542
0.120756	16410	829	8210	419	6217	494
0.124256	17820	880	8330	443	7489	545
0.127806	17410	917	8866	463	6319	538
0.131406	15300	848	7753	422	6022	505
0.135056	16320	865	7099	407	5768	500
0.138756	14360	823	7268	417	5473	476
0.142506	15210	858	7300	450	6678	558
0.146306	13280	833	7154	430	5991	523

MOMENTUM = 175 GEV/C CONTINUED

-T IN (GEV/C)**2; S = DSIGMA/DT AND E = ERROR IN MICROBARNS/(GEV/C)**2

	P+ P		PI+ P		K+ P	
-T	S	E	S	E	S	E
0.150156	14020	804	6370	391	4832	447
0.154056	12480	755	6502	394	5388	477
0.158006	11510	730	6582	411	5697	495
0.162006	11700	757	6253	389	5951	503
0.166056	12220	748	7154	415	5455	480
0.170156	11130	725	7012	416	4222	438
0.174306	10380	680	5640	368	5273	459
0.178506	9720	645	5721	353	4277	431
0.182756	10210	671	5086	337	4752	427
0.187056	9338	626	4608	318	4558	414
0.191406	7682	558	4840	321	4148	395
0.195806	9339	630	4925	326	4066	420
0.200256	7590	549	4192	306	4737	432
0.204756	7799	554	4362	299	3594	401
0.209306	8862	586	4243	304	4144	386
0.213906	7478	530	4264	296	3152	346
0.218556	6618	503	3365	260	3641	360
0.223256	5910	480	3661	267	2980	334
0.228006	5736	476	3493	267	3126	324
0.232806	6358	484	3580	284	3003	321
0.237656	5226	436	3495	259	2710	303
0.242556	5155	465	3666	263	3062	320
0.247506	6300	488	2900	258	2342	287
0.252506	5338	440	3141	244	2764	306
0.257556	5463	449	2745	236	2755	335
0.262656	4523	410	2736	238	2736	308
0.267806	4527	404	2699	226	2212	273
0.273006	3948	389	2706	241	3085	334
0.278256	3582	370	2397	226	1986	266
0.283556	3430	359	2418	219	2240	298
0.288906	3218	394	2326	229	1549	262
0.294306	3409	381	2150	217	1956	267
0.299756	3120	360	2190	219	2014	280
0.305256	2795	354	1825	196	2248	291
0.310806	3246	370	2076	223	1841	270
0.316406	2769	340	1646	200	1194	216
0.322056	2291	311	2051	214	1533	246
0.327756	2378	326	1571	192	1664	264
0.333506	2204	318	1959	227	1135	221
0.339306	2114	321	1449	193	1356	249
0.345156	1520	272	1637	205	1726	282
0.351056	2145	358	2244	244	1438	261
0.357006	1401	268	1359	192	1073	265
0.363006	1533	288	1434	203	730	193
0.369056	1079	253	735	151	1543	294
0.375156	2020	351	1502	219	1225	265
0.381306	1912	360	877	177	1109	267
0.387506	1340	306	1104	202	1145	275
0.393756	1642	349	1253	221	784	235
0.400056	1283	319	851	189	688	228
0.406406	1511	364	896	204	935	279
0.412806	536	218	550	160	855	268
0.419256	1410	389	1218	263	727	272
0.425756	768	289	923	231	946	313

MOMENTUM = 175 GEV/C

-T IN (GEV/C)**2; S = DSIGMA/DT AND E = ERROR IN MICROBARNS/(GEV/C)**2

	P- P		PI- P		K- P	
-T	S	E	S	E	S	E
0.001806	185300	10190	112800	2060	111200	2969
0.002256	149600	7748	81680	1500	80860	2109
0.002756	117400	6809	65230	1204	59820	1739
0.003306	116600	6082	52230	1015	48660	1419
0.003906	103400	5139	45410	874	38840	1158
0.004556	91250	4762	40180	757	36150	1066
0.005256	98300	4466	38560	729	34130	998
0.006006	89670	3946	35330	659	30260	874
0.006806	83180	3989	34070	627	28490	824
0.007656	88590	3753	31890	587	27070	762
0.008556	80850	3491	31620	561	25080	743
0.009506	80200	3324	30370	538	24500	711
0.010506	77980	3231	29020	512	23320	658
0.011556	78380	3217	29270	517	22960	683
0.012656	75800	3190	28110	489	21990	627
0.013806	77420	3037	27630	473	22140	613
0.015006	75220	2917	26240	458	20960	584
0.016256	70650	2845	26310	444	21750	597
0.017556	75380	2886	26610	446	20230	582
0.018906	70950	2843	25810	441	20330	564
0.020306	66460	2806	25370	432	20370	555
0.021756	68280	2646	24520	424	19360	540
0.023256	63790	2651	23950	414	18090	539
0.024806	65490	2621	24380	423	18130	537
0.026406	64990	2691	22640	404	18810	533
0.028056	63390	2670	22950	407	18190	526
0.029756	61740	2586	22320	412	17320	531
0.031506	59640	2648	21350	395	17080	519
0.033306	53520	2510	21710	403	16720	524
0.035156	57230	2528	20720	385	15040	486
0.037056	52430	2436	20200	393	16050	510
0.039006	54190	2511	19640	383	15190	497
0.041006	52410	2464	19020	376	15460	495
0.043056	52010	2471	19600	379	16200	512
0.045156	48360	2317	18760	372	14360	490
0.047306	45130	2337	19000	377	13960	486
0.049506	45020	2347	18030	376	14390	495
0.051756	44450	2345	18000	383	13260	500
0.054056	47190	2561	17230	379	14130	515
0.056406	42020	2423	17680	388	13260	519
0.058806	36280	2406	16460	371	13100	496
0.061256	40590	2518	15720	378	13090	524
0.063756	35390	2334	15370	375	12550	514
0.066306	37220	2341	15000	369	11860	517
0.068906	37740	2396	14480	375	11820	496
0.071556	31840	2198	14080	367	12540	518
0.074256	32480	2231	14080	376	10660	487
0.077006	30150	2146	13060	348	10400	467
0.079806	31520	2232	12560	354	10060	475
0.082656	30240	2277	13150	364	10640	498
0.085556	32290	2339	12340	345	9432	460
0.088506	25630	2090	11790	343	9286	478
0.091506	23120	1926	12270	352	8637	460
0.094556	24120	1963	11240	337	8480	448
0.097656	26090	2058	10670	323	9410	466
0.100806	24190	2000	10910	335	8546	457
0.104006	24310	1985	9764	318	8263	438
0.107256	21700	1970	9967	313	7757	434
0.110556	18730	1747	9712	313	7324	414
0.113906	19380	1884	9582	306	7861	439
0.117306	17330	1795	9563	308	8238	441
0.120756	17150	1805	8602	302	6948	410
0.124256	17980	1862	8658	298	6995	406
0.127806	17170	1698	7730	288	6309	381
0.131406	15100	1703	8195	287	5455	375
0.135056	12160	1436	7228	281	6409	398
0.138756	15530	1642	7824	288	6418	391
0.142506	10500	1475	7141	270	5794	379
0.146306	11990	1436	6552	262	4564	352

MOMENTUM = 175 GEV/C CONTINUED

-T IN (GEV/C)**2; S = DSIGMA/DT AND E = ERROR IN MICROBARNS/(GEV/C)**2

	P- P		PI- P		K- P	
-T	S	E	S	E	S	E
0.150156	11760	1439	6458	264	6282	402
0.154056	10570	1486	6922	272	5413	368
0.158006	10540	1351	6126	255	5423	371
0.162006	13520	1555	6033	257	5608	383
0.166056	8747	1238	5818	244	5162	352
0.170156	9590	1294	6053	248	4201	331
0.174306	9399	1305	5543	252	4795	371
0.178506	8525	1245	5496	245	4603	339
0.182756	10650	1388	5010	240	5206	360
0.187056	10160	1358	4775	229	4173	337
0.191406	8651	1263	5029	232	4335	345
0.195806	6650	1109	4565	229	3751	308
0.200256	7640	1193	4258	214	3784	312
0.204756	7136	1330	4127	222	3430	294
0.209306	6686	1085	4141	205	3549	293
0.213906	7655	1211	4144	218	3957	338
0.218556	6071	1072	4302	225	3514	303
0.223256	6667	1111	3995	211	2935	290
0.228006	6924	1154	3934	209	2756	288
0.232806	7514	1188	3770	211	2989	278
0.237656	2802	722	3057	186	3101	282
0.242556	5676	1036	2955	189	2957	277
0.247506	6485	1128	3412	197	2938	282
0.252506	4634	944	3253	200	1899	224
0.257556	4622	942	2814	177	2471	275
0.262656	4959	990	2913	183	2392	255
0.267806	4358	928	2239	160	2445	258
0.273006	3376	817	2535	171	1874	225
0.278256	3844	880	2607	174	2723	275
0.283556	2953	787	2569	177	2627	297
0.288906	3863	908	2626	180	1877	235
0.294306	4032	923	2443	173	2505	270
0.299756	3899	917	2267	175	1955	241
0.305256	2396	721	2235	168	1727	227
0.310806	2197	693	1961	157	1589	219
0.316406	2289	722	1877	157	1709	261
0.322056	1389	565	2078	174	1579	224
0.327756	2165	720	1638	151	1641	232
0.333506	2795	840	1592	152	1591	236
0.339306	1723	649	1510	156	1442	221
0.345156	1350	602	1546	154	1355	224
0.351056	810	466	1615	158	1658	248
0.357006	1974	744	1164	151	707	165
0.363006	572	403	1323	161	1200	217
0.369056	301	301	1256	147	1184	222
0.375156	897	516	1372	154	1297	231
0.381306	3145	991	1153	144	1171	280
0.387506	1321	658	1205	169	953	272
0.393756	1691	754	1199	152	851	198
0.400056	688	486	633	111	916	208
0.406406	1822	812	647	116	1022	226
0.412806	744	524	662	118	834	207
0.419256	2179	971	954	183	1101	257
0.425756	1649	821	901	173	925	229

MOMENTUM = 200 GEV/C

-T IN (GEV/C)**2; S = DSIGMA/DT AND E = ERROR IN MICROBARNS/(GEV/C)**2

	P+ P		PI+ P		K+ P	
-T	S	E	S	E	S	E
0.001806	147800	4877	105100	3405	98250	3916
0.002256	120600	3498	70460	2411	66950	2673
0.002756	106000	2864	57350	1821	44800	2148
0.003306	90310	2410	44970	1477	43030	1600
0.003906	89170	2175	41940	1319	32920	1382
0.004556	82990	1912	38500	1092	28930	1232
0.005256	77390	1736	34020	1028	25020	1072
0.006006	75630	1657	31140	926	21150	1020
0.006806	76170	1517	31440	853	22540	930
0.007656	74990	1476	28950	783	20650	873
0.008556	70890	1418	27840	763	21450	800
0.009506	70880	1340	26510	719	19360	769
0.010506	69500	1271	26890	718	19650	747
0.011556	68380	1243	26420	661	19380	694
0.012656	68720	1198	25200	641	18960	690
0.013806	68250	1133	25320	622	18440	665
0.015006	63540	1103	24280	597	17970	605
0.016256	64080	1092	24340	585	18320	613
0.017556	63020	1057	25050	559	17490	589
0.018906	59810	1030	23040	539	17160	572
0.020306	59030	976	24000	541	16410	566
0.021756	59760	973	24000	526	16270	563
0.023256	56730	931	22280	506	15720	509
0.024806	56920	933	22010	502	16140	512
0.026406	55620	907	21560	487	15210	505
0.028056	53860	883	21630	484	16160	511
0.029756	53200	869	21360	476	14760	496
0.031506	50400	842	21270	451	15370	479
0.033306	51690	840	21040	471	15130	493
0.035156	49620	823	19460	451	14280	469
0.037056	48850	814	20120	442	15360	486
0.039006	47490	796	19280	440	13550	458
0.041006	45660	794	18850	434	14340	486
0.043056	45850	793	18880	436	14030	462
0.045156	43370	772	17710	416	12820	461
0.047306	43030	766	17180	407	12730	455
0.049506	41740	764	17240	418	12790	462
0.051756	41130	754	17840	432	12890	463
0.054056	40910	748	16340	417	12570	447
0.056406	37810	716	15880	406	11370	450
0.058806	36510	713	16400	424	11880	451
0.061256	36630	739	16220	423	11850	474
0.063756	33850	714	14760	415	10550	459
0.066306	34370	708	14480	407	11590	477
0.068906	33500	708	14660	410	10130	449
0.071556	30670	692	13940	412	9808	450
0.074256	30420	692	13800	414	10430	450
0.077006	30240	673	13610	395	9884	446
0.079806	29140	659	13170	394	9767	433
0.082656	28810	658	13870	409	10270	463
0.085556	26420	647	12670	392	10060	450
0.088506	26050	639	11830	384	9584	431
0.091506	24820	620	11630	374	9341	419
0.094556	25170	613	10450	365	9305	439
0.097656	23050	608	10310	357	7649	412
0.100806	22880	591	11160	372	7189	374
0.104006	22130	588	10460	359	7673	404
0.107256	20370	576	8985	338	7933	403
0.110556	20140	552	9148	334	7363	414
0.113906	20080	566	8859	337	7104	390
0.117306	18480	543	9300	349	7218	386
0.120756	17420	529	8222	324	7404	399
0.124256	17280	534	9139	346	6895	384
0.127806	17850	547	7775	323	6482	382
0.131406	15600	523	7949	335	5868	370
0.135056	15650	512	6956	311	6382	377
0.138756	14910	518	7279	334	6388	400
0.142506	15000	519	7749	332	5833	385
0.146306	12600	494	6848	315	5944	381

MOMENTUM = 200 GEV/C CONTINUED

-T IN (GEV/C)**2, S = DSIGMA/DT AND E = ERROR IN MICROBARNS/(GEV/C)**2

	P+ P		PI+ P		K+ P	
-T	S	E	S	E	S	E
0. 150156	12920	488	6307	333	5113	362
0. 154056	13370	509	6644	322	5398	378
0. 158006	12260	504	6200	318	4515	352
0. 162006	11530	494	5523	324	4832	368
0. 166056	12160	528	5893	330	4142	369
0. 170156	10940	489	4841	292	4063	348
0. 174306	9324	460	5487	357	4795	404
0. 178506	10600	495	4715	310	4475	382
0. 182756	9061	453	5210	323	3474	333
0. 187056	8363	436	4881	314	3392	330
0. 191406	7917	433	4556	300	3474	341
0. 195806	8413	443	4388	303	3462	339
0. 200256	6840	410	4783	308	3028	309
0. 204756	7877	436	3559	267	3421	372
0. 209306	6760	393	4016	281	2930	301
0. 213906	6568	374	4688	299	2877	295
0. 218556	6470	384	3658	251	3298	353
0. 223256	5986	352	3732	248	3670	340
0. 228006	5410	369	3551	242	2377	280
0. 232806	5150	319	2780	227	3204	293
0. 237656	5408	314	3529	233	3009	280
0. 242556	4709	310	3389	222	2825	265
0. 247506	4353	279	2875	201	2414	258
0. 252506	4262	272	2669	199	2887	261
0. 257556	4119	266	2666	206	2158	241
0. 262656	4323	262	2719	190	2442	252
0. 267806	4017	258	2474	180	2213	223
0. 273006	3822	249	2373	196	2353	243
0. 278256	3373	227	1962	158	1821	217
0. 283556	2871	222	2522	185	1549	182
0. 288906	3147	226	2176	174	2032	209
0. 294306	3076	214	2131	179	1565	183
0. 299756	2753	204	2236	169	1715	212
0. 305256	2640	194	1728	144	1793	192
0. 310806	2766	195	2122	157	1437	169
0. 316406	2540	201	2039	158	1726	190
0. 322056	2273	178	1656	139	1265	159
0. 327756	2055	174	1902	154	1624	203
0. 333506	1693	150	1477	129	1310	177
0. 339306	1946	168	1504	136	1427	192
0. 345156	1752	168	1529	145	1469	174
0. 351056	1719	168	1718	146	1042	170
0. 357006	1451	158	1307	128	1246	163
0. 363006	1633	152	1037	121	937	138
0. 369056	1409	154	1388	130	1551	180
0. 375156	1400	156	1251	125	1002	146
0. 381306	1331	138	1143	117	1170	156
0. 387506	1099	125	1161	128	1344	166
0. 393756	835	110	870	103	1188	159
0. 400056	1056	124	922	106	862	135
0. 406406	1152	128	997	111	1073	150
0. 412806	781	107	790	111	825	133
0. 419256	1000	123	901	107	907	142
0. 425756	1031	123	727	95	727	125
0. 432306	848	125	806	112	772	127
0. 438906	787	127	713	111	785	133
0. 445556	1016	127	589	106	930	147
0 452256	710	106	584	88	573	115
0. 459006	816	118	566	91	477	148
0. 465806	682	109	715	104	771	141
0. 472656	458	89	487	105	600	124
0. 479556	483	93	438	82	551	121
0. 486506	455	92	258	64	309	92
0. 493506	669	117	570	100	714	147
0. 500556	539	107	294	73	642	142
0. 507656	508	108	379	85	516	131
0. 514806	355	94	370	88	568	144
0. 522006	269	84	640	121	585	218
0. 529256	410	109	428	103	437	136
0. 536556	228	85	416	107	389	136
0. 543906	427	117	481	115	392	137

MOMENTUM = 200 GEV/C

-T IN (GEV/C)**2; S = DSIGMA/DT AND E = ERROR IN MICROBARNS/(GEV/C)**2

	P- P		PI- P		K- P	
-T	S	E	S	E	S	E
0.001806	169100	9867	114200	3415	118000	4234
0.002256	137300	6840	78930	2407	75110	2837
0.002756	126200	5955	61020	1938	62320	2215
0.003306	100200	5135	51870	1541	50940	1806
0.003906	98170	4480	47840	1338	44960	1514
0.004556	98650	4001	44560	1165	38710	1330
0.005256	94090	3650	39480	1063	34880	1231
0.006006	82600	3509	36900	933	30820	1066
0.006806	90980	3208	33420	872	28270	985
0.007656	82600	3042	32890	817	28470	908
0.008556	82670	2776	32160	784	26660	902
0.009506	78220	2655	28470	724	26200	826
0.010506	79100	2709	30080	708	24910	762
0.011556	77190	2460	28540	667	23130	731
0.012656	70800	2372	28500	637	23620	703
0.013806	75290	2331	28180	623	23210	695
0.015006	74600	2223	27030	589	21210	646
0.016256	69600	2136	26390	562	21500	613
0.017556	71320	2111	25440	552	21200	612
0.018906	66480	2012	25390	546	20130	590
0.020306	69690	1955	25610	523	20470	566
0.021756	67260	2027	24910	513	19110	560
0.023256	65370	1886	24930	502	19990	561
0.024806	63150	1857	23970	493	18470	528
0.026406	61950	1824	23280	477	18120	514
0.028056	61300	1725	22450	460	18420	505
0.029756	56320	1730	22580	461	17740	499
0.031506	58530	1720	22820	462	17160	499
0.033306	55570	1626	21780	444	16650	474
0.035156	51530	1609	20780	432	16810	485
0.037056	53240	1622	20700	442	16690	481
0.039006	54170	1656	20670	425	15710	471
0.041006	53350	1654	19520	420	15600	464
0.043056	47860	1559	19320	414	15500	472
0.045156	48050	1552	18500	414	15610	466
0.047306	47150	1569	18440	409	14680	455
0.049506	45470	1529	18510	406	13620	449
0.051756	43610	1500	17160	395	14040	437
0.054056	44470	1516	17250	393	14300	455
0.056406	42790	1524	17040	397	14200	439
0.058806	43040	1553	17090	405	13470	449
0.061256	40890	1469	15760	393	13770	446
0.063756	37430	1483	15800	387	12880	439
0.066306	35830	1418	15110	389	12910	452
0.068906	35130	1476	14740	390	12450	443
0.071556	36840	1489	14290	394	11970	461
0.074256	33570	1413	14370	399	12330	447
0.077006	29690	1331	13300	372	9759	413
0.079806	29940	1334	13210	379	10730	432
0.082656	31850	1443	12980	375	11050	430
0.085556	27730	1331	12160	368	10340	426
0.088506	28250	1403	12700	387	10300	439
0.091506	25880	1290	12540	371	9442	429
0.094556	28790	1336	11470	368	10310	438
0.097656	24560	1288	10710	349	9247	399
0.100806	25940	1316	10450	352	8912	408
0.104006	23210	1309	10160	335	8480	400
0.107256	19870	1143	10490	341	8167	397
0.110556	20790	1250	9829	340	8546	403
0.113906	20650	1251	9422	329	7818	378
0.117306	19140	1160	8912	320	7184	365
0.120756	19290	1132	8793	331	7571	384
0.124256	18030	1125	8039	319	7160	359
0.127806	19410	1201	8367	325	7515	400
0.131406	17440	1133	7937	298	6480	344
0.135056	16570	1048	7301	290	6944	358
0.138756	15650	1077	7289	294	6782	357
0.142506	12700	955	7449	304	5916	335
0.146306	11530	965	6794	293	5431	314

MOMENTUM = 200 GEV/C CONTINUED

-T IN (GEV/C)**2. S = DSIGMA/DT AND E = ERROR IN MICROBARNS/(GEV/C)**2

	P- P		PI- P		K- P	
-T	S	E	S	E	S	E
0.150156	13770	961	6777	283	6127	334
0.154056	13060	941	6535	289	6090	346
0.158006	11300	930	6386	278	5486	322
0.162006	11820	903	6367	289	5347	317
0.166056	11190	871	5834	261	4642	306
0.170156	11980	915	6349	284	5172	320
0.174306	9675	870	5643	260	4804	303
0.178506	9695	857	5494	265	4422	296
0.182756	8654	773	4991	253	4405	302
0.187056	9323	802	4328	245	4045	282
0.191406	9639	817	4682	246	4062	291
0.195806	6789	753	4495	227	3948	284
0.200256	7786	741	4515	232	4160	298
0.204756	7018	713	4222	237	4490	298
0.209306	6752	698	4485	230	3221	285
0.213906	5348	617	3792	211	4017	303
0.218556	5333	620	3966	235	3514	262
0.223256	5059	660	3991	233	3196	252
0.228006	5256	619	3555	206	3662	270
0.232806	5271	621	3251	202	3290	275
0.237656	4199	606	3050	205	2703	250
0.242556	4935	603	3325	205	3233	264
0.247506	3720	520	2971	193	2664	250
0.252506	3263	547	2759	186	2195	219
0.257556	3207	488	2700	187	2441	244
0.262656	3936	539	2685	192	2575	227
0.267806	4355	566	2573	182	2318	215
0.273006	3614	511	2452	169	1975	196
0.278256	2761	512	2456	170	2067	202
0.283556	3000	540	2561	176	1599	193
0.288906	2424	415	2288	163	1968	207
0.294306	2830	458	2286	172	2180	209
0.299756	2743	439	1911	147	1769	195
0.305256	2223	386	1659	134	1753	178
0.310806	2039	384	1608	159	1933	207
0.316406	1527	403	1652	136	1655	176
0.322056	2346	414	1759	145	1205	169
0.327756	3043	463	1715	154	1747	182
0.333506	2018	373	1420	127	1241	153
0.339306	1923	369	1320	123	1053	172
0.345156	1391	318	1479	140	1426	182
0.351056	1402	312	1334	131	1233	153
0.357006	1908	366	1422	127	1010	138
0.363006	1156	381	1182	117	1192	168
0.369056	1012	269	1177	126	1053	143
0.375156	1258	304	1135	116	1077	163
0.381306	947	262	954	105	1144	150
0.387506	809	242	963	107	829	146
0.393756	1244	300	1060	112	1048	144
0.400056	1613	350	924	118	996	144
0.406406	687	228	945	118	800	128
0.412806	1004	385	797	111	789	128
0.419256	966	278	1017	115	556	110
0.425756	554	208	836	104	523	130
0.432306	885	265	618	115	755	150
0.438906	81	296	787	102	913	143
0.445556	609	229	876	111	579	117
0.452256	600	225	695	112	711	153
0.459006	891	280	589	91	716	131
0.465806	266	153	602	92	640	124
0.472656	462	205	467	84	486	142
0.479556	374	186	538	90	520	115
0.486506	378	189	341	94	737	137
0.493506	98	98	551	93	384	101
0.500556	318	182	518	94	294	91
0.507656	321	185	486	91	596	131
0.514806	0	0	373	80	355	145
0.522006	110	110	369	81	434	114
0.529256	113	112	558	101	317	99
0.536556	118	118	229	66	398	113
0.543906	250	176	285	76	525	134

APPENDIX D

Additive Quark Model Amplitude

In this Appendix we summarize the theoretical arguments used by Bialas et al.[1.17] to arrive at the nuclear amplitude of Eq. 1.5. The t dependence of the Additive Quark Model (AQM) amplitude is written as follows:

$$f_n^{ff}(t) = A\ G_a(t)\ G_p(t)\ A_{qq}(s,t)\ , \qquad \text{D.1}$$

where A is a constant, G_a and G_p are the electromagnetic form factors of the incident particle a and of the target proton (Eqs. 1.3a-c), and $A_{qq}(s,t)$ is the quark-quark scattering amplitude. We note that in the Chou-Yang[1.16] model A_{qq} is unity.

Bialas et al. employ the optical approach of Glauber and assume the scatter of particles is purely diffractive and dependent on the structure and interaction of the particles in impact space. In Figure D.1, the impact space parameter, b, is defined. The Fourier transform parameter of b is q, which is equal to $(-t)^{1/2}$.

We first assume that pions and kaons are composed of two quarks, while protons are made up of three. These quarks appear point-like when probed by electromagnetic processes, since their gluon cloud is neutral. However, when probed by nuclear processes the gluon cloud participates and gives the quark a finite spatial extent. We associate a radius, r_q, with this volume. A quark with an 'active' gluon cloud

Figure D.1

Additive Quark Model Scattering

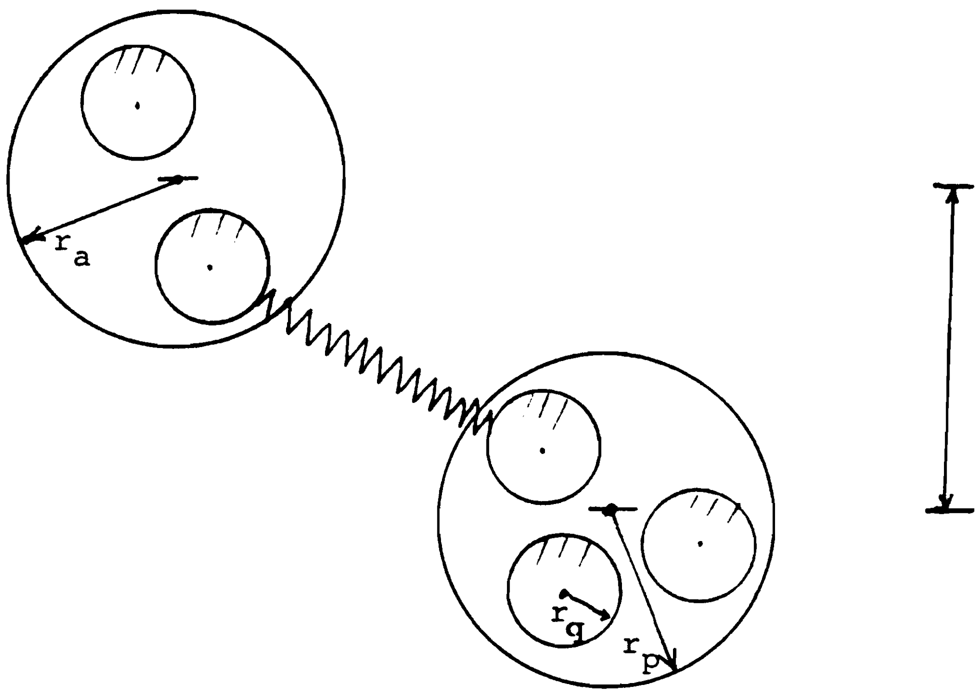

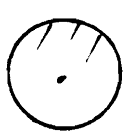

dressed quark

is called a dressed quark.

Next we assume that the quark distribution within particle a in impact space is given by a function chosen so that its Fourier transform gives the electromagnetic form factors. Specifically, when this function is evaluated over two quarks, it yields the monopole form for pions and kaons (1.3b,c). Similarly, when evaluated over three quarks, it yields the dipole form for the protons (1.3a). The single quark-quark scattering amplitude in impact space is then assumed to be given by $\exp(-b^2/r_q^{\,2})$, whose Fourier transform is $\exp(ut/2)$, where $u = r_q^{\,2}/2\hbar^2$. Alternatively, Levin and Shekter[1.18] give the reduced slope, u, as $u = 2\,\alpha' \ln(s/s_0)$, where α' is the derivative of the Regge trajectory, and thus indicate that the quark radius should increase with increasing energy.

These quark distributions and single quark-quark scattering amplitude are used in a Glauber analysis, where the scattering matrix is expanded in terms of the number of quark-quark scatters. We assume that at low t the hadronic interactions of 'quasi-free' dressed quarks are dominated by single quark-quark scattering. Then, to first order in this expansion the nuclear amplitude is given by

$$f_n^{\,ff}(t) = A\, G_a(t)\, G_p(t) \exp(ut/2)\ . \qquad \text{D.2}$$

Multiple quark-quark scattering terms become significant with increasing -t. The dip at $-t = 1.4$ (GeV/c)^2 seen in pp scattering is interpreted to be the interference between single and double quark-quark scattering. In Schiz et al.[1.11] we noted significant departure of the pp data from Eq. D.2 above $-t = 0.4$ (GeV/c)^2. We have restricted our use of the AQM form factor amplitude to -t less than 0.36 $(GeV/c)^2$.

REFERENCES AND NOTES

1.1 Real part measurements for pp scattering:

A. A. Vorobyov et al., Phys. Lett. 41B, 639 (1972).

P. Jenni et al., Nucl. Phys. B129, 232 (1977);

K. J. Foley et al., Phys. Rev. Lett. 19 (1967);

V. D. Apokin et al., Sov. J. Nucl. Phys. 25, 51 (1977);

E. Jenkins et al., Fermilab Pub. 78/35-EXP (1978); Submitted to Sov. J. Nucl. Phys.; also published as D. Gross et al., Phys. Rev. Lett. 41, 217 (1978);

U. Amaldi et al., Phys. Lett. 43B, 231 (1973);

U. Amaldi et al., Phys. Lett. 66B, 390 (1977).

1.2 Real part measurements for π^-p scattering:

P. Baillon et al., CERN 75-10 (1975); also published in Nucl. Phys. B105, 365 (1976)

K. J. Foley et al., Phys. Rev. 181, 1775 (1969);

V. D. Apokin et al., Phys. Lett. 56B, 391 (1975);

J. P. Burq et al., Phys. Lett. 77B, 438 (1978).

1.3 Real part measurements for π^+p scattering:

P. Baillon et al., CERN 75-10;

K. J. Foley et al., Phys. Rev. 181, 1775 (1969);

V. D. Apokin et al., Sov. J. Nucl. Phys. 25, 51 (1977).

1.4 Real part measurements for K^+p scattering;

P. Baillon et al., CERN 75-10;

P. Baillon et al., Nucl. Phys. B107, 189 (1976);

R. K. Carnegie et al., Phys. Lett. 59B, 308 (1975);

D. W. S. Leith et al., SLAC report, unpublished;

V. D. Apokin et al., Sov. J. Nucl. Phys. 25, 51 (1977).

1.5 Real part measurements for K^-p scattering:

P. Baillon et al., CERN 75-10;

P. Baillon et al., Nucl. Phys. B107, 189 (1976);

J. R. Campbell et al., Nucl. Phys. B64, 1 (1973);

R. K. Carnegie et al., Phys. Lett. 59B, 308 (1975);

R. J. Deboer et al., Nucl. Phys. B106, 125 (1976);

R. W. Meijer, Thesis, Amsterdam University, 1973.

1.6 Real Part measurements for $\bar{p}p$ scattering:

P. Jenni et al., Nucl. Phys. B94, 1 (1975);

P. Jenni et al., Nucl. Phys. B129, 232 (1977);

D. W. S. Leith et al., SLAC report, unpublished;

K. J. Foley et al., Phys. Rev. Lett. 19, 857 (1967).

1.7 L. N. Hand et al., Rev. Mod. Phys. 35, 335 (1963).

1.8 A. Quenzer et al., Phys. Lett. 76B, 512 (1978) and the references therein.

1.9 E. Dally et al., submitted to XIX International Conference on High Energy Physics, Tokyo, August, 1975.

1.10 G. B. West and D. R. Yennie, Phys. Rev. 172, 1413 (1968).

1.11 A. Schiz et al., submitted to Phys. Rev.

1.12 C. W. Akerlof et al., Phys. Rev. D14, 2864 (1976);

D. S. Ayres et al., Phys. Rev. D15, 3105 (1977).

1.13 R. K. Carnegie et al., Phys. Lett. 59B, 313 (1972).

1.14 G. Barbiellini et al., Phys. Lett. 39B, 663 (1972); J. P. Burq et al., Phys. Lett. 77B, 438 (1978).

1.15 H. A. Bethe, Ann. Phys. 3, 190 (1958); In Ref. 1.1 Amaldi(1973) discusses the bases for ignoring spin effects at high energies.

1.16 T. T. Chou and C. N. Yang, Phys. Rev. 170, 1591 (1968).

1.17 A. Bialas et al., Acta Phys. Pol. 8B, 855 (1977); N. W. Dean, Phys. Rev. 1D, 2703 (1970).

1.18 E. M. Levin and V. M. Shekhter, Proc. of IXth Winter LNPI School on Nuclear Physic and Elementary Particles (Leningrad 1974), Vol. III.

1.19 The quark-quark scattering amplitude is written in impact parameter space (b-space) as $\exp(b^2/r_q^2)$; private communication, H. Miettenen. A similar parametrization is used Ref. 1.17.

1.20 M. Gell-Mann et al., Phys. Rev. 95, 1621 (1954).

1.21 R. J. Eden, P. V. Landshoff, D. I. Olive, and J. C. Polkinghorne, "The Analytic S-Matrix", pp 3, 16 (Cambridge University Press, London and New York, 1966).

1.22 A. Martin, Nuovo Cimento 42, 930 (1966); 44, 1219 (1966).

1.23 J. B. Bronzan et al., Phys. Lett. 49B, 272 (1974).

1.24 R. E. Hendrick and B. Lautrup, Phys. Rev. D11, 529 (1975); T. R. Englemann and R. E. Hendrick, Phys. Rev. D16, 2891 (1977). R. E. Hendrick provided a numerical tabulation of his results for which we are grateful.

1.25 G. Hohler et al., Kernforschungzentrum Karlsruhe, KFK 2457, April, 1977.

1.26 O. Dumbrajs, University of Helsinki, HU-TFT-78-15, April, 1978.

1.27 H. J. Lipkin, Phys. Rev. D17, 366 (1978).

1.28 R. J. Eden, "High Energy Collisions of Elementary Particles," (Cambridge University Press, London, 1967), p. 194.

2.1 A. Schiz, Thesis, Yale University, 1979; also A. J. Slaughter et al., to be published.

2.2 D. S. Ayres et al., Phys. Rev. D15, 3105 (1977).

2.3 D. S. Ayres, "SAS Facility Threshhold Cerenkov Counter Operating Instructions", Argonne National Laboratory Report, unpublished.

2.4 R. Anderson et al., Nucl. Instrum. Methods 135, 267 (1976).

2.5 M. Benot et al., Nucl. Instrum. Methods 105, 431 (1972).

2.6 R. D. Majka, "Sigma Minus-Proton Elastic Scattering at 23 GeV/c", Thesis, Yale University, 1974.

2.7 W. Frieze et al., Nucl. Instrum. Methods 136, 93 (1976).

2.8 S. Dhawan, "A Fast Readout and Geometrical Reconstruction System for Proportional Wire Chambers", Yale University, unpublished.

3.1 S. Dhawan and R. D. Majka, "A Hardware Scatter Detector," IEEE Transactions on Nuclear Science, Vol. NS-22 (1975).

3.2 Digital Equipment Corp., Maynard, Massachussetts.

4.1 G. Moliere, Z. Naturforsch. 3a, 78 (1953);
H. A. Bethe, Phys. Rev. 89, 1256 (1953).

4.2 M. Sogard, Phys. Rev. D9, 1486 (1974).

4.3 F. James and M. Roos, CERN Computer 7600 Interim Program Library, D506 and D516.

5.1 A. S. Carroll et al., Phys. Rev. Lett. 33, 932 (1974).

5.2 V. Bartenev et al., Phys. Rev. Lett. 31, 1088 (1973).

5.3 R. Schamberger, Jr. et al., Phys. Rev. D17, 1268 (1978).

A.1 I. S. Gradshteyn and I. M. Ryzhik, "Table of Integrals, Series, and Products," (Academic Press, Inc., New York, 1965).

ACKNOWLEDGMENTS

I've never had so finicky a lover, always demanding that I understand her whimsy from her being and then describe the difference to a tenth of a per cent. I am most indebted to Jean Slaughter, Joe Lach, and Alan Schiz for their day to day interest, enthusiasm, and encouragement during this vexing quest.

I am grateful to my advisor, Jack Sandweiss, and my other colleagues: Charles Ankenbrandt, Muzaffer Atac, Robert Brown, Stanley Ecklund, Peter Gollon, James MacLachlan, Richard Majka, Jay Marx, Peter Nemethy, Arthur Roberts, Laurant Rosselet, and Gil Shen, whose hard work and dedication made this experiment possible.

To Peter Martin for his creative resourcefulness and to the Staff of the 5th floor Gibbs, I am thankful, especially for providing a home here where the tall grasses grow and the bison roam. I also thank Adrian Disco for the jewel-like high resolution PWC's, Satish Dhawan for the design of much of the electronics, Irving Winters for sundry mechanical designs, and to William Frieze for his work on early parts of the experiment.

My thanks also go to the many people at Fermilab for their helpful and efficient efforts during the data acquisition and analysis, especially the Meson Lab and Computer Operations Groups. Thanks go to Jon Blomquist, Garvie Hale, and Ed Steigmeyer for their invaluable efforts in the set-up of the experiment. I would like to thank Emily

Luisada for her most patient and careful work on the figures in the thesis. In addition, I thank the Research Services Department for use of their word processor to type the thesis.

I thank the Ford Foundation for the support they provided during my early years of graduate school through the Doctoral Fellowships for Mexican-Americans and Puerto Ricans. This experiment was funded by the Department of Energy.

A mi madre y a mis hermanas por el aliento, cariño, y amor que siempre me han dado, soy y sere agradecido.